Design, Synthesis, and Characterization of New

Fluorescent Probes for in vivo Redox Visualization

Paul R. Oleynik

Master of Science

Department of Chemistry

Faculty of Science

McGill University

Montreal, Quebec, Canada

June 1, 2007

A thesis submitted to McGill University in partial fulfilment of the

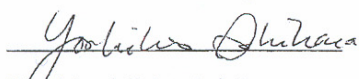*requirements of the degree of Master of Science*

Dedication

This document is dedicated to my parents, Robert and Gail Oleynik.

Paul Oleynik

801 Sherbrooke West, Rm 202

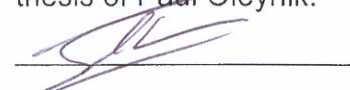Otto Maass Chemistry Bld.

Montreal, QC, Canada

H3A 2K6

Additional copyright clearance from the *Journal of the American Chemical Society* to include a copy of "Design and Synthesis of a BODIPY- Adduct for Use as an Off/On Fluorescent Antioxidant Indicator" (*J. Am. Chem. Soc.*; **2007**; 129; 1842-1843.) is not needed, as approved by the Copyright Subcommittee of the Joint Board/Council Committees on Publications and stated on their website (http://pubs.acs.org/copyright/forms/dissertation.pdf):

Acknowledgements

First and foremost I would like to thank my research supervisor, Professor Gonzalo Cosa, for his constant guidance, selflessness, and seemingly endless knowledge of the physical sciences. I wish him nothing but luck at the beginning of what I am sure will be a long and influential adventure in the sciences.

I offer many thanks to the Chemistry Department of McGill University for their financial and administrative support. Specifically, the help of Chantal Marotte has been over and above her duties, allowing me to focus on my studies and not the black hole of administration. Additionally, I would like to thank Jean-Marc Gauthier for making my teaching assistant duties some of my more enjoyable times at McGill.

Financial assistance from Fonds de Recherche sur la Nature et les Technologies, the Canada Innovation Foundation, and the Natural Science and Engineering Research Council of Canada is much appreciated.

Many thanks to my colleagues An Thien Ngo, Jeff Quesnel, Katerina Kurmova, Pierre "Habibi" Karam, Melanie Burger, Elisa Fuller, and Catrina Pheeney for their acceptance of my constant shenanigans in the Cosa research group. I would also like to thank all of my colleagues within the McGill Chemistry Department. The departmental student and faculty body truly make it a special place to study.

Finally, and most importantly, I wish to thank my parents, Robert and Gail Oleynik, my sister Katie Oleynik, and my brother John Oleynik, as well as my best friend, Jennifer Banfill. They have always allowed me to make my own mistakes while at the same time showing me how to learn from them. Nothing I do would be possible without them.

TABLE OF CONTENTS

7

List of Tables

List of Schemes

List of Figures

11

ABSTRACT

We have initiated a research program intended to prepare lipid soluble free radical sensitive fluorescent probes which can readily report the antioxidant activity within the lipid bilayers. This work provides a substantial amount of information useful in the rational design of pyrromethane dye-based off-on fluorescent probes/switches for redox visualization. In this thesis we report the photophysical properties of a newly prepared Trolox®-PM605 dye (B-TOH) which exhibits a marked off-on fluorescence behaviour in the presence of radicals in homogeneous and microheterogeneous solutions. The absorption and fluorescence spectra, fluorescence quantum yields, and fluorescence lifetimes for this probe when dissolved in organic solvents, as well as in dimirystoyl phosphatidylcholine (DMPC) lipid vesicle suspensions in water are reported herein. The analogous photophysical properties were measured for PM605, the precursor fluorophore used in B-TOH synthesis, its deacylated derivative PM-OH, and a control probe 3,5-Di-tert-butyl-4-hydroxybenzoic acid-PM605 (PM-BHB, which is expected to have a lower reactivity towards radicals) adduct whose synthesis is further described herein. We also report the emission time profile of B-TOH, PM-BHB, and PM-OH following their prolonged exposure to peroxyl radicals in organic solvents and liposome water suspensions. Via careful electrochemical analysis and HPLC oxidation product studies, the observed emission growth of B-TOH is shown to occur via the deactivation of a Photoinduced Electron Transfer (PET) process, operative only in reduced B-TOH. Following exposure of B-TOH to free radicals and subsequent oxidation, PET is surpressed. In summary, we report a novel hydrophobic fluorescent antioxidant indicator with optimum off/on ratio properties for homogeneous solution studies. Antioxidant depletion and the onset of radical mediated oxidation can be directly monitored following emission

enhancement over time, thus dramatically facilitating real-time studies of oxidative processes.

RESUME

Nous avons initié un programme de recherche qui a pour but de développer des sondes fluorescentes, sensibles aux radicaux libres, qui soient solubles dans les solutions lipidiques. Ces sondes devront pouvoir rapporter les activités anti-oxidantes des bi-couches lipidiques. Ce travail fournit des informations importantes pour la conception rationnelle de colorants dérivés du pyrrométhane qui pourront servir d'indicateurs fluorescents "on-off" de la visualisation des réactions redox. Dans cette thèse, nous rapportons les propriétés du nouvel indicateur Trolox-PM605 (B-TOH) qui montre un comportement fluorescent "on-off" marqué en présence de radicaux en solutions homogènes et micro-homogènes. Les spectres d'absorption et de fluorescence, les taux de fluorescence quantique, et la durée de vie de la fluorescence pour cette sonde quand dissoute dans des solvants organiques ainsi que dans des vésicules lipidiques de dimirystoyl de phoshatidylcholine (DMPC) en suspensions dans l'eau sont également rapportées. Les propriétés analogues photophysiques du PM605 (le précurseur fluorophore utilisé pour la synthèse du B-TOH) et du PM-OH (son dérivé acétyle) ainsi que celles d'une sonde contrôle, le 3,5-Di-tert-butyl-4-hydroxybenzoic acid-PM605 (PM-BHB, dont il est attendu d'observer une plus faible réactivité envers les radicaux libres) ont ainsi été mesurées. Nous rapportons également le profil temporel d'émission du B-TOH, du PM-BHB ainsi que du PM-OH, à la suite de leur exposition prolongée aux radicaux peroxydes en solution dans des solvants organiques ou des suspensions aqueuses de liposomes. De précises analyses électrochimiques et des études des produits d'oxidation HPLC ont permis l'observation de la croissance de l'émission du B-TOH, qui se déroule via la désactivation d'un processus de Transfert d'Electron Photo-induit (TEP), ce processus ne s'opérant que dans le contexte du B-TOH réduit. A la suite de l'exposition du B-TOH aux radicaux libres provoquant son oxydation, le TEP est supprimé. En

15

conclusion, nous décrivons un nouvel indicateur d'antioxydant, hydrophobique et fluorescent, qui possède un ratio "on-off" optimal pour les études des solutions homogènes. La déplétion des anti-oxidants et l'émergence de l'oxidation par radicaux peut ainsi être directement observée en suivant les variations de fluorescence au cours du temps. Ce processus facilitant de façon spectaculaire l'études des processus oxidatifs.

List of Symbols

A – Pre-exponential factor

c – Speed of light

°C – Degrees in celcius

$\Delta G°_{ET}$ – Standard Gibb's free energy change for electron transfer

e – Efficiency of escape

$\Delta E°$ - Standard potential

E_a – Activation energy

F – Fluorescence

h – Planck's constant

I – Intensity

J_{AB} – J coupling between A and B

k – Rate constant

k' – Pseudo-first order rate constant

k_{coup} – Coupling rate constant

k_i – Initiation rate constant

k_{inh} – Inhibition rate constant

k_{ISC} – Intersystem crossing rate constant

k_{nr} – Nonradiative rate constant

k_o – Oxidation rate constant

k_p – Propagation rate constant

k_q – Quenching rate constant

k_{rad} – Radiative rate constant

K_P – Partition constant

$K_{P/OW}$ – Octanol/Water partition constant

K_{SV} – Stern-Volmer constant

λ – Wavelength

λ_{exc} – Excitation wavelength

λ_{max} – Wavelength of maximum intensity

m/z – Mass-to-charge ratio

η - NOE enhancement

ν – Frequency

π – Pi (as in electrons)

Φ_{FL} – Quantum yield of fluorescence

R – Gas constant

s – Seconds

S_0, S_1, S_2, ..., S_n – Singlet energy levels

σ - NMR frequency shift

t – Time

T – Temperature

T_0, T_1, T_2, ..., T_n – Triplet energy levels

τ – Fluorescence lifetime/induction period

τ_{nr} – Nonradiative lifetime

τ_{rad} – Radiative lifetime

v/v – Volume-to-volume ratio

ω - Born correction term

List of Abbreviations

α-TOH - α-tocopherol

ABAP – 2,2´-Azobis-(2-methylpropionamidine) dihydrochloride

AIBN – 2,2'-Azobis(2-methylpropionitrile)

ATP – Adenosine Triphosphate

A.U. – Arbitrary Units

BDE – Bond Dissociation Energy

B-TOD – Deuterated 8-((±) 6-Hydroxy-2,5,7,8-tetramethylchromane-2-
carbonyloxy)methyl-2,6-diethyl-1,3,5,7-tetramethyl pyrromethene
fluoroborate

B-TOH – 8-((±) 6-Hydroxy-2,5,7,8-tetramethylchromane-2-
carbonyloxy)methyl-2,6-diethyl-1,3,5,7-tetramethyl pyrromethene
fluoroborate

cm – Centimeters

DCFH – 2',7'-Dichlorofluorescin

DMAP – 4-Dimethylaminopyridine

DMPC – 1,2-Dimyristoyl-*sn*-Glycero-3-Phosphocholine

DNA – Deoxyribonucleic Acid

EDC – 1-ethyl-3-(3-dimethylaminopropyl) carbodiimide hydrochloride

EPR – Electron Paramagnetic Resonance

Equiv. – Equivalents

ESI – Electron spray ionization

eV – Electron volts

HOMO – Highest Occupied Molecular Orbital

HPLC – High Performance Liquid Chromatography

HRMS – High Resolution Mass Spectrometry

IR – Infrared

ISC – Intersystem Crossing

KIE – Kinetic Isotope Effect

kJ – Kilojoules

LUMO – Lowest Unoccupied Molecular Orbital

MHz – MegaHertz

μM – Micromolar

Min – Minutes

mM – Millimolar

MM2 – Molecular Mechanics 2 Force Field

Mol – Moles

MS – Mass Spectrometry

NADPH – Nicotinamide Adenine Dinucleotide Phosphate

ND:YAG – Neodymium-doped Yttrium Aluminium Garnet

nM – Nanomolar

NMR – Nuclear Magnetic Resonance

NOE – Nuclear Overhauser Effect

NOESY – Nuclear Overhauser Effect Spectroscopy

PET – Photoinduced Electron Transfer

PM-BHB – 3,5-Di-turt-butyl-4-hydroxybenzyloxymethyl-2,6-diethyl -1,3,5,7-
tetramethyl pyrromethene fluoroborate

PM-OH – 8-Hydroxymethyl-2,6-diethyl -1,3,5,7-tetramethyl pyrromethene
fluoroborate

PUFA – Polyunsaturated Fatty Acid (also called LH)

ROS – Reactive Oxygen Species

SOD – Super oxide dismutase

SOMO – Semi Occupied Molecular Orbital

Tert-Butyl – Tertiary butyl

THF – Tetrahydrofuran

Trolox – 6-Hydroxy-2,5,7,8-tetramethylchroman-2-carboxylic acid

UV – Ultraviolet

Vis – Visible

1. INTRODUCTION

This introduction will describe first the chemistry of reactive oxygen species (ROS), lipid peroxidation, and the protective behaviour of vitamin E, followed by an overview of fluorescence and how this phenomenon is applied in modern fluorescent probes.

1.1 REACTIVE OXYGEN SPECIES, LIPID PEROXIDATION, AND THE CHEMISTRY OF VITAMIN E

1.1.1 The Chemistry and Biology of Reactive Oxygen Species

Molecular oxygen (O_2) appeared in significant amounts in the Earth's atmosphere roughly 2.5 billion years ago due to oxygenic photosynthesis by cyanobacteria, combined with an abundance of carbon dioxide (CO_2) and water (H_2O).[1-3] The increasing concentration of molecular oxygen in the atmosphere allowed for the evolution of aerobic respiration, leading to the development of complex eukaryotic organisms.[4]

For all currently living aerobic species, molecular oxygen is a central molecule in cellular respiration. Certain derivatives of oxygen are however highly toxic to cells. In the 1950s, Gerschman et al. proposed that oxygen free radicals (or reactive oxygen species (ROS)) are responsible for toxic effects in aerobic organisms.[5-7] A variety of enzymes were discovered by McCord and Fridovich in the 1960s that were found to be responsible for detoxification of oxygen in aerobes but were absent in anaerobes (leading to oxygen-induced damage in these organisms).[8-11] The presence of such enzymes suggested that if the ROS were not scavenged, they would critically injure cells. This hypothesis was confirmed in the case of the super oxide radical anion (O_2^-) ROS by Carlioz and Touati via the construction of Super-Oxide Dismutase (SOD)-

deficient strains E. coli in 1986; these organisms showed remarkable growth defects if exposed to air.[12]

The observed toxicity of oxygen species is due to the rare nature of molecular oxygen; it is a stable biradical with two spin-aligned, unpaired electrons in its π-antibonding orbitals (Figure 1-1).[13,14] The biradical nature of oxygen restrict it to accepting electrons one at a time during a redox reaction, making this process, and the subsequent chemical reations, energetically unfavourable. Indeed, molecular oxygen, with a redox potential of -0.16 V, is a poor univalent electron acceptor (see Scheme 1-1). Consequently, molecular oxygen itself is a poor oxidant and is fairly benign to biomolecules.
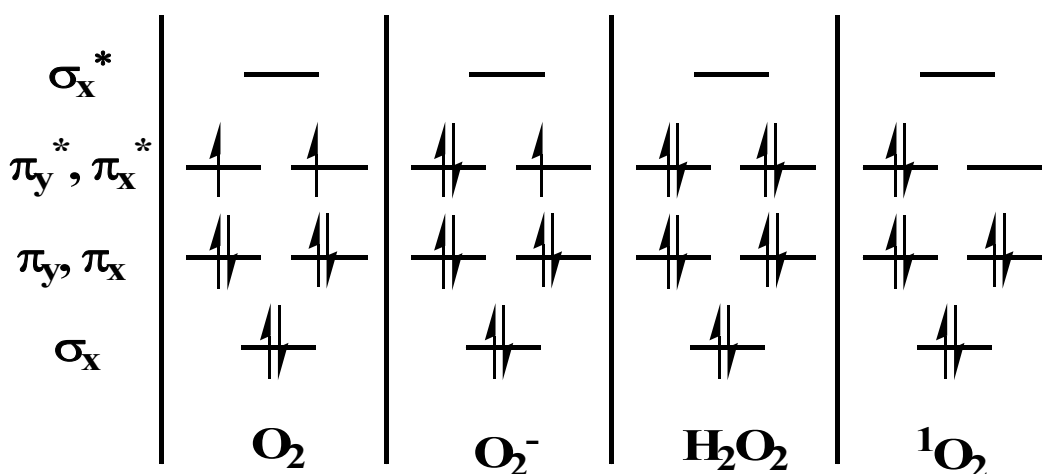
Figure 1-1. Molecular orbital diagrams of the Reactive Oxygen Species (ROS) molecular oxygen (O_2), superoxide (O_2^-), hydrogen peroxide (H_2O_2), and singlet oxygen ($^1O_2$).[14]

Reduction of molecular oxygen produces the ROS molecules of superoxide radical anion ($O_2^{\cdot-}$), hydrogen peroxide (H_2O_2), peroxyl radical ($ROO^\cdot$), and the hydroxyl radical ($HO^\cdot$) (Figure 1-1, Scheme 1-1). In addition, energy transfer to molecular oxygen via a variety of biomolecular processes can flip one of the unpaired electrons to give singlet oxygen ($^1O_2$) (see Figure 1-1). These ROS molecules are much stronger oxidants

than molecular oxygen, as are indicated in their redox potentials, which are outlined in Scheme 1-1. Hence, the ROS molecules, in thermodynamic terms, are very reactive molecules, leading to their destructive properties.

$$O_2 \xrightarrow[\text{-0.16 V}]{e^-} O_2^{\cdot-} \xrightarrow[\text{+0.94 V}]{e^- + 2H^+} H_2O_2 \xrightarrow[\text{+0.38 V}]{e^- + H^+} HO^{\cdot} \xrightarrow[\text{+2.33 V}]{e^- + H^+} H_2O$$
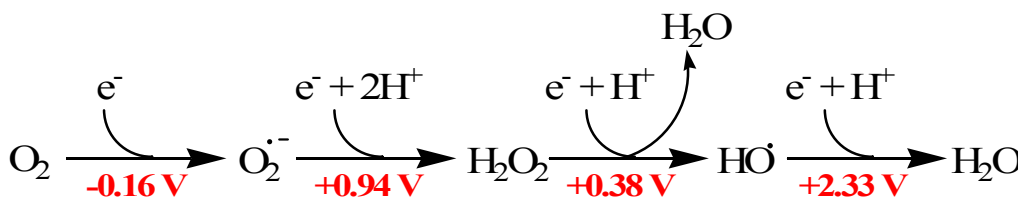
Scheme 1-1. Redox potentials for Reactive Oxygen Species demonstrating the strong oxidant capability of these molecules.[14]

In cells, ROS are continuously taken from environmental sources and produced as byproducts in a number of metabolic-related mechanisms.[15,16] Mitochondria, the power plants of cells, where aerobic respiration takes place, consume more than 90% of oxygen in aerobic organisms. These organelles are the main site of ROS generation and are, hence, an important site for cellular redox studies. Indeed, as noted by Chang *et al.*,[17] overproduction of H_2O_2 and other ROS from the mitochondrial electron transport chain leads to oxidative stress and the subsequent functional decline of organ systems. Additionally, several electron-transfer enzymes involved in the electron transport chain in the mitochondria have been associated with ROS production. NADPH-dependent oxidase, for example, catalyzes the production of superoxide via reduction of molecular oxygen by NADPH.[18] Also, a variety of peroxidises have been found to generate the highly reactive hydroxyl radical from hydrogen peroxide.[19] The superoxide anion is formed from an electron escaping from the energy producing mitochondrial electron transport systems, which normally is used to reduce oxygen to water in order to produce adenosine triphosphate (ATP), the energy currency of the cell.[20] Peroxyl radicals are generated by a combination of oxygen with

alkyl radicals (R˙) or via decomposition of alkyl peroxides (ROOH).[21] As discussed below, these radicals can abstract hydrogen atoms from biomolecules, often being involved in chain reactions. The wide range of ROS types and mechanisms of production, coupled with its destructive nature make these systems an important field of study.

Enzymatic and nonenzymatic antioxidant systems in cells regulate the destructive power of ROS. Examples of enzymatic antioxidant systems include superoxide dismutase, catalase, and glutathione peroxidise, while examples of nonenzymatic approaches include vitamins E and C, and carotenes.[22,23] Production and accumulation of ROS molecules beyond the ability of the enzymatic and nonenzymatic antioxidant systems to properly scavenge them can oxidatively damage many important biomolecules including proteins, lipids, and DNA, leading to the onset of oxidative stress.[4,13,14] The efficiency of antioxidant systems decreases with age and diseases, resulting in an accumulation of oxidized biomolecules.[24] Many diseases are associated with ROS-induced damage. Among others, atherosclerosis, vasospasms, cancers, trauma, stroke, asthma, hyperoxia, arthritis, heart disease, age pigments, dermatitis, cataractogenesis, retinal damage, hepatitis, liver disease, and periodontis have been shown to involve ROS-induced oxidation of biomolecules.[21,25,26]

1.1.2 The Chemistry and Biology of Lipid Peroxidation

The oxygen-dependent deterioration of lipids has been observed for centuries, mainly through the rancidity of food. Rancidity is caused by the autoxidation (oxidation under mild conditions) of lipid molecules in foods.

Modern studies of lipid peroxidation can be thought to have begun with Criegee et al. in the 1940s when he established that hydroperoxides

are the primary product of the oxidation of hydrocarbons.[27] Criegee's results were applied to lipid systems, which are essentially complicated hydrocarbons, by Farmer et al.[28] In addition, Ingold made significant contributions to this field after moving from the study of radicals and their intermediates in plastics and oils to investigations on the role of oxidation in the ageing process, including many pioneering studies involving Vitamin E, from the 1960s to the present time.[29-34] Several product studies in the following decades provided a mechanistic understanding of the oxidation of specific lipid molecules.[35] With the introduction of High Performance Liquid Chromatography (HPLC), multiple products generated during lipid oxidation could be characterized, leading to the first demonstration of free radical induced oxidation of phospholipids by Porter in 1980[35] and a new era of understanding of lipid peroxidation.

The work discussed above, and subsequent developments,[26,29-37] have lead to the conclusion that lipid peroxidation is a free-radical chain reaction that is initiated by the presence of ROS. Many of the processes that create free radical initiators of lipid radical chain reactions occur within or near membranes, making them susceptible to ROS damage.[38] The free radical chain reaction is commenced by an initiator "In", forming a carbon centred radical "R·". The initiation step, with its characteristic rate of generation "R_g", is associated with a number of environmental factors such as heat, light, or enzymatic processes, among others.[31]

The newly formed radicals react rapidly with an oxygen molecule to form a peroxyl radical (ROO·),[39] a reactive intermediate capable of damaging the lipid bilayer following hydrogen atom abstraction from polyunsaturated fatty acids (reaction 1 in Scheme 1-2).[35] As seen in Scheme 1-2, the peroxyl radical can next attack LH (where L stands for a polyunsaturated fatty acid) to form a hydroperoxide ROOH and a new carbon centred radical L· at a much slower rate (reaction 2 in Scheme 1-2).[33] The newly formed lipid-based carbon centred radical L· can then

propagate the chain reaction as shown in reactions 3 and 4 of Scheme 1-2.[40] As the level of hydroperoxides increases the polarity of the lipid-phase will also increase due to the additional hydrogen bond donors, causing the newly developed hydrophilic part of the molecule to migrate to the lipid/water interface. This has the effect of changing the mobility of the lipid and the resistance to thermodenaturation, potentially resulting in the formation of new lipid rafts in the membrane.[21] The propagation step, as with all continually fed chain reactions, will continue until it is terminated following the reaction (disproportionation or addition) of two chain carriers to give non-reactive products.

Initiation

$$In \longrightarrow R^{\bullet} \xrightarrow{O_2} ROO^{\bullet} \qquad (Rate = R_g) \ (1)$$

$$ROO^{\bullet} + LH \longrightarrow ROOH + L^{\bullet} \qquad (Rate = R_i) \ (2)$$

Propagation

$$L^{\bullet} + O_2 \xrightarrow{k_{ox}} LOO^{\bullet} \qquad k_{ox} \sim 1\text{-}10 \times 10^8 \ M^{-1}s^{-1} \ (3)$$

$$LOO^{\bullet} + LH \xrightarrow{k_p} LOOH + L^{\bullet} \qquad k_p \sim 1 \times 10^1 \ M^{-1}s^{-1} \ (4)$$

Termination

$$LOO^{\bullet} + TOH \xrightarrow{k_{inh}} LOOH + TO^{\bullet} \qquad k_{inh} \sim 3 \times 10^6 \ M^{-1}s^{-1} \ (5)$$

$$LOO^{\bullet} + TO^{\bullet} \xrightarrow{k_{coup}} T(O)OOL \qquad k_{coup} \sim 1\text{-} 8 \times 10^8 \ M^{-1}s^{-1} \ (6)$$

$$AscH + TO^{\bullet} \xrightarrow{k_{reg}} Asc^{\bullet} + TOH \qquad k_{reg} \sim 3 \times 10^5 \ M^{-1}s^{-1} \ (7)$$
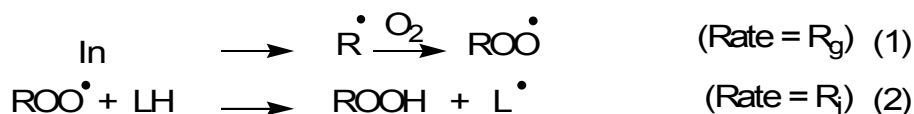
Scheme 1-2. Initiation, propagation, and termination of the free radical induced peroxidation of esters of polyunsaturdated fatty acids (LH).[40]

Natural lipid systems from living organisms do not oxidize regularly given their antioxidant defence mechanisms (discussed above). The array of antioxidant molecules fall into two classes of compounds based on their mode of action: preventative antioxidants act at the initiation stage by reducing the rate of chain initiation, whereas chain-breaking antioxidants

interfere with the propagation step by reacting with a propagation molecule to form non-reactive products.[32]

Based on its chemical reactivity towards radicals and its physiological concentration (~30 uM in plasma[37]), the most important antioxidant against membrane peroxidation is the lipid-soluble chain-breaking antioxidant Vitamin E. Vitamin E, in fact, refers to a family of structurally similar phenolic compounds called tocopherols that differ in the number and position of methyl groups on the aromatic ring (Figure 1-2).[31] Tocopherols are characterized by their phenolic "head" group, which is responsible for their antioxidant activity, and their phytyl (hydrocarbon) "tail", which is responsible for their lipophilicity. The most potent antioxidant form of Vitamin E is the fully methylated form α-tocopherol (α-TOH, where the H represents the phenolic hydrogen) (Figure 1-2).

x-TocH	R_1	R_2
α	CH_3	CH_3
β	H	CH_3
γ	CH_3	H
δ	H	H
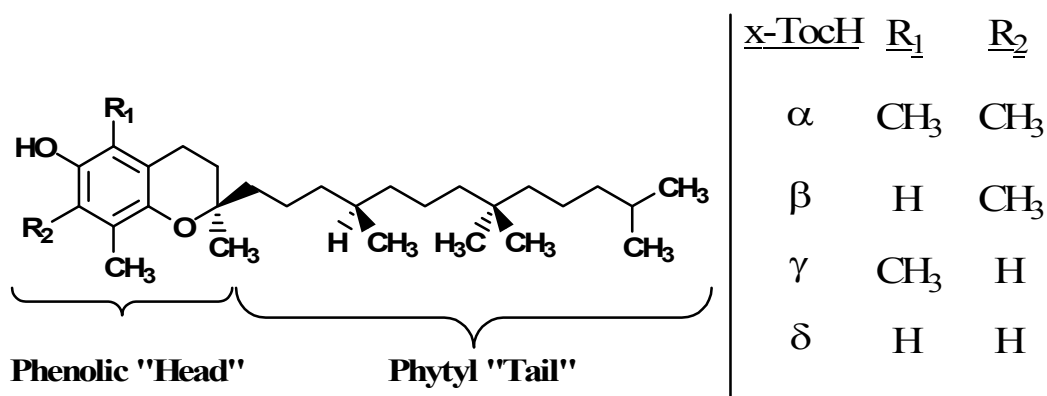
Figure 1-2. Generic structure of the most reactive lipophilic antioxidant, Vitamin E (α-tocopherol). Different substitution patterns give rise to the family of compounds. The phenolic "head" group contains the antioxidant activity, while the long alkyl tail acts as a lipid anchor.[31]

α-tocopherol is considered a good antioxidant since it fulfills two criteria: first, chain-carrying peroxyl radicals preferentially react with α-tocopherol over other oxidizable moieties (in Scheme 1-2, reaction 5 is preferred over reaction 4), such as polyunsaturated fatty acids (PUFAs); and, second, the newly formed α-tocopherol radical (α-TO·) is stable

enough to not oxidize another lipid molecule (α-TO$^{\cdot}$ is not a chain carrier or chain initiator). In solution, α-TOH traps two chain propagating peroxyl radicals (LOO$^{\cdot}$) thus effectively terminating two free radical chain autooxidations.[41-44]   A first peroxyl radical is scavenged yielding a hydroperoxide and α-TO$^{\cdot}$, the latter reacts with a second peroxyl radical to give various chromanones such as 8a-(alkyldioxy)tocopherone (α-TO(OOL), Scheme 1-2).[45,46]   An induction period is observed in lipid oxidation studies in the presence of α-TOH, the end of which signals the consumption of α-TOH and the onset of the lipid chain autooxidation.[43,47-49]
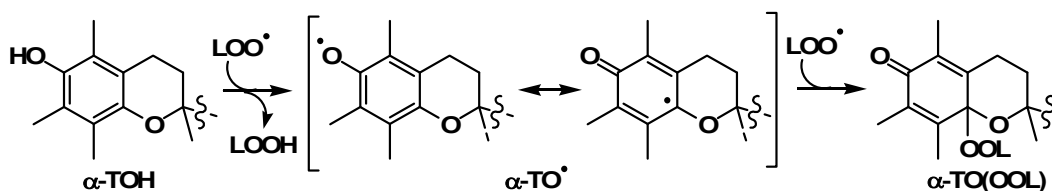
Scheme 1-3. Peroxyl radical scavenging by α-tocopherol (α-TOH) and α-tocopherol radical (α-TO$^{\cdot}$) in homogeneous solution.

The initial rate of oxidation including α-tocopherol (α-TOH) inhibition is given by:

$$\frac{-d[O_2]}{dt} = \frac{k_3[RH]R_g}{2k_5[\alpha-TOH]} \qquad (1\text{-}1)$$

where k_3 and k_5 and are the rates of reactions 3 and 5 (Scheme 1-2), respectively, [RH] is the concentration of oxidizable lipid, and R_g is the rate of generation of peroxyl radicals. The 2 in the denominator of Equation 1-1 represents the fact that two peroxyl radicals are scavenged per α-tocopherol. An important value for oxidation studies is the rate of generation of radicals R_g, which can be calculated via the induction period τ (where τ is the time it takes to consume all of the α-tocopherol and commence lipid peroxidation)[50] according to Equation 1-2.

$$\tau = 2[\alpha-TOH]/R_g \qquad (1\text{-}2)$$

Since the induction period τ indicates the complete consumption of an antioxidant, it can provide valuable information regarding the effectiveness of a molecule as an antioxidant. HPLC product studies are used to monitor the concentration of a particular antioxidant with time, which allows for the determination of the end of the induction period, however this method is an invasive one. The induction period technique was used to conclude that vitamin E is the major lipid-soluble, chain-breaking antioxidant in human membranes.[31]

Flourimetry offers a particularly important platform in which to analytically study ROS, lipid peroxidation, and antioxidant loads on account of its extreme sensitivity. Indeed, many fluorescent probes have been devised to monitor free radicals both *in vivo* and *in vitro*.[51] Notably, most if not all of these methods measure the induction period τ in the form of the time it takes to begin radical-induced destruction of the flourophore probe. Unfortunately, these methods do not account for the oxidative stress responsible for the depletion of the system's antioxidant load until it has been surpassed. Further, probes that work by turning off can report a fluorescent quencher rather than free radicals (i.e. they lack specificity). Therefore, lipid peroxidation studies both in solution and within live cell membranes would dramatically benefit from using a real time off/on fluorescent indicator of the antioxidant status, i.e., a probe capable of reporting via emission enhancement the depletion of α-tocopherol and the onset of the lipid chain autooxidation.

1.2 PRINCIPLES OF FLUORESCENCE AND FLUORESCENT PROBES

"Fluorescence is a dominant methodology used extensively in biotechnology, flow cytometry, medical diagnostics, DNA sequencing, forensics, and genetic analysis, to name a few."

- Joseph R. Lakowicz[52]

1.2.1 Principles of Fluorescence

1.2.1.1 Introduction to the Phenomenon of Fluorescence and the Jablonski Diagram

Fluorescence is a type of luminescence (emission of light occurring from electronically excited states) occurring from the emission of a photon caused by the return of an excited electron to its ground state after being electronically excited.[52] Fluorescence is an allowed transition, occurring with a rate constant anywhere between 10^{-12} and 10^{-9} s. Fluorescence differs from phosphorescence, another type of luminescence, in that in fluorescence the excited electron is paired (via opposite spin) to the second electron in the ground-state orbital (a singlet excited state). Phosphorescence, on the other hand, occurs when the excited electron is in a triplet excited state (where the excited electron has the same angular momentum as the second electron in the ground-state orbital). Phosphorescence is a spin-forbidden transition and, hence, occurs at a much longer time-scale (10^{0} to 10^{-6} s).[52] The differences between the two types of luminescence is shown in Figure 1-3.
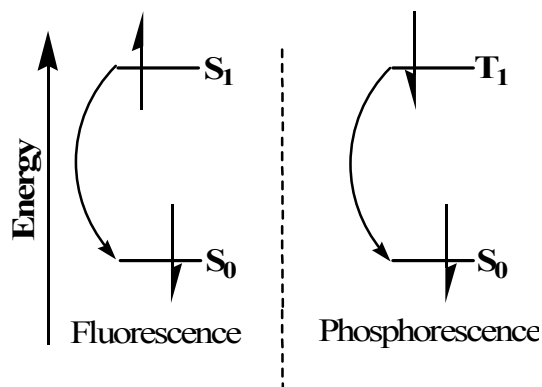
Figure 1-3. Frontier orbital energy diagram showing the difference between fluorescence and phosphorescence. In fluorescence, the excited electron returning to the ground state is of opposite spin to the second

electron in the ground state (spin-allowed transition). In phosphorescence, the excited electron returning to the ground state has the same spin as the second electron already in the ground state and therefore must undergo a change in the spin angular momentum upon returning to the ground state (spin-forbidden transition).

Absorption and emission of light, as well as the various molecular processes that can occur in excited states are best diagrammed by what is called a Jablonski diagram,[53] named after Professor Alexander Jablonski. A typical Jablonski diagram is depicted in Figure 1-4. In this figure, S_0, S_1, and S_2 represent the singlet ground, first, and second electronic states, respectively, with each electronic energy state containing a number of vibrational energy levels (depicted 0, 1, 2, etc.).
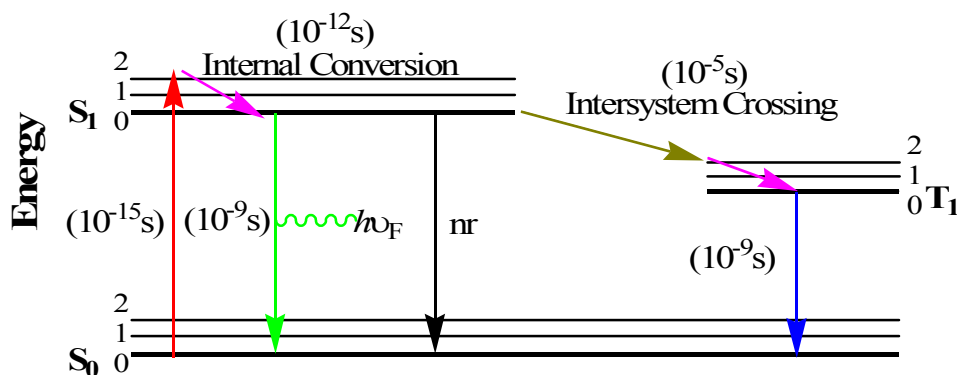
Figure 1-4. A typical Jablonski diagram showing absorption (red arrow), internal conversion (pink arrow), emission (green arrow), non-radiative decay (black arrow), intersystem crossing (brown arrow), and phosphorescence (blue arrow). The time each process takes is also shown.

As shown in Figure 1-4, absorption of energy in the form of light instantaneously ($\sim 10^{-15}$ s) excites an electron to a higher electronic (and possibly a higher vibrational) state (shown as a red arrow in Figure 1-4), which is followed by rapid ($\sim 10^{-12}$ s) relaxation to the lowest vibrational

energy state of the electronic excited state (referred to as internal conversion, see pink arrow in Figure 1-4). Following excitation, the excited flourophore can deactivate/react following a number of parallel reaction pathways involving non-radiative deactivation (k_{nr}), intersystem crossing (k_{ISC}), radiative deactivation (fluorescence, k_{rad}), intermolecular fluorescence quenching (k_qx[Quencher]) (see Figure 1-4 and Scheme 1-4).

$$S_0 \xrightarrow{\text{h}\nu} S_1{}^*$$

$$S_1{}^* \xrightarrow{k_{nr}} S_0$$

$$S_1{}^* \xrightarrow{k_{ISC}} T_1{}^*$$

$$S_1{}^* \xrightarrow{k_{rad}} S_0 + \text{h}\nu$$

$$S_1{}^* \xrightarrow{k_q[Q]} \textbf{Products}$$
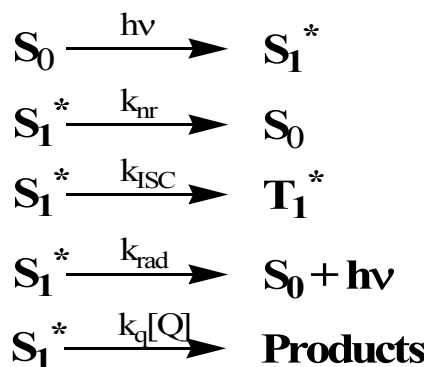
Scheme 1-4. Kinetic scheme of the excitation of a flourophore $S_1{}^*$, followed by the possible deactivation pathways available to it. These include non-radiative, intersystem crossing to the triplet state $T_1{}^*$, radiative, and quenching deactivation.

1.2.1.2 Fluorescence Lifetimes and Fluorescence Quantum Yields

Two of the most important characteristics of fluorescence are the fluorescence lifetimes and fluorescence quantum yields. Fluorescence lifetimes are important as they dictate the time available for a flourophore to relay information from its emission. Fluorescence emission is a stochastic process where the fluorescence lifetime τ of a flourophore is the average time the molecule spends in the excited state before returning to the ground state. Fluorescence then follows an exponential decay as shown in Equation 1-3.

$$I(t) = I_0 e^{-t/\tau} \qquad (1\text{-}3)$$

where $I(t)$ is the fluorescence intensity at time = t, I_0 is the initial intensity, and τ is the fluorescence lifetime. When $t = \tau$, $I(t)/I_0$ becomes equal to $1/e$ (or 0.37), so τ is defined as the time when 37% of the original fluorescence intensity remains. Given the parallel deactivation pathways discussed in Scheme 1-4, the fluorescence lifetime is described by Equation 1-4.

$$\tau = \frac{1}{k_{rad} + k_{nr} + k_{ISC} + k_q[Quencher]} \tag{1-4}$$

The fluorescence quantum yield Φ_{FL} is the number of photons emitted relative to the number of photons absorbed,[52] therefore the largest possible quantum yield is 1. Kinetically, the quantum yield is represented by:

$$\Phi_{FL} = \frac{k_{rad}}{k_{rad} + k_{nr} + k_{ISC} + k_q[Quencher]} \tag{1-5}$$

This characteristic is important in determining the efficiency of fluorescence of a flourophore, and in determining the behaviour of the flourophore in different environments.

1.2.1.3 Fluorescence Quenching

Fluorescence quenching is any process that decreases the fluorescence intensity of a flourophore. Quenching can occur via a variety of processes, more generally involving chemical reactions upon encounter with the quencher (photochemical process) or energy transfer to the quencher, or assisted ISC in the presence of the quencher where the latter two constitute photophysical processes.

The decrease in emission intensity due to the action of a quencher is described by the Stern-Volmer equation:

$$\frac{I_0}{I} = 1 + K_{SV}[Quencher] = 1 + k_q\tau^o[Quencher] \tag{1-6}$$

where I_0 is the initial emission intensity, I is the emission intensity in the presence of quencher at a concentration of [Quencher], K_{SV} is the Stern-Volmer constant, k_q is the quenching rate constant, and τ^o is the fluorescence lifetime in the absence of quencher. From Equation 1-8, the Stern-Volmer constant K_{SV} can be obtained as the slope from a plot of I_0/I versus the concentration of quencher [Quencher] (known as a Stern-Volmer plot). Hence, the K_{SV}, as well as the quenching rate constant are easily measured experimentally.

Knowledge gained about the phenomenon of fluorescence has lead to applications in a wide variety of problems in the chemical and biological world. Fluorescent molecules are used to probe interactions of molecules with other molecules and with solvents, diffusion, distances, conformational changes, and binding interactions, to name a few. Fluorescent spectroscopy and intelligently designed fluorescent probes are constantly progressing, providing significant contributions to scientific understanding.

1.2.2 Fluorescent Probes

Cellular events occur in an extremely dynamic fashion in a constrained small environment, making observation of and information about such events difficult to acquire. Well designed fluorescent probes (known as extrinsic or unnatural flourophores) and instrumentation are able to provide the spatial and temporal resolution necessary to directly observe these events. In fact, recent advances in single-molecule spectroscopy have allowed the observation of these events (and flourophores) individually.[54-58] Such fluorescent probe-based studies are possible due to the extremely high sensitivity of flourophores to their chemical environment, making them easy to manipulate into chemical switches (on/off, off/on).

Pioneering work in fluorescent probes applied to biological systems was reported by Tsien's group for a fluorescent probe designed to sense Ca^{2+}.[59-62] Since then, a variety of fluorescent probes for various biomolecules have been reported and applied to systems, greatly contributing new information related to cellular physiology. Information on many designed flourophores can be found in the Molecular Probes catalogue.[63]

Flourophores for *in vitro* studies will generally have the following characteristics: they absorb and emit in the visible range of frequencies where most cellular biomolecules do not absorb or emit light; they contain reactive functional groups facilitating the coupling to other chemical moieties; they have a high quantum yield of fluorescence to avoid large loading of the flourophores;[52] and, they are highly photostable. The last point is very important when choosing a flourophore in the design of a fluorescent probe. This concern arises from the fact that flourophores will photobleach (stop fluorescing) upon continuous illumination. A flourophore which can withstand high light excitation intensities (like those seen in fluorescence microscopy) without photobleaching is considered to be photostable.

Traditionally, fluoresceins and rhodamines were popular families of flourophores used as labels in fluorescent probes, with BODIPY dyes becoming popular more recently because of their tunability in the visible range, high quantum yield of fluorescence, large extinction coefficient, and insensitivity to solvent polarity and pH.[52]
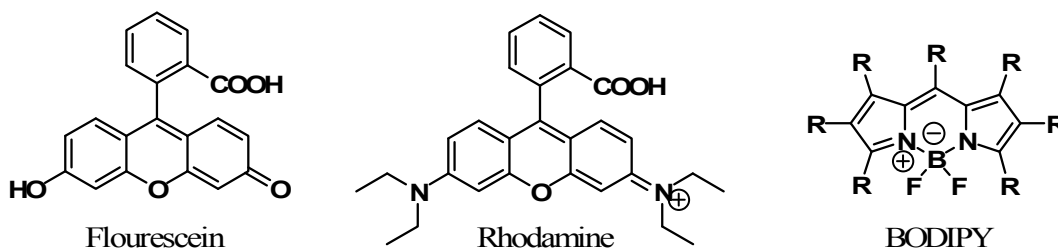
Figure 1-5. Generic structures of the commonly employed flourophores in fluorescent probes fluorescein, rhodamine, and BODIPY.

Because of the large variety of approaches to designing fluorescent probes, all of the types of fluorescent probes will not be reviewed here. A thorough presentation of fluorescent probes is presented within Lakowicz's Principles of Fluorescent Spectroscopy, 3rd Edition[52] and de Silva's "Signal Recognition Events with Fluorescent Sensors and Switches".[64] Membrane probes, fluorogenic probes, biomimetic probes, and receptor-reporter type probes[64] are the most pertinent to the current research and are discussed below. Membrane labelling is accomplished by choosing a flourophore that is hydrophobic and will hence partition into membranes. An added advantage of membrane probes is that hydrophobic flourophores will often have much lower fluorescence quantum yields in aqueous solutions on account of aggregation and subsequent self-quenching, causing the aqueous fraction to become virtually invisible. The depth of the probe within the membrane can be customized by covalent linkage to various hydrophobic chains of different length. Membrane probes are of particular interest for studying events within lipid membranes, membrane potentials, events occurring at the lipid-water interface, and diffusion within membranes.

Fluorogenic probes,[65-67] or off/on probes, are dyes that are originally non- or weakly fluorescent until an event of interest occurs, thereby causing an observable increase of fluorescence. The advantage of these probes is that, if designed correctly, only the event of interest will

be observed, compared to on/off type probes where many events can cause quenching of fluorescence, giving a false signal.

Biomimetic probes are structural analogues of biomolecules which have either been slightly modified to make the new molecule fluorescent, or by linking a flourophore to the parent molecule. These probes have the advantage of having the same chemistry as the parent molecule of study and will therefore behave in a similar manner. Ideally, the flourophore will have no effect on this behaviour. An example of a successful biomimetic probe is the fluorescent cholesterol analogue dehydroergosterol, which has been used as a probe for interactions of steroids with membranes.[68-70]

Finally, receptor-reporter type probes have a flourophore covalently linked to a receptor moiety. The flourophore is responsible for photonic excitation and emission and is hence the reporter moiety. The receptor moiety is responsible for interacting with the species to be detected. A linker, or spacer, joins the two moieties. Many of these probes will operate via quenching of the reporter by the receptor. The fluorescence is initially unquenched for "on/off" probes, becoming quenched by the receptor after reaction with an analyte. Conversely, "off/on" probes are initially quenched by the receptor, with the quenching being cancelled upon reaction of the receptor. Since the receptor often must interact with important biomolecules, these types of probes are frequently designed to be biomimetic, borrowing receptor interaction from biosystems. The quenching of such probes often occurs via Photoinduced Electron Transfer (PET) (discussed in detail below in Section 2.2.2). Hence, receptor-reporter probes can be intelligently designed from knowledge of the optical, guest (analyte) binding, and redox properties of the components.

In the end, fluorescent probes have provided information regarding chemical and biological systems that has previously been unobtainable. This field is rapidly evolving, and new probes are constantly being

developed, allowing experiments on systems that were previously unattainable.

1.3 RESEARCH GOALS

Methods for studying ROS production have been improving since their discovery. As discussed above, these studies began with enzyme studies, moved onto HPLC product studies, and currently use visualization produced via highly sensitive fluorescent probes. Fluorescent probes for the detection of ROS are promising tools for understanding the role of ROS within cells. Traditionally, the fluorogenic probe dichlorodihydrofluorescein (DCFH, $C_{24}H_{16}O_7Cl_2$) has been used for detection of ROS, however it suffers from low selectivity and low photostability.[51,71] Recently, many new probes have been developed for specific ROS systems with high selectivity and photostability.[51]

Currently, peroxyl radical formation and lipid peroxidation studies have used a fluorescence probe where the response is reported after the antioxidant load has been surpassed.[72] Alternatively, invasive product studies on cell extracts are employed .[73] These approaches do not provide necessary direct real-time observation of peroxyl radical formation in the presence of natural antioxidants. Conversely, a well-designed fluorescent radical probe would provide the sensitivity and spatial resolution needed for direct observation of ROS production *in vitro* and *in vivo*.

Our goal is to design, prepare, and characterize such a probe for peroxyl radicals in lipid membranes. Such a probe should be a real-time lipophilic off/on fluorescent probe of antioxidant status; that is, a probe capable of reporting via emission enhancement the depletion of α-tocopherol, the major antioxidant in cellular lipid membranes. This probe would further signal the onset of lipid chain autoxidation. To this end, we have designed a receptor-reporter type biomimetic fluorogenic membrane

probe where the receptor moiety contains the chromanol moiety of α-tocopherol linked to a BODIPY flourophore (see below for details).

2. RESULTS AND DISCUSSION

2.1 DESIGN AND SYNTHESIS OF AN OFF/ON FLUORESCENT ANTIOXIDANT PROBE

Our main goal is to develop a real-time lipophilic off/on fluorescent probe of antioxidant status; that is, a probe capable of reporting via emission enhancement the depletion of α-tocopherol, the major antioxidant in cellular lipid membranes. Such a probe will further signal the onset of lipid chain autoxidation. In order to avoid complications involving absorption or emission due to biomolecules, the probe must absorb and emit in the visible range of frequencies where most cellular biomolecules do not absorb or emit light. The following section describes the design and synthesis of our fluorescent probe 8-((±) 6-hydroxy-2,5,7,8-tetramethylchromane-2-carbonyloxy)methyl-2,6-diethyl-1,3,5,7-tetramethyl pyrromethene fluoroborate (herein referred to as **B-TOH**, see Figure 2-1) which fulfill the conditions mentioned above.

2.1.1 Design of the Fluorescent Probe B-TOH

Our strategy involves preparing a two segment, receptor–reporter[64,74-76] type free radical scavenger fluorescent probe that fulfills the following solubility, reactivity, and spectroscopic requirements: (i) the antioxidant probe partitions in hydrophobic media; (ii) the radical scavenging reactivity of the receptor segment compares to that of α-tocopherol; (iii) the reporter segment absorbs and emits in the visible region of the spectrum; and (iv) the reporter segment undergoes an observable emission enhancement upon radicals being scavenged by the receptor segment.

We chose for the receptor segment commercially available Trolox,[31,37] an α-tocopherol derivative, to match the reactivity of the probe towards free radicals with that of α-tocopherol. Trolox preserves the electronic and steric characteristics of the chromanol moiety of α-tocopherol and hence should have a radical scavenging reactivity that compares to that of α-tocopherol. In order for the probe to partition within hydrophobic media, we coupled to Trolox a dipyrrometheneboron difluoride (BODIPY) fluorescent probe which is known to be retained in phospholipid bilayers.[77] Importantly, BODIPY has an absorption maximum at 543 nm and a fluorescence maximum at 575 nm in ethanol,[78] both of which are in a window that is relatively free of absorption and emission by cellular biomolecules. We thus prepared the Trolox-BODIPY adduct **B-TOH** or **1** (see Figure 2-1).

In addition to **1**, we also prepared a control receptor-reporter probe 3,5-Di-tert-butyl-4-hydroxybenzyloxymethyl-2,6-diethyl -1,3,5,7-tetramethyl pyrromethene fluoroborate or **PM-BHB**, from herein referred to as **2** (see Figure 2-1), that has the commercially available 3,5-Di-tert-butyl-4-hydroxybenzoic acid as the receptor segment. **2** will have a lower reactivity towards ROS for a number of reasons. Its tert-butyl groups sterically protect the reactive phenol site making phenolic hydrogen abstraction by a peroxyl radical difficult. Additionally, the lack of an oxygen atom para- to the phenol will destabilize phenoxyl radicals relative to **1**.[31] In fact, the para- conjugated electron withdrawing carboxylic acid will strengthen the O-H bond of the phenol relative to Trolox making hydrogen abstraction by radicals more difficult. The bond dissociation energy (BDE) of the O-H bond in 3,5-Di-tert-butyl-4-hydroxybenzoic acid is reported to be 84.27 kcal/mol via EPR spectroscopy.[79] This is significantly stronger than the phenolic O-H bond of α-tocopherol, whose BDE is reported to be 5.34 kcal/mol weaker at 78.93 kcal/mol (via EPR spectroscopy).[80]

B-TOH/1   **PM-BHB/2**
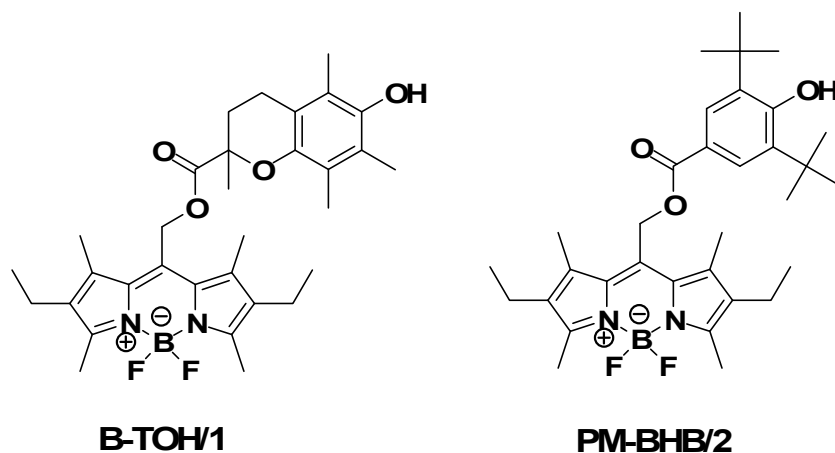
Figure 2-1. Structures of the Trolox-BODIPY adduct antioxidant probe, **B-TOH** or **1**, and the control **PM-BHB** or **2**.

2.1.2 Synthesis of the Fluorescent Probes

The following synthesis methodology was first developed by Mr. Yoshihiro Ishihara,[81] a summer student in our research lab. It was utilized to prepare material for use in the current study. In order to construct **1** and **2**, the BODIPY flourophore PM605 was first deacetylated using lithium hydroxide in a 1:1 (v/v) mixture of distilled deionized water and tetrahydrofuran (this solvent mixture was used for solubility reasons) to yield 8-Hydroxymethyl-2,6-diethyl -1,3,5,7-tetramethyl pyrromethene fluoroborate, a primary alcohol (herein referred to as **PM-OH** or **3**) (quantitative yield) (Scheme 2-1).[82]

Scheme 2-1. Deacetylation of PM605 to form the primary alcohol **PM-OH** or **3**.

Ester formation between **3** and the carboxylic acids of both Trolox and/or 3,5-Di-tert-butyl-4-hydroxybenzoic acid were carried out using EDC/DMAP activated coupling in chloroform under Ar (37% and 45% yield, respectively) (Scheme 2-2).[83]
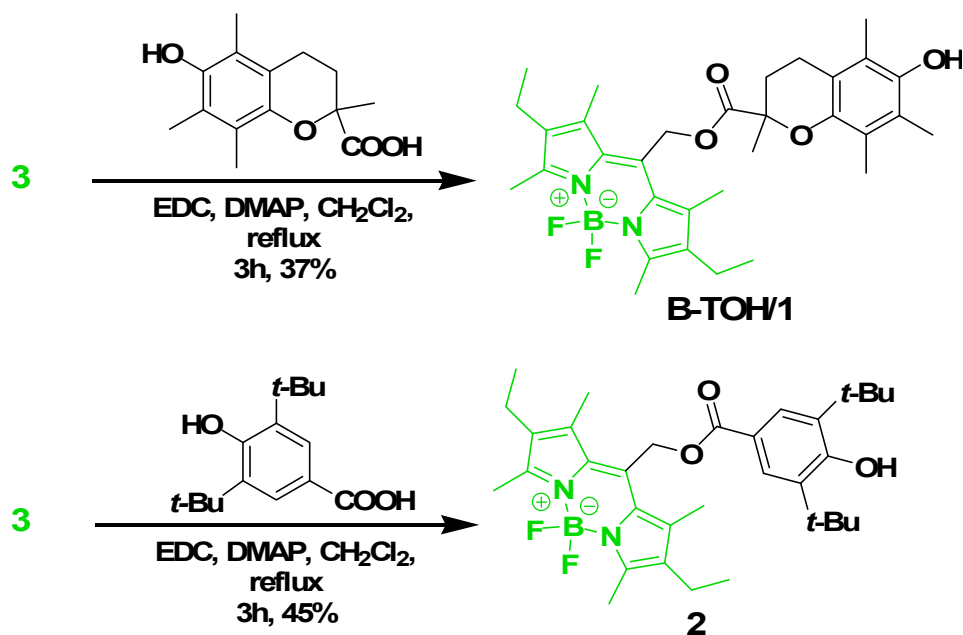
Scheme 2-2. Synthesis of the Trolox-BODIY adduct **1** and 3,5-Di-tert-butyl-4-hydroxybenzoic acid-BODIPY adduct **2** from **3**.

2.2 PHOTOPHYSICAL PROPERTIES OF FLUORESCENT PROBES

The knowledge of the photophysical properties of **1**, **2**, and **3** will provide insights into the modes of action of these molecules.

2.2.1 Absorbance, Quantum Yield, and Fluorescence Lifetime Analysis of Fluorescent Probes

1, **2**, and **3** were dissolved in methanol, acetonitrile, toluene, and hexanes for homogeneous solution studies and their photophysical properties were determined in order to gain insight into the effect of the modifications introduced into the PM605 chromophore. Specifically, the absorption and fluorescence spectra (Figure 2-2) and the fluorescence lifetime decay curves (Figure 2-3) were obtained. Solutions were made to have absorbencies below 0.10 (2.9 μM) to avoid self absorption.

The shape of the absorption and fluorescence spectra (Figure 2-2) of all probes studied are similar to those of the parent BODIPY flourophore PM605,[78] indicating that the modifications described in Section 2.1.2 do not significantly alter the electronic structure of the BODIPY reporter moiety. Hence, previously reported information regarding the BODIPY flourophore (i.e. molar extinction coefficient, electronic transitions, etc.) are valid for these newly synthesized molecules. The absorption maxima show a hypsochromic shift with increasing solvent polarity in all cases (Table 2-1), as observed with other non-polar pyrromethene-BF$_2$ dyes.[84] This effect indicates that the first excited state of the BODIPY flourophore is less polar than the ground state in all cases.
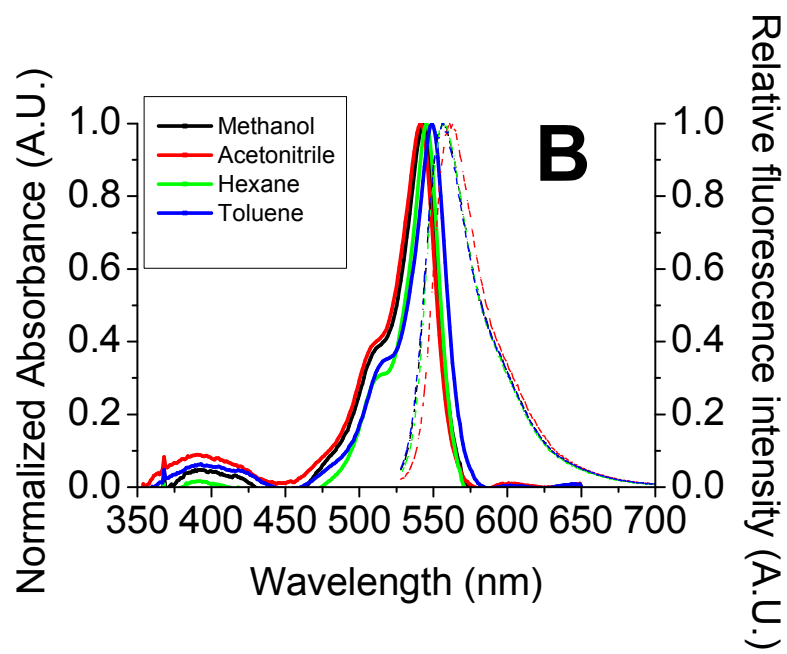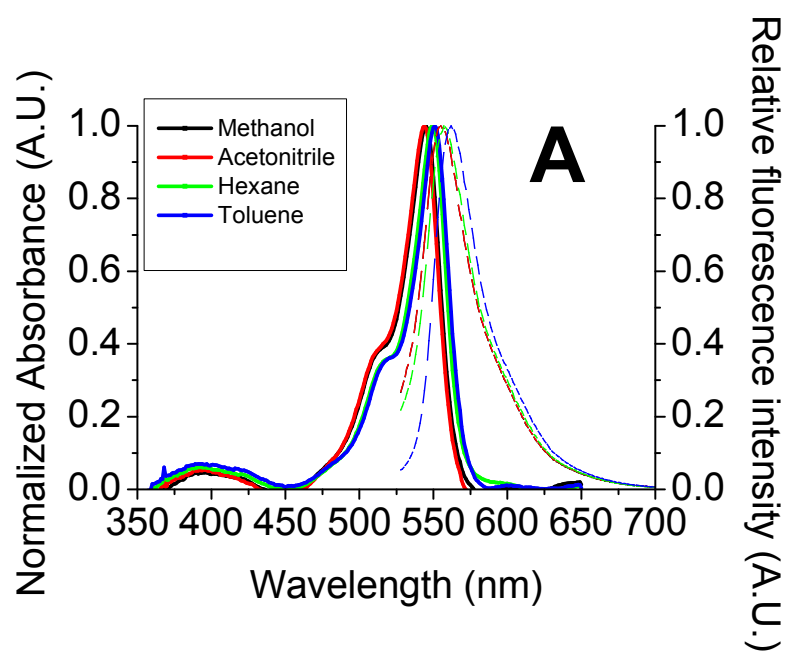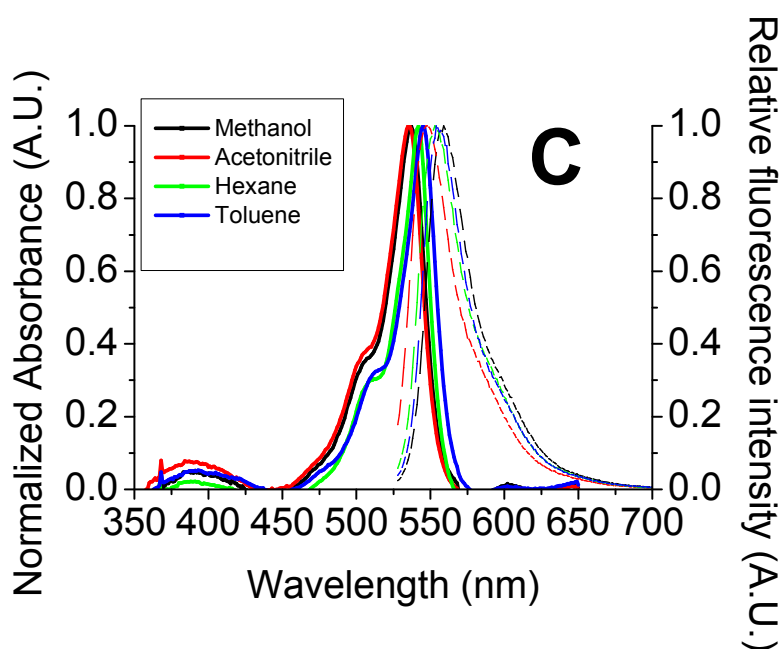
Figure 2-2. Normalized absorption (solid lines) and fluorescence (dashed lines) spectra of (A) **1**, (B) **2**, (C) **3** in methanol (black), acetonitrile (red), hexane (green), and toluene (blue). Dye solutions were prepared in order to have absorbences lower than 0.1 at the excitation wavelength (which varied from 515 to 525 nm).

The fluorescence quantum yield Φ_{FL} of **1** in hexane, methanol, acetonitrile, and toluene is 30-, 20-, 15-, and 10-fold smaller, respectively, than that of PM605. The fluorescence quantum yield Φ_{FL} of **2** and **3** (Table 2-1) are similar to the reported value of 0.74 for PM605 in ethanol.[78] The decrease in the fluorescence quantum yield of **1** can be rationalized by an intramolecular quenching of the excited BODIPY reporter flourophore via the Trolox receptor moiety (see section 2.2.2).

Further information of the intramolecular fluorescence quenching in **1** appears in the fluorescence lifetime analysis of the probes. Figure 2-3 shows the fluorescence decay profiles for **1**, **2**, and **3** in hexane and acetonitrile. The fluorescence lifetimes are presented in Table 2-1. Note the biexponential decay observed in **1**, which is most likely due to

impurities and/or probe oxidation upon loading (each decay component is displayed in Table 2-1, including their weighted scores a_1 and a_2). The fluorescence lifetimes of both **2** and **3** fall between 7 and 8 ns; however, the fluorescence lifetime of **1**, at under 1 ns, is much shorter in organic solvents. The short lifetime of **1** compared to those of **2** and **3** indicates there is a reduction in the probability of an excited electron in **1** returning to its ground state via a radiative pathway (see also equations 1-4 and 1-5).
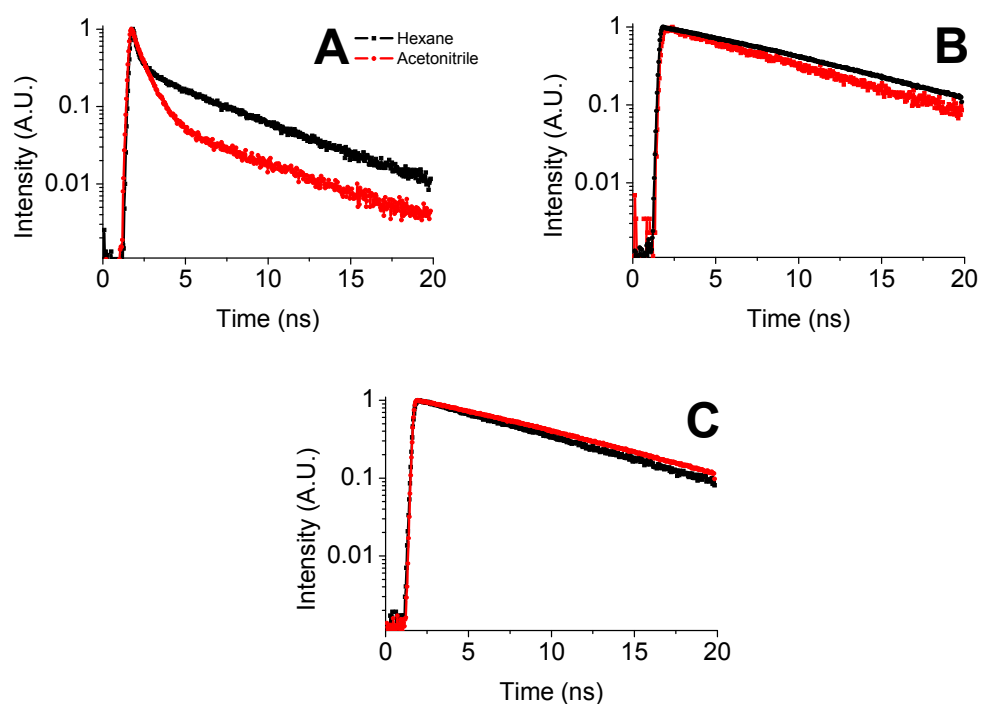
Figure 2-3. Normalized fluorescence decay profiles for (A) **1**, (B) **2**, (C) **3** in hexane (black) and acetonitrile (red). Dye concentrations were such that absorbences were from 0.05 to 0.2 to avoid emission self-absorption from occurring.

Table 2-1. Steady state absorption and fluorescence emission maxima and average lifetimes determined for the probes under study while dissolved in hexanes, toluene, acetonitrile, and methanol, as well as

embedded in DMPC lipid vesicles. Also shown are the decay, radiative, and non-radiative fluorescence lifetime values.

Compound	Solvent	Abs λ_{max} (nm)	Em λ_{max} (nm)	Φ_{FL}	τ_1 (ns)	a_1 (ns)	τ_2 (ns)	a_2 (ns)	τ_{dec} (average) (ns)	τ_{rad} (ns)	τ_{nr} (ns)
1	hexanes	549	557	0.02	0.15	0.90	3.35	0.10	0.46	8.99	0.16
	toluene	551	562	0.07	-	-	-	-	-	-	-
	acetonitrile	544	555	0.05	0.61	0.96	4.40	0.04	0.79	11.6	0.64
	methanol	545	555	0.04	-	-	-	-	-	-	-
2	hexanes	545	557	0.67	-	-	-	-	7.76	11.5	23.5
	toluene	549	556	0.69	-	-	-	-	-	-	-
	acetonitrile	541	561	0.75	-	-	-	-	7.14	9.55	28
	methanol	544	556	0.66	-	-	-	-	-	-	-
3	hexanes	542	553	0.95	-	-	-	-	7.34	7.75	138
	toluene	545	554	0.73	-	-	-	-	-	-	-
	acetonitrile	535	548	0.97	-	-	-	-	7.39	7.58	288
	methanol	537	549	0.83	-	-	-	-	-	-	-

The intramolecular quenching observed in **1** was explored via intermolecular quenching of **3** by Trolox in a Stern-Volmer experiment. From the ratio of the emission of **3** recorded without (I_0) and with (I) increasing Trolox concentration versus [Trolox] (Figure 2-4), the quenching of **3** by Trolox was found to be fairly efficient. Indeed, a Stern-Volmer quenching constant (K_{SV}) of 19.3 M^{-1} is obtained in acetonitrile (Figure 2-4). Given the fluorescence decay lifetime τ = 7.42 ns in acetonitrile (Table 2-1), and the measured K_{SV} (where $K_{SV} = k_q\tau$), upon applying Equation 1-8 we calculate a bimolecular quenching constant k_q of 2.6 x 10^9 M^{-1} s^{-1}. The Stern-Volmer plot of 3,5-Di-tert-butyl-4-hydroxybenzoic acid with **3** in Figure 2-4 shows no quenching, which is consistent with the high quantum yield of fluorescence and long fluorescence lifetime of **2**.

Knowing the parameters for the intermolecular quenching of **1**, we can then calculate the "effective concentration" of Trolox in **1** by applying equation 1-6 as follows: the ratio I_0/I is equal to Φ_3/Φ_1 (given that the chromophore is the same in both cases). Using the k_q and τ^o values

measured experimentally for **3**, we can obtain the "effective Trolox concentration" in the receptor-reporter probe **1**. A value of 0.90 M Trolox is thus calculated.
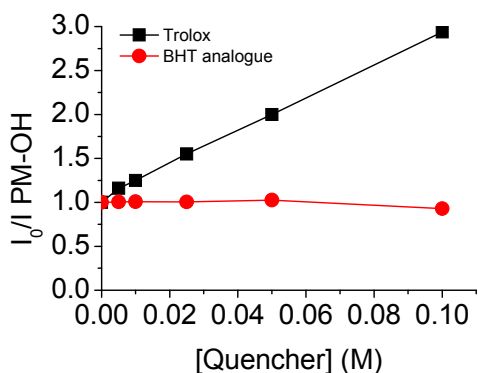
Figure 2-4. Stern-Volmer plots of the quenching of 1 μM **3** with either Trolox (black squares) or 3,5-Di-tert-butyl-4-hydroxybenzoic acid (red circles) as quenchers in acetonitrile. **3** was excited at 510 nm and fluorescence emission was detected at the maximum (548 nm).

In the end, the Trolox receptor moiety in **1** is intramolecularly quenching the BODIPY reporter moiety. This quenching is not present in **2** or **3**, as confirmed by their long fluorescent lifetimes and high quantum yields of fluorescence, as well as by the lack of quenching seen in the Stern-Volmer experiment involving **2**. We next proceeded to verify that the intramolecular quenching proceeds via Photoinduced Electron Transfer (PET) (see Section 2.2.2).

2.2.1.1 Photophysical Properties of 1 in Microheterogeneous Solutions

Compound **1** was incorporated into 1,2-Dimyristoyl-*sn*-Glycero-3-Phophocholine (DMPC) lipid vesicles to study it in a microheterogeneous environment and its photophysical properties were determined in order to

gain insight into the effect of this environment on **1**. As with homogeneous solutions, the absorption and fluorescence spectra (Figure 2-5) and the fluorescence lifetime decay curve (Figure 2-6) were obtained.

The absorption spectra of **1** in DMPC lipid vesicles resembles that of **1** in hexanes, with a maximum at 549 nm (compared to 549 nm in hexanes)(Figure 2-5), which is consistent with the flourophore embedded in the bilayer lipid core rather than at the water/lipid interphase. The fluorescence emission maximum is at 556 nm, which is consistent with the emission of **1** in all solvents studied except toluene. Additionally, the shape of the absorption and fluorescence spectra are similar to those observed in organic solvents (Figure 2-2a) indicating that there are no significant differences in the electronic structure of **1** dissolved in organic solvents or embedded within lipid membranes.
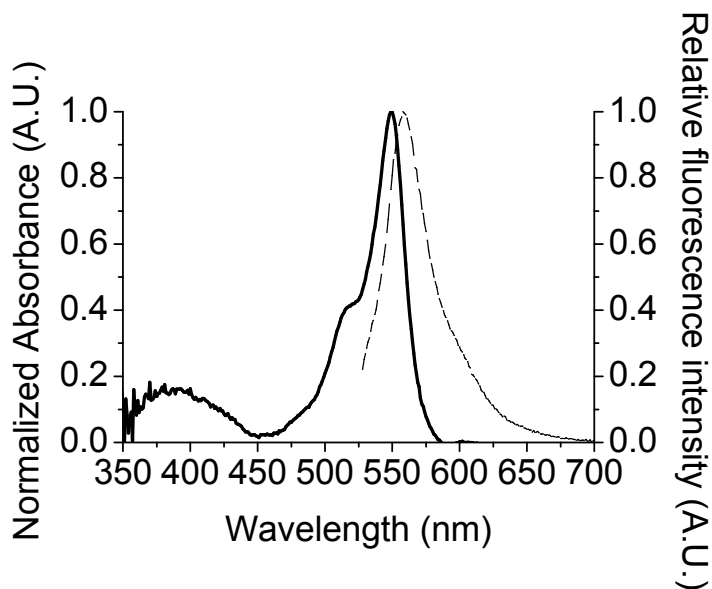
Figure 2-5. Normalized absorption (solid line) and fluorescence (dashed line) spectra of 0.54 μM **1** embedded in 11 μM DMPC in lipid vesicle suspensions. Fluorescence was acquired following excitation at 218 nm. Dye solutions were prepared in order to have absorbences lower than 0.1 at the excitation wavelength.

Figure 2-6 shows the fluorescence decay profiles for **1** in hexane, acetonitrile, and DMPC lipid vesicles, as well as **3** in acetonitrile for visual comparison. The fluorescence lifetimes of **1** in hexane and acetonitrile as reported in Table 2-1 are 0.15 and 0.61 ns, respectively. However, upon incorporation of **1** into lipid vesicles, the fluorescence lifetime increases to 2.50 ns. Taking into account the very short fluorescence lifetime of **1** and the relatively long fluorescence lifetime of **3** (~7 ns) in homogeneous solution, a lifetime of 2.50 ns for **1** in lipid vesicles indicates that the intramolecular quenching in **1** is partially deactivated upon incorporation into lipids. The fluorescence quantum yield of **1** relative to **2** incorporated into lipids was determined to be 0.30, indicating that the increased lifetime of **1** in lipids must be due to a deactivation of intramolecular quenching. We speculate that the intramolecular quenching occurs via a Photoinduced Electron Transfer (PET) process, which is discussed below.
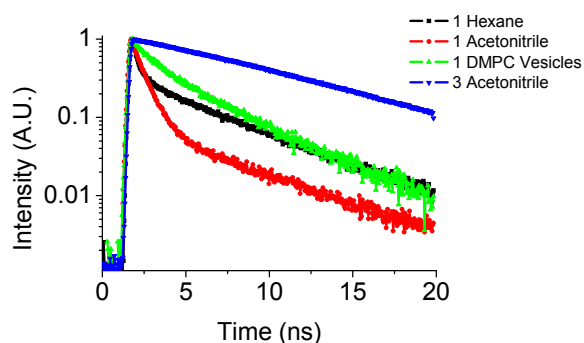
Figure 2-6. Normalized fluorescence decay profiles **1** in hexane (black), acetonitrile (red), DMPC lipid vesicles (green), and **3** in acetonitrile (blue) for comparison. BODIPY concentrations were such that absorbencies were from 0.05 to 0.2 to avoid emission self-absorption from occurring.

2.2.2 Photoinduced Electron Transfer in 1 and 2: Electrochemical Studies

As outlined in Chapter 1, fluorescence quenching may occur via a variety of mechanisms. In the current case, we speculate that Photoinduced Electron Transfer (PET) from Trolox to BODIPY is the active mechanism. In PET, a host-guest complex can return to the ground state without emission of a photon.[64] This occurs because the highest occupied molecular orbital (HOMO) (which becomes the semi-occupied molecular orbital (SOMO) after excitation) of the excited flourophore can accept an electron from the HOMO of the quencher (as illustrated in Figure 2-7), which blocks the excited electron (residing in the LUMO of the flourophore) from returning to the HOMO of the flourophore, thereby blocking fluorescence emission.
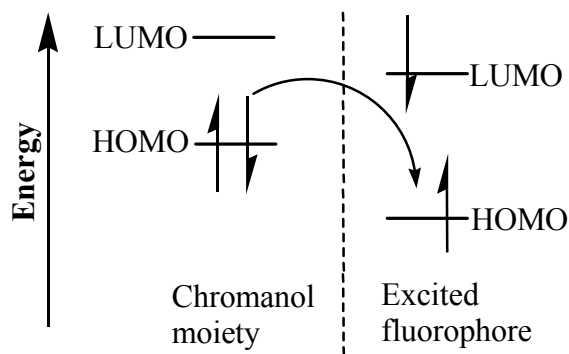
Figure 2-7. Frontier orbital energy diagram discribing Photoinduced Electron Transfer. After excitation, the HOMO of the excited flourophore can accept an electron from the HOMO of quencher, thereby quenching fluorescence.

To validate the feasibility of the PET hypothesis for quenching of BODIPY (A = electron acceptor) by Trolox (D = electron donor) the standard Gibbs free energy changes ΔG^0_{eT} for the formation of solvent-separated radical ion pairs must be evaluated. The Gibbs free energy may be calculated by the Rehm-Weller equation:[85]

$$\Delta G^o_{eT} = [E^o_{D^{+\bullet}/D} - E^o_{A/A^{-\bullet}}] - \Delta E_{oo} + \omega \qquad (2\text{-}1)$$

where ω is a correction term based on the Born equation to account for the solvation and interaction of radical ions formed upon reduction/oxidation, E_{00} corresponds to the energy of the first singlet state, $E^{0}(A/A^{-\cdot})$ is the one-electron redox potential for the electron acceptor, and, $E^{0}(D^{+\cdot}/D)$ is the one-electron redox potential for the electron donor.

A value of -0.1 eV is estimated for the Born correction term. The energy of the first excited singlet state E_{00} for PM605 was calculated from the intersection point of the normalized absorption and emission spectra in acetonitrile (Figure 2-8). E_{00} reports the HOMO-LUMO energy bandgap calculated according to:

$$E_{00} = hc / \lambda \qquad (2\text{-}2)$$

where h is Planck's constant, c is the speed of light, and λ is the wavelength corresponding to the HOMO-LUMO energy bandgap determined. From Equation 2-2 we find a singlet energy E_{00} of 2.22 eV. The one-electron redox potential for α-tocopherol $E^{0}(D\cdot+/D)$ is reported to be +0.5 to +0.6 eV (vs Fc/Fc+).[86]
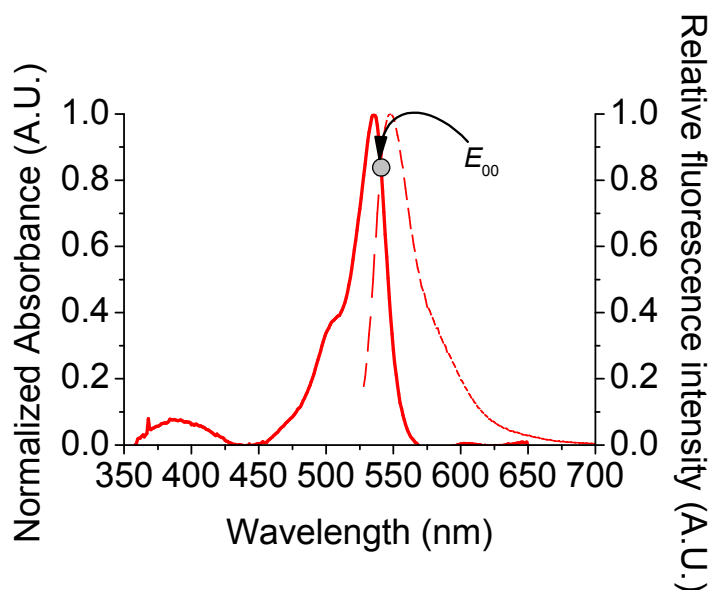
Figure 2-8. Normalized absorption (solid line) and fluorescence (dashed line) spectra of **3** in acetonitrile. The wavelength corresponding to the

HOMO-LUMO energy bandgap occurs at the intersection of the normalized spectra at 541 nm.

Because the one-electron redox potentials of BODIPY are unknown it was necessary to determine them via cyclic voltammetry. Figure 2-9a shows the cyclic voltammogram of PM605 acquired in Ar-saturated 0.1 M Tetrabutylammonium hexafluorophosphate vs a Fc/Fc+ internal standard (see 2 in Figure 2-9a). Based on this data we determine the (irreversible) one-electron reduction potential of PM605 E_0(A/A·-) to be -1.52 eV (vs Fc/Fc+) (see 1 in Figure 2-9a). Additionally, the (reversible) oxidation of PM605 occurs at 0.698 eV (vs Fc/Fc+) (see 3 in Figure 2.9-a). The standard free energy for PET from α-tocopherol to BODIPY was calculated via Equation 2-1 with all of the previous data.

$$\Delta G_{eT}^0 = [(+0.60 eV) - (-1.52 eV)] - 2.22 eV - 0.10 eV = -0.2 eV$$

The value of ΔG^0_{eT} obtained indicates that PET is thermodynamically feasible (note the error in E^0(D·+/D) determination for α-tocopherol, which ranges between 0.5 and 0.6 eV). Consistent with a low driving force for PET (i.e. ΔG^0_{eT} ranges between -0.3 eV and -0.1 eV), the intermolecular quenching rate constant of **3** by Trolox is one order of magnitude smaller than the diffusion controlled value, i.e. k_q = 2.6 x 10^9 M^{-1} s^{-1} < k_d = 2 x 10^{10} in acetonitrile. In conclusion, PET is a plausible mechanism responsible for the intramolecular quenching observed in **1** and the intermolecular quenching of **3** by Trolox.
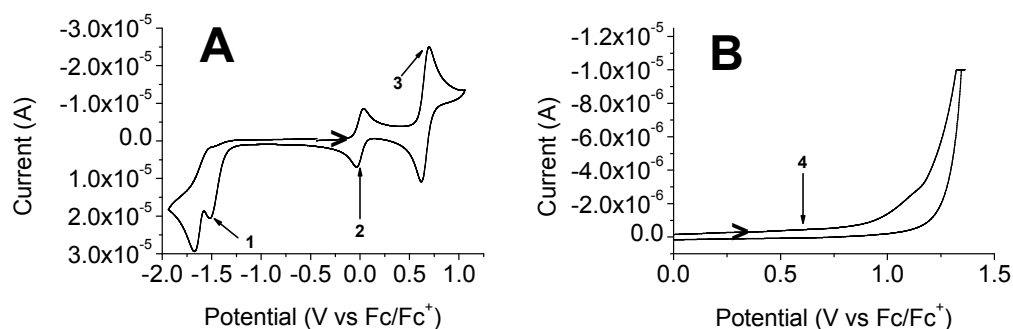
Figure 2-9. Cyclic voltammograms of a) PM605 and b) 3,5-Di-turt-butyl-4-hydroxybenzoic acid in degassed, Ar-saturated acetonitrile (0.1 M Tetrabutylammonium hexafluorophosphate) versus Fc/Fc⁺. Scan rate = 20 mV s⁻¹. The scan direction is indicated by an arrow. 1 indicates the first (irreversible) reduction of PM605. 2 indicates the (reversible) reduction of the internal standard, ferrocene. 3 indicates the (reversible) oxidation of PM605. 4 shows the point at which 3,5-Di-tert-butyl-4-hydroxybenzoic acid should oxidize in order for PET to be thermodynamically favourable in compound **2** (see above discussion).

As discussed above, no intramolecular quenching of the BODIPY reporter exists in **2** as revealed by the high quantum yields and relatively long lifetimes of **2**, as well as the lack of intermolecular quenching of **3** by 3,5-Di-turt-butyl-4-hydroxybenzoic acid (section 2.2.1). It is, therefore, expected that PET should be an endergonic process ($\Delta G^0 > 0$) in this case. For PET to be favourable in **2**, the one electron redox potential of the 3,5-Di-turt-butyl-4-hydroxybenzoic acid must be larger than 0.6 eV according to Equation 2-1.

$$\Delta G^0_{eT} = [(E^0_{D^{+\bullet}/D}) - (-1.52 eV) - 2.22 eV - 0.10 eV \leq 0 eV$$

$$\therefore E^0_{D^{+\bullet}/D} \leq -1.52 eV + 2.22 eV + 0.10 eV = 0.8 eV$$

$$-1.52 eV + 2.22 eV + 0.10 eV \leq E^0_{D^{+\bullet}/D}$$

Figure 2-9b shows the cyclic voltammogram of 3,5-Di-tert-butyl-4-hydroxybenzoic acid acquired in Ar-saturated 0.1 M Tetrabutylammonium

hexafluorophosphate. The one-electron redox potential (vs Fc/Fc+) is not observed below 1.25 eV, at which point solvent oxidation occurs. More importantly, the oxidation of 3,5-Di-tert-butyl-4-hydroxybenzoic acid does not occur below 0.6 eV (see 4 in Figure 2-9b). This indicates that PET is endergonic, and hence not favourable, in molecule **2**.

The receptor moiety of **1** is not electronically conjugated to the reporter moiety, hence electrons must move through space for intramolecular PET to occur, which would be facilitated by π-stacking of the receptor and the reporter moieties. Since the receptor and reporter moieties of **1** both contain aromatic systems, it is possible that π-stacking exists in this molecule forming a sandwich complex. Indeed, a molecular mechanics modelling (MM2) energy minimization clearly demonstrates π-stacking in **1** (Figure 2-10). In this model, the distance between the two aromatic groups is calculated to be 3.79 Angstroms. At this distance the π-orbitals will overlap, allowing for π-π interaction which will facilitate electron transfer. The π-stacking may be disrupted upon incorporation of **1** into lipid vesicles since BODIPY would prefer to be buried within the lipid membrane where as the phenol of the Trolox moiety would prefer the lipid-water interface, leading to the observed partial disruption of the intramolecular quenching of 1 in lipid vesicles (Section 2.2.1.1). Alternatively, at the water-lipid interface, PET might not be strongly exergonic.
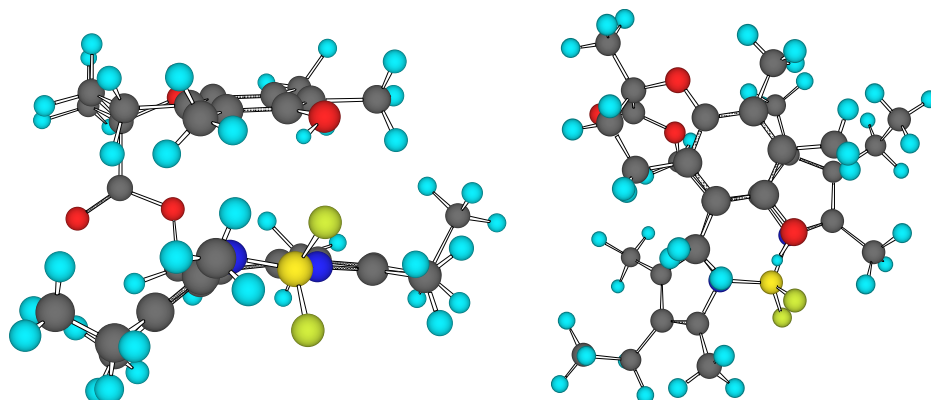
Figure 2-10. MM2 optimized geometry of **1** showing π-stacking between the Trolox receptor moiety and the BODIPY reporter moiety from a side view (left) and top view (right). Atom labels are as follows: Hydrogen (light blue), Carbon (black), Oxygen (red), Nitrogen (dark blue), Fluorine (green), Boron (yellow).

NOESY experiments were performed in an attempt to gain experimental evidence for the through-space proximities predicted by the simulations (see above). In this type of experiment, the nuclei must be within 5 Å for an NOE to be observed. Given their predicted proximity to the H atoms on the Trolox moiety, the methylene (A, 2.37 ppm, q, 6H) and the methyl (B, 1.04 ppm, t, 4H) hydrogens in the ethyl group of the BODIPY reporter moiety in **1** (see Figure 2-11) were irradiated for the 1D NOESY experiments.
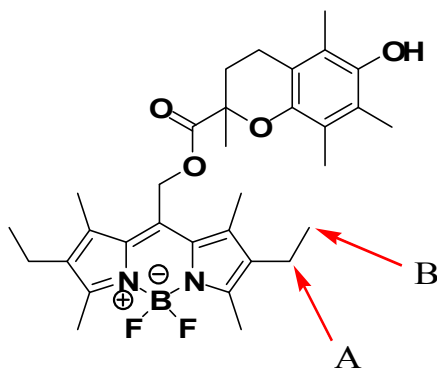
Figure 2-11. Structure of **1**, the red arrows indicate the methylene (A) and methyl (B) groups chosen for irradiation in the 1D NOESY experiments.

The 1D NOESY spectrum obtained upon irradiating the methylene group (Figure 2-12) shows some extent of signal enhancement arising most probably from interactions with hydrogen atoms in the Trolox moiety. However, at present, no conclusive evidence has been obtained regarding the receptor-reporter distance. Future work involving 2D NOESY will tackle this important issue.
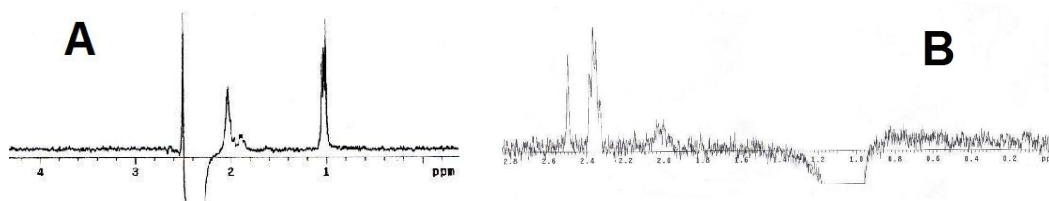
Figure 2-12. 1D NOESY spectra of **1** in CH_3Cl where the methylene groups (A) and, seperatively, the methyl groups (B) of BODIPY are irradiated (see Figure 2-11 and description for details).

2.3 BEHAVIOUR OF FLUORESCENT PROBES UNDER OXIDATIVE STRESS

To be applicable to oxidative systems the behaviour of **1** must be characterized under various free radical exposure conditions. Conditions

should include various generation rates of peroxyl radicals to determine how the probe behaves under strong and weak oxidative stress. Conditions should also involve homogeneous and heterogeneous solution studies and in the presence of competing antioxidants.

2.3.1 Time-resolved Fluorescence Studies of Probes in Homogeneous Solution

The emissive properties of **1**, **2**, and **3** were investigated in the presence of peroxyl radicals generated via thermolysis of 0.8 mM 2,2'-Azobisisobutyronitrile (AIBN) in air saturated toluene. AIBN, like all azo radical initialors, thermally decompose at a constant rate in a temperature-dependent manner to yield two carbon-centred radicals R$^{\cdot}$, which trap molecular oxygen with a reaction rate constant of 10^8 s^{-1} to yield two peroxyl radicals (Scheme 2-3).[30,50]
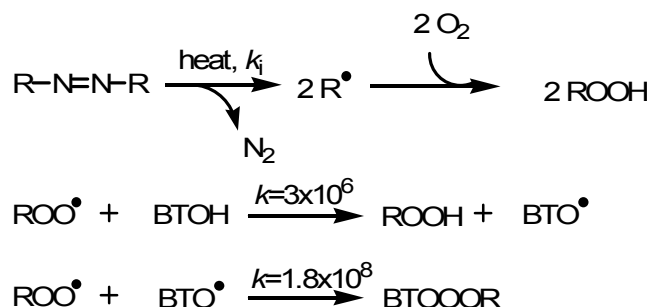
Scheme 2-3. Thermolytic cleavage of azo initiators to form peroxyl radicals and their subsequent reactions with **1**. In the case of AIBN, R = C(CH$_3$)$_2$CN. In the case of ABAP, R = C(CH$_3$)$_2$CNHNH$_2$.

Peroxyl radicals formed can then react with **1** as shown in Scheme 2-3 (see also Schemes 1-2 and 1-3). In Scheme 2-3, the carbon-centred radicals R$^{\cdot}$ will react with 1 with a bimolecular rate constant value similar to the biomolecular rate constant for trapping O$_2$ (k~10^8); however, in aerated solutions the concentration of molecular oxygen [O$_2$] will be

roughly 1 mM, leading to a pseudo-first order rate constant k' of 10^5 M^{-1} in air saturated samples. The concentration of **1** in our experiments will be on the micromolar range, leading to a pseudo-first order rate constant k' of *ca.* 10^2 M^{-1}. Hence, at these concentrations **1** will not compete with molecular oxygen in the first line of Scheme 2-3.

Scheme 2-3 represents the generation of peroxyl radicals. The rate at which peroxyl radicals are generated is calculated by:

$$R_g = 2e[Initiator]k_i \qquad (2\text{-}3)$$

where R_g is the rate of generation of peroxyl radicals, e is the efficiency of escape of the geminal radical pair, [*Initiator*] is the concentration of the radical initiator, and k_i is the rate constant of radical initiation. We have used a value of 0.64 for e as measured at 30°C.[86] A concentration of AIBN ([*Initiator*]) of 0.8 mM was used for all homogeneous experiments. k_i was calculated via the Arrhenius equation:

$$k_i = Ae^{-E_a/RT} \qquad (2\text{-}4)$$

where A is the pre-expontial factor, E_a is the activation energy, R is the gas constant, and T is temperature. For the thermolysis of AIBN, a pre-exponential value A of 2.89×10^{15} s^{-1} and an activation energy E_a of 130.23 kJ mol^{-1} were used (as reported by Akzo Chemie).[87] Equations 2-4 and 2-5 were used to calculate theoretical rates of generation of peroxyl radicals from 0.8 mM AIBN at 0, 37, 65, and 75 °C (Table 2-2).

In toluene under air, a *ca.* 9-fold increase in the fluorescence emission of 3.1 μM **1** in 0.8 mM AIBN was observed at 37, 65, and 75 °C (Figure 2-13). The initial rapid growth period is followed by a slow decay at all temperatures (initial rates of emission growth are listed in Table 2-2). Control experiments at 75 °C in the absence of AIBN reveal no changes in either absorption or emission over time (Figure 2-13). The rate of emission enhancement increases with increasing temperature, which is consistent with a larger generation rate of peroxyl radicals (as predicted with Equations 2-4 and 2-5, Table 2-2) (Figure 2-13). No fluorescence

emission enhancement is observed upon incubation at 0 °C, a temperature at which the peroxyl radical generation rate R_g from a 0.8 mM AIBN solution is negligible (as predicted with Equations 2-3 and 2-4, Table 2-2).
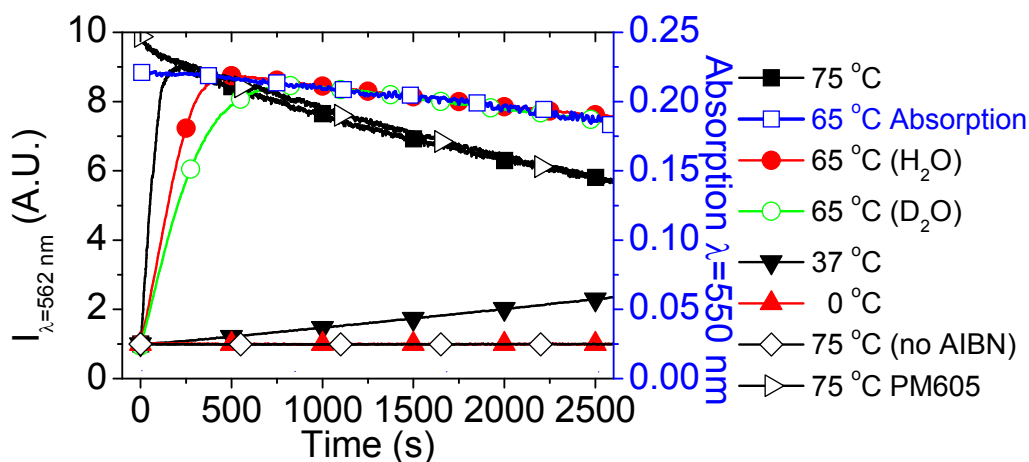
Figure 2-13. Emission intensity time profiles for **1** solutions incubated at 75, 65, 37, and 0 °C with AIBN and at 75 °C without AIBN. Also shown are the absorption time profile for **1** at 65 °C with AIBN and the emission intensity time profile for PM605 at 75 °C with AIBN. A deuterated (1% (*v/v*) D$_2$O) second run of **1** at 65 °C illustrates the KIE. Experiments were done with 3.1 μM dye and 0.8 mM AIBN in toluene under air. Data points were taken every 5 s.

The intramolecular emission quenching outlined in section 2.2 is deactivated and the emission is restored upon reaction of **1** with peroxyl radicals. We thus observe no changes in the absorption intensity during the emission enhancement period (see blue line, open squares (absorption), and compare to the red line, closed circles (emission) in Figure 2-13). These results indicate that there are no changes to the BODIPY fluorophore electronic structure during the emission enhancement period. This is consistent with the receptor acting as an antioxidant.

We further observe that after reaching the maximum fluorescence signal both the fluorescence emission and absorption decay at parallel rates. Once the antioxidant receptor is consumed the peroxyl radicals are free to attack the BODIPY flourophore reporter, resulting in the parallel absorption and emission decay with time. PM605 in the presence of peroxyl radicals decays at a rate similar to the decay of BODIPY in **1** under the same conditions (compare the 75 °C black lines in Figure 2-13). BODIPY has been shown to degrade in the presence of peroxyl radicals.[72]

As discussed above, the receptor moiety acts as an antioxidant, undergoing hydrogen abstraction from the OH group in the phenol moiety upon encounter with peroxyl radicals. To confirm this hypothesis, a kinetic isotope effect (KIE) experiment was performed for **1** at 65 °C. In this method, D_2O was added to a solution of **1** in toluene, thereby causing exchange with the most labile hydrogen atom (the phenolic hydrogen), and the organic toluene layer was isolated. A ca. 2-fold KIE was observed in the rate of emission enhancement (Figure 2-13, Table 2-2), which is consistent with a rate-limiting step involving hydrogen atom abstraction from the phenol of **1**. The KIE value of 4 was measured for α-tocopherol in styrene at 30 °C.[30] Discrepancy in the KIE (once the temperature difference has been accounted for) indicates some differences in the reactivity of **1** when compared to that of α-tocopherol, however the result nonetheless confirms the phenol as the site of attack during the fluorescence enhancement period.

The observed time lag for reaching maximum emission (also known as the induction period) can provide valuable information regarding the oxidative state of the system of interest (see Figure 2-14). We have calculated the rate of generation of peroxyl radicals R_g via the inhibitor method,[30,50,88] following the antioxidant consumption directly via emission enhancement, rather than doing HPLC product studies. As seen in Chapter 1, in homogeneous solution α-tocopherol, and hence **1**, can

scavenge two peroxyl radicals per antioxidant. Therefore, from a known concentration of antioxidant and the time required to reach maximum emission τ, the generation rate of peroxyl radicals R_g can be directly calculated via:

$$R_g = 2[B-TOH]/\tau \qquad (2\text{-}5)$$

Using Equation 2-5, R_g was calculated at 75, 65, and 37 ^{o}C for **1** and deuterated **1** (**B-TOD**) (Table 2-2). These experimental values determined via Equation 2-5 were consistent with theoretical values calculated using Equations 2-3 and 2-4 (see Table 2-2). This confirms that **1** is a reliable antioxidant probe in homogeneous solutions. *Further, our results show that by monitoring the emission increase we can precisely determine the end of the induction period due to the presence of an antioxidant. Thus, 1 is uniquely positioned to report via fluorescence enhancement the consumption of α-tocopherol, and the end of the induction period in a radical chain reaction of lipid peroxidation.*
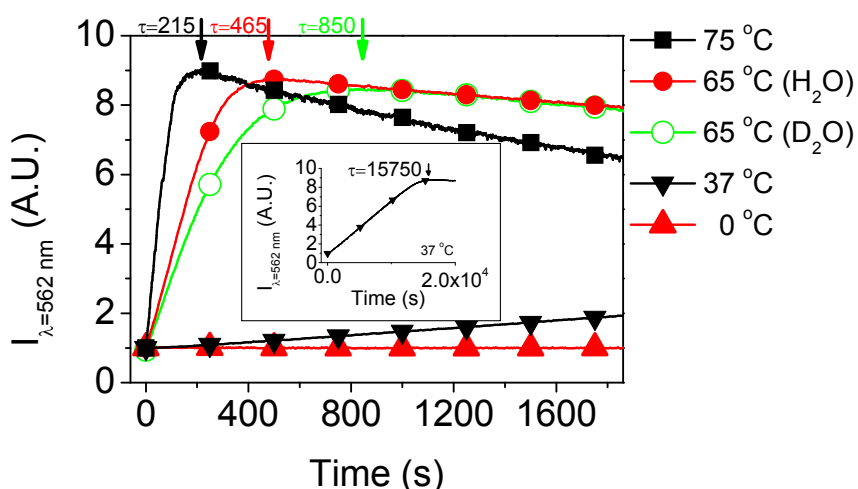
Figure 2-14. Emission intensity time profiles for solutions of **1** incubated at 75 ^{o}C, 37 ^{o}C and 0 ^{o}C with AIBN. Also shown are two runs at 65 ^{o}C to illustrate the KIE. In these runs solutions of **1** in toluene were stirred (60 minutes) in the presence of either 1%v/v D_2O or 1%v/v H_2O. The phases

were then separated and the AIBN was dissolved in the organic phase incubated at 65 °C. All runs were done in 3.1 μM dye and 0.8 mM AIBN in toluene under air. Excitation was performed at 516 to 518 nm, and emission was recorded at 562 nm. Datapoints were taken every 5 seconds. Inset: full range of the emission intensity time profile measured at 37 °C.

Table 2-2. Kinetic parameters of **1** determined from the fluorescence time trajectories.

Sample	τ Highest emission time point	R_g (s^{-1}) Determined via Equation 2-3	R_g (s^{-1}) Determined via Equation 2-4	Initial Rates of emission enhancement (s^{-1})
75 °C, B-TOH	21 x 10^1 s	2.9 x 10^{-8}	8.4 x 10^{-8}	8.22 x 10^{-2}
65 °C, B-TOH	46 x 10^1 s	1.3 x 10^{-8}	2.2 x 10^{-8}	2.70 x 10^{-2}
65 °C, B-TOD	85 x 10^1 s	7.3 x 10^{-9}	N.A.	2.09 x 10^{-2}
37 °C, B-TOH	15.7 x 10^3 s	3.9 x 10^{-10}	3.4 x 10^{-10}	5.04 x 10^{-4}
0 °C, B-TOH	N.A.	N.A.	3.7 x 10^{-13}	0

2.3.2 HPLC Product Studies of B-TOH in Homogeneous Solution Studies

Two separate HPLC product studies were done following incubation of **1** with AIBN in acetonitrile: one involving UV absorption and fluorescence detection (Figure 2-15), and a second involving UV absorption and mass spectrometry (MS) detection (Figures 2-16). In both cases, the retention time of **1** was larger than that of the dominant oxidized **1** product observed. The oxidized **1** in turn had retention times

larger than **3**. PM605 appeared at retention times different to those of **3**, **1** and oxidized **1**. The UV absorption vs. fluorescence analysis and UV-visible absorption vs. MS analysis are described below. Two proposed mechanisms could account for the deactivation of the intramolecular quenching in **1** leading to its marked fluorescence enhancement following reaction with peroxyl radicals. Our MS, UV-visible and fluorescence HPLC results support the formation of chromanones upon reaction of the receptor segment in **1** with peroxyl radicals (see also Scheme 1.3).

2.3.2.1 Fluorescence and UV Absorption HPLC

Acetonitrile solutions containing **1** and AIBN were injected and analyzed via HPLC following extended incubation periods (0, 0.5, 1 and 3 minutes) under air at 70 °C. Acetonitrile solutions of **3** and PM605 were eluted under identical conditions. Retention times were obtained for pure **1** (12.9 minutes), **3** (11.5 minutes), PM605 (13.3 minutes), and the product formed upon radicals scavenging by the receptor segment in **1** (oxidized **1**) (12.4 minutes) (Figure 2-15).

Following incubation of 0.180 mM **1** with 22 mM AIBN at 70 °C under air, a decrease in the **1** absorption peak and the appearance of a newly formed product whose retention time is different from those of **1**, **3**, and PM605 is readily observed (Figure 2-15). Prolongued incubation (3 minutes) leads to a substantial, *ca*. 50%, consumption of **1**, the dominant formation of the species with retention time of 12.42 minutes, as well as the appearance (minor peak) of a new species with a retention time of 11.9 minutes (see Figure 2-15 bottom right). We can not exclude that the retention time 11.9 minute species is a secondary product arising from subsequent reaction of oxidized **1** with free radicals. The following analysis focuses on the dominant product whose retention time is 12.4

min. on a Zorbax SB C8 column (and 16.8 minutes on a Zorbax SB C18 column, see below).

Changes in the corresponding emission chromatograms are more evident than in the absorption chromatograms. The formation of a new emissive species whose chromatogram emission peak is as intense as that of **1** is observed after 0.5 minutes incubation, whereas the absorption of the new species is undetectable in the absorption chromatogram (less than 5% of **1** absorption). Following 1 minute incubation, the newly formed species absorption peak is *ca.* 10 fold less intense than that of **1**, yet its emission is 2 fold larger (Figure 2-15 bottom row, left). Considering that the absorption extinction coefficients for **1** and its oxidized product reveal no significant differences at 228 nm, the wavelength at which the absorption chromatogram was acquired (see Figures 2-15, 2-17, and discussion below), the previous HPLC studies are consistent with the formation of a highly emissive species (10 to 20 fold more emissive than **1**) following radical-mediated oxidation of **1**.
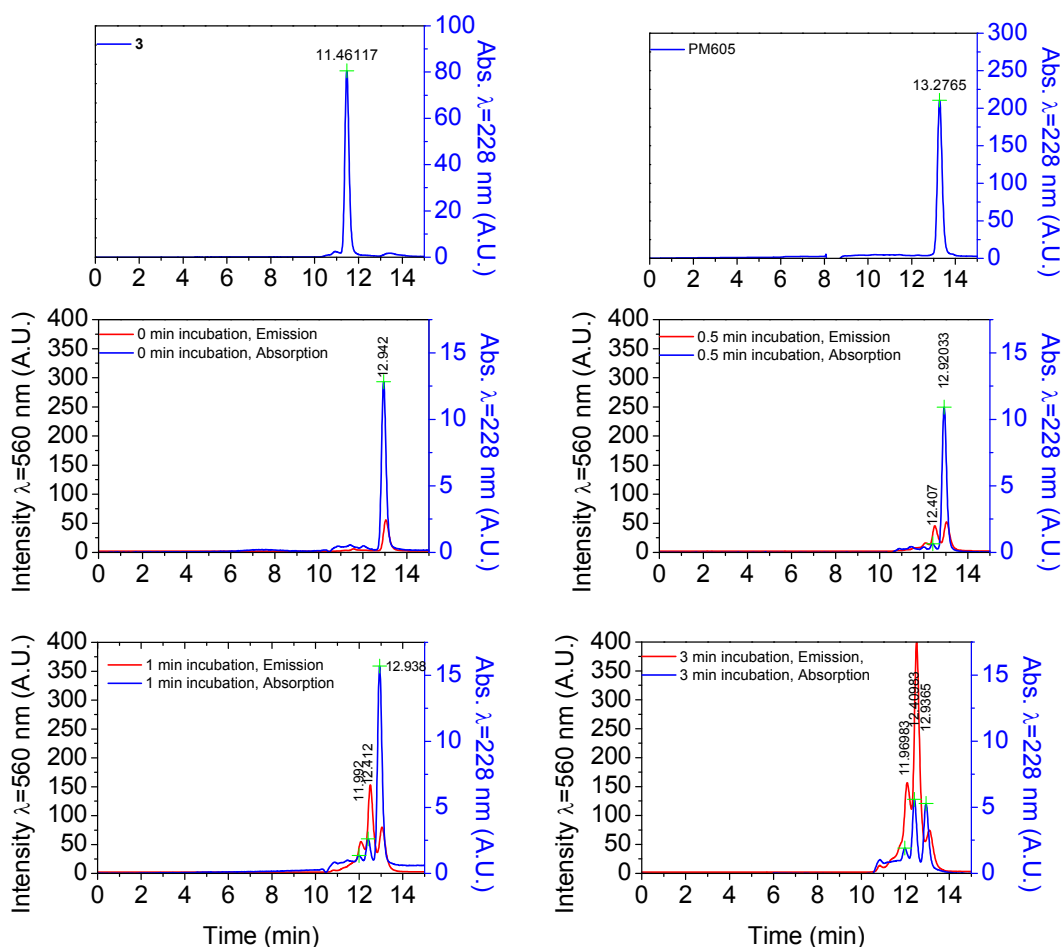
Figure 2-15. Top row: absorption chromatograms of: Left: **3**; Right: PM605. Middle and bottom rows: absorption (blue trace) and fluorescence (red trace) chromatograms of: a 0.180 mM **1** sample following incubation at 70 °C with AIBN 22 mM in air equilibrated acetonitrile: middle row, left: 0 minute incubation period, middle row, right: 0.5 minute incubation period; bottom row, left: 1 minute incubation period and bottom row, right: 3 minutes incubation period. All chromatograms were recorded following the absorption over time at 228 nm, and the emission over time at 560 nm upon excitation at 550 nm.

2.3.2.2 MS and UV-Visible Absorption HPLC Studies

Acetonitrile solutions containing **1** and AIBN were injected and analyzed via HPLC following extended incubation periods under air at 70 °C. Acetonitrile solutions of **3** and PM605 were eluted under identical conditions. Retention times were obtained for pure **1** (17.6 minutes), **3** (13.5 minutes), PM605 (14.6 minutes), and the product formed upon radical scavenging by the reporter segment in **1** (16.8 minutes) (Figure 2-16).
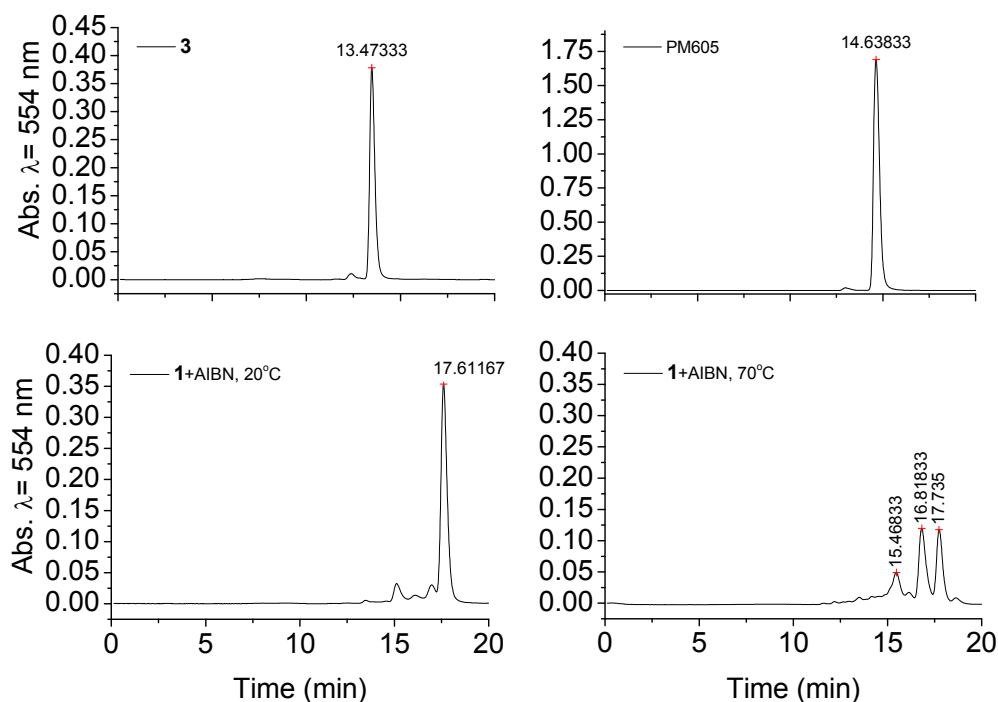
Figure 2-16. Absorption chromatograms of: Top row, left: **3**; top row, right: PM605; bottom row, left: a 0.430mM **1** sample with AIBN 11 mM kept at room temperature; bottom row, right: a 0.430mM **3** sample following 30 minutes incubation at 70 °C with AIBN 11 mM in air equilibrated acetonitrile. All chromatograms were recorded following the absorption over time at 554 nm.

Following incubation of 0.430 mM **1** with 11 mM AIBN at 70 °C under air, a decrease in the **1** absorption peak and the appearance of a newly formed product with a retention time different to that of **1**, **3** and PM605, is readily observed (Figure 2-16). The chromatogram has a significant resemblance to that obtained following 3 minute incubation of 0.180 mM **1** with 22 mM AIBN at 70 °C under air (shown in Figure 2-16 bottom right,).

The absorption spectrum of the newly formed species matches that of **1** in all the visible range. Differences however appear at wavelengths below 325 nm (Figure 2-17). An analysis of the absorption spectra of Trolox, **2**, **1**, and oxidized the **1** product reveals that the **1** absorption band centered at 297 nm and the shoulder at 225 nm (which can be assigned to absorptions from the chromanol chromophore in **1**) disappear following reaction of **1** with peroxyl radicals. In addition, the molar absorption coefficient of the oxidized **1** product reveals a 2 fold increase at 240 nm in comparison to that of **1** or **3**.

The disappearance of the **1** absorption band at ca. 297 nm (corresponding to the 292 nm band in Trolox), and the 2 fold enhancement of the molar absorption coefficient at 240 nm (from 15,000 to 30,000 M^{-1} cm^{-1}) in going from **1** to oxidized **1** are consistent with oxidation of the chromanol to chromanone/s. An analysis based on Woodward's rules for enones indicate that the formed tocopherone/s should have an intense ($\varepsilon \sim 1 \times 10^4$ M^{-1} cm^{-1}) absorption in the 240 nm to 250 nm region, which is similar to the observed molar extinction coefficient enhancement at 240 nm obtained for the oxidized **1** product.
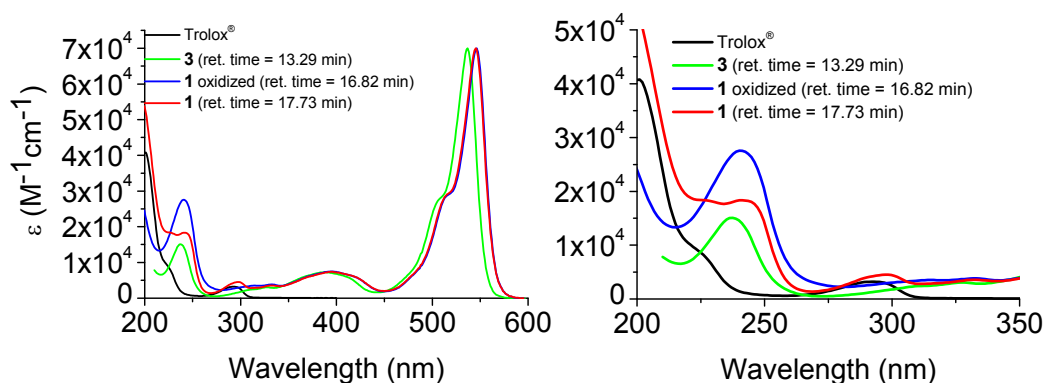
Figure 2-17. Molar absorption coefficients for Trolox, **3**, PM605, **1** and oxidized **1**. In all cases but Trolox, the absorption spectra were extracted at the indicated retention times from the HPLC 3D data (absorbance *vs.* time *vs.* wavelength) and further analyzed with Origin® software. Spectra were normalized to the λ_{max} absorption coefficient value of 70,000 $M^{-1}\,cm^{-1}$, an average of the reported absorption coefficient for PM605 in various solvents.[82] Trolox absorption coefficient was obtained from a Beer-Lambert analysis. Note the absorption peaks of Trolox at 292 nm and the shoulder at *ca.* 225 nm.

The newly formed species has a molecular weight equal to or larger than that of **1**. This is revealed by the presence of a fragment with m/z= 565, i.e. one unit less than the molecular ion peak of **1**, at the elution time corresponding to the major product obtained following **1** oxidation (Figure 2-18). A comparison of the mass spectra for **1** and the oxidized **1** product, extracted from the HPLC 3D data (intensity vs. time vs. m/z) reveal the presence of ion fragments whose m/z value is one unit higher for **1** than for oxidized **1**. Thus we find peaks at m/z 566 (**1** molecular ion peak), 546 (loss of HF) and 318 for **1** and m/z 565, 545 and 317 for oxidized **1**. These results support the hypothesis that the oxidation product results from the addition of a reactive species to **1** (which would lead to a m/z=565 fragment upon ionization), rather than the fragmentation of **1** (which would give rise to a molecular ion peak with m/z << 566). Arguably, the oxidation product arises from the addition of a peroxyl radical to the chromanyl

radical in **1** to yield tocopherones as seen with a-tocopherol (see Scheme 1.3).[31,89,90]
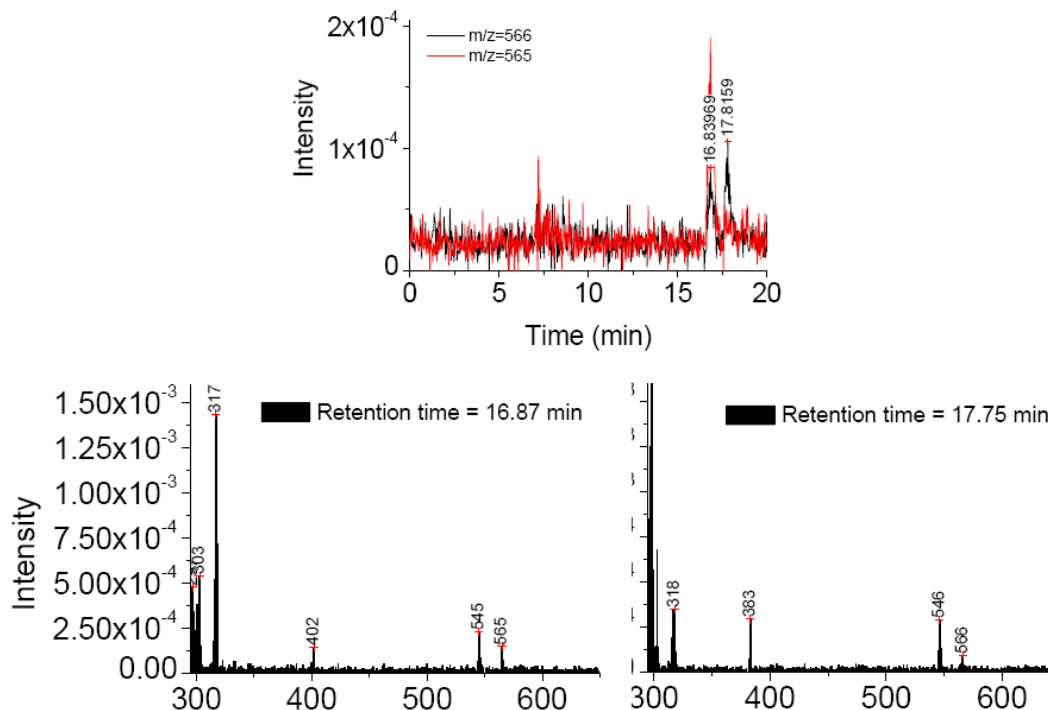
Figure 2-18. Top: HPLC m/z chromatograms of a 0.430mM **1** sample following 30 minutes incubation at 70 °C with AIBN 11 mM in air equilibrated acetonitrile. Red trace: m/z=565. Black trace: m/z=566. Also shown at the bottom are the mass spectra corresponding to: Left) oxidized **1**, retention time 16.87 m. Right) **1**, retention time 17.75 m.

Two proposed mechanisms could account for the deactivation of the intramolecular quenching in **1** leading to its marked fluorescence enhancement following reaction with peroxyl radicals. Our MS, UV-visible and fluorescence HPLC results rule out the radical-mediated dissociation of **3** from **1**, and support the formation of chromanones upon reaction of the receptor segment in **1** with peroxyl radicals (see also Scheme 1.3).

2.3.3 Time-resolved Fluorescence Studies of 1 in the Presence of Antioxidants

Compound **1**, with a reactivity similar to that of α-tocopherol, is a good antioxidant probe at the micro- and nano-molar levels in the presence of other antioxidants. As illustrated in Figure 2-19, the previously observed 9-fold increase in the fluorescence emission of 3.1μM of **1** in 0.8 mM AIBN was observed at 65 °C in aerated toluene in the presence of a variable concentration of the antioxidant Trolox.
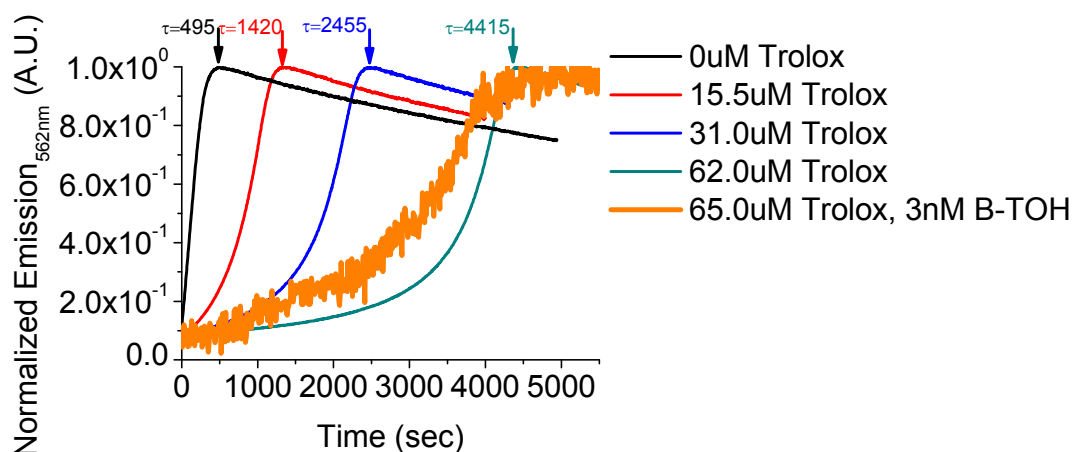
Figure 2-19. Emission intensity time profiles for 3.1 μM (fine lines) and 3.1 nM (bold line) **1** solutions incubated at 65.0 °C with 0.8 mM AIBN in the presence of 15.5 μM, 31.0 μM, 62.0 μM, and 65.0 μM (in the 3.1 nM **1** case, bold line) antioxidant (Trolox). All reactions were done in toluene. Datapoints were taken every 5 s.

The rate of increase of fluorescence is a linear function of the concentration of Trolox. Specifically, the time of complete emission growth directly correlates to the concentration of Trolox (τ = 63.5[Trolox] + 473, see Figure 2-20). It is important to note that the rate of fluorescence increase has two regimes in the presence of a competing antioxidant; a

slow growth followed by rapid growth. As seen before, there is a decay of fluorescence observed after reaching the maximum fluorescence intensity that is due to peroxyl radical attack on the BODIPY flourophore after the receptor phenol has been oxidized.
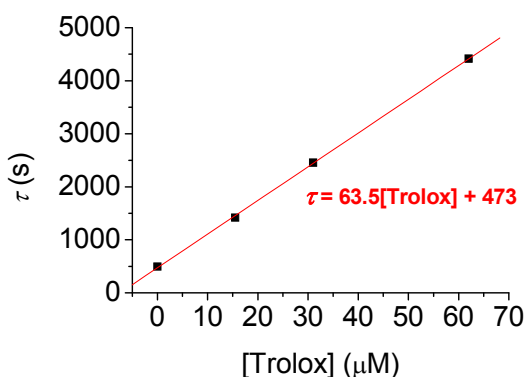
Figure 2-20. A plot of emission growth time (τ) of 3.1 μM **1** with 0.0 μM, 15.5 μM, 31.0 μM, and 62.0 μM Trolox demonstrating the linear relationship between τ and the concentration of Trolox [Trolox].

Additionally, **1** provided an observable fluorescence response to the presence of peroxyl radicals when **1** was at the nano-molar level in the presence of micro-molar concentrations of antioxidant (bold orange line, Figure 2-19). This demonstrates the high sensitivity of this probe in the presence of antioxidants. Further, our results show that by monitoring the emission increase we can precisely determine the end of the induction period due to the presence of an antioxidant. Thus, **1** is uniquely positioned to report via fluorescence enhancement the consumption of α-tocopherol, and the end of the induction period in a radical chain reaction of lipid peroxidation.

2.3.4 Time-resolved Fluorescence Studies of Probes in Microheterogeneous Environment

Oxidative stress affects a variety of biological systems accounting for many pathological effects; hence, real-time probes of oxidative status in these systems are of great benefit to biological research (as discussed in Chapter 1). Being lipophilic, **1** was designed to be applied to lipid membrane oxidation studies. Before **1** can be applied to such studies, however, its behaviour must be fully characterized in these systems as has been performed in homogeneous environments (Section 2.3.1).

2.3.4.1 Thermodynamics of Probe-Lipid Interactions

First, the octanol:water partition coefficient of **1** was determined via absorbance spectroscopy to be quite high at 406.8 +/- 20.6, allowing for the quantification of the hydrophobicity of **1**. The octanol:water partition $K_{P/OW}$ is defined as:

$$K_{P/O:W} = \frac{[B-TOH]_O}{[B-TOH]_W} \qquad (2\text{-}6)$$

where [B-TOH]$_O$ and [B-TOH]$_W$ are the concentrations of **1** in octanol and water, respectively. The octanol:water partition coefficient for **1** is comparable to that of α-tocopherol (549 +/- 9.62).[91] Hence, **1** should partition into lipid membranes in a manner similar to α-tocopherol.

Secondly, a spectroscopic titration technique was used to quantify binding of **1** to the DMPC lipid vesicles. The analytical binding constant K_p was determined as follows:[92]

$$K_p = \frac{[B-TOH]_l}{[B-TOH]_w[DMPC]} \qquad (2\text{-}7)$$

where [B-TOH]$_l$, [B-TOH]$_w$, and [DMPC] are the concentrations of **1** bound to the liposome or free in the bulk aqueous phase, and the phospholipid

concentration, respectively. The constant K_p can be related to the fluorescence emission spectra of **1** by the following relation:

$$F = \frac{F_0 + K_p F_\infty [DMPC]}{1 + K_p [DMPC]} \tag{2-8}$$

Where F_0 and F_∞ are the fluorescence intensities of **1** free in the bulk aqueous phase and totally bound to DMPC lipid vesicles, respectively.

F_∞ is often difficult to determine experimentally, therefore Equation 2-8 can be modified to:

$$\frac{1}{F - F_0} = \frac{1}{F_\infty - F_0} + \frac{1}{F_\infty - F_0} \frac{1}{K_p} \frac{1}{[DMPC]} \tag{2-9}$$

Therefore, K_p is obtained by recording fluorescence intensities of **1** at various concentrations of DMPC and plotting $1/(F\text{-}F_0)$ vs. $1/[DMPC]$. Figure 2-21 shows the fluorescence response of 2.11 μM **1** to the gradual addition of preformed DMPC lipid vesicles, suggesting **1** is binding to the lipid vesicles.
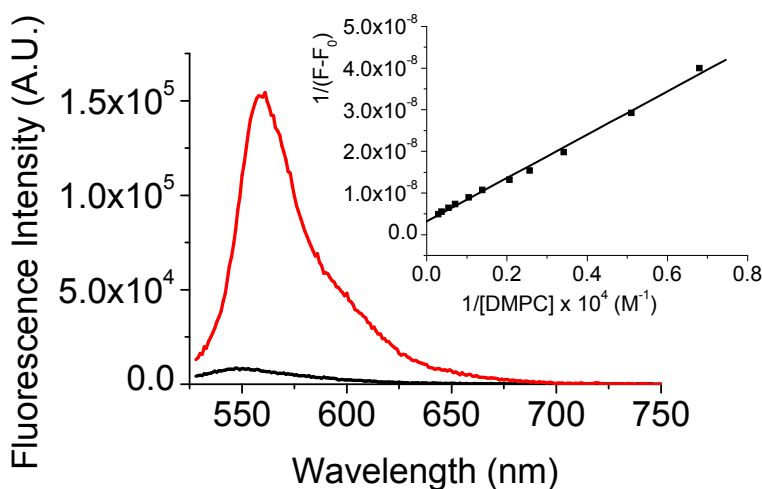
Figure 2-21. Emission spectra (λ_{exc} = 518) of 1 (2.11 μM) at 35 °C in the absence (black line) or presence (red line) of DMPC (3.48 mM) lipid vesicles made in phosphate buffer (pH 7.2). The inset represents $1/(F\text{-}F_0)$ versus $1/[DMPC]$ and the line of best fit corresponding to Equation 2-9.

In order to quantify the binding of **1** to the lipid vesicles, K_p was evaluated by recording the fluorescence emission spectra of the above solution of **1** with lipid concentrations from 0 to 3.48 mM DMPC. Applying Equation 2-9, the fluorescence titration of **1** with DMPC lipid vesicles is shown in the inset of Figure 2-21, from which the analytical binding constant K_p was calculated to be 615 M^{-1} at a pH of 7.2 and a temperature of 35 ^{o}C. From Equation 2-9, it can be calculated that at a DMPC concentration of 11 mM, 87.1% of **1** is associated with lipid vesicles. This DMPC concentration was used in the studies involving **1** embedded in lipid vesicles.

2.3.4.2 Time-resolved Fluorescence Studies of Probes in DMPC Lipid Model Membranes

The emissive properties of **1** and **2** were investigated in the presence of peroxyl radicals generated via thermolysis of 1.0 mM 2,2´-Azobis-(2-methylpropionamidine) dihydrochloride (ABAP) in air saturated DMPC lipid vesicle suspensions in phosphate buffer (pH = 7.2). ABAP is a water-soluble azo radical initiator, hence it thermally decompose at a constant rate in a temperature-dependent manner to yield two carbon-centred radicals R˙, which trap molecular oxygen with a constant reaction rate of 10^8 s^{-1} to yield two peroxyl radicals, similar to AIBN (Scheme 2-3).[30,50]

In DMPC lipid vesicles suspension in phosphate buffer under air, a *ca*. 3-fold increase in the fluorescence emission of 0.54 μM **1** in 1.0 mM ABAP was observed at 37 $^\circ$C (Figure 2-22). As with homogeneous solution studies, the intramolecular emission quenching outlined in section 2.2 is deactivated and the emission is restored upon reaction of **1** with peroxyl radicals. Also as observed in homogeneous solution studies, the initial rapid growth period is followed by a decay of fluorescence due to

attack of the flourophore by peroxyl radicals. **3** in the presence of peroxyl radicals decays at a rate similar to the decay of BODIPY in **1** under the same conditions (see Figure 2-22).
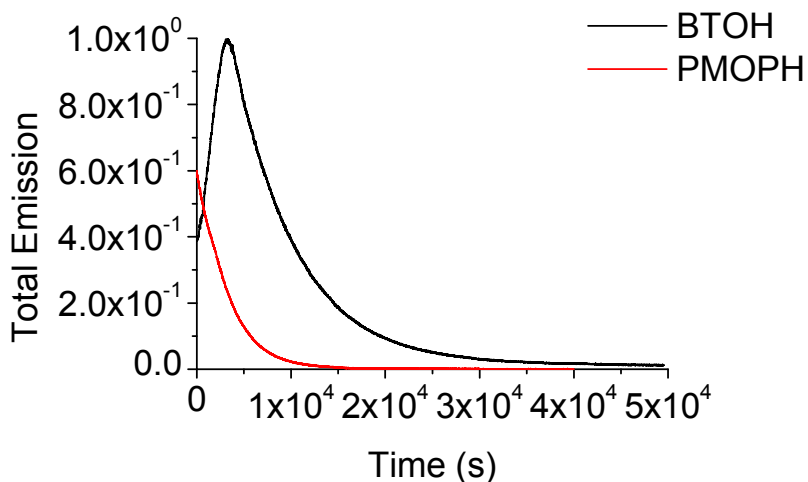
Figure 2-22. Emission intensity time profiles for **1** and **2** embedded in DMPC lipid vesicles suspensions incubated at 37 °C with ABAP. Experiments were done with 0.54 μM dye and 1.0 mM AIBN in pH = 7.2 phosphate buffer under air. Data points were taken every 5 s.

The less dramatic increase in fluorescence of **1** incorporated into lipid vesicles can be attributed to an initial partially deactivated intramolecular quenching of **1**.

3. CONCLUSIONS AND FUTURE WORK

A novel lipophilic fluorogenic radical probe, **B-TOH**, has been designed, synthesized, characterized, and its mode of action investigated. This probe is capable of reporting on the antioxidant status of the system via direct, real-time observation of a 9-fold increase in emission in the presence of peroxyl radicals in homogeneous solution and a 3-fold increase emission in lipid vesicle suspensions.

B-TOH is a two segment, receptor-reporter type fluorescent probe that has the following properties: the BODIPY reporter moiety allows it to partition into hydrophobic media; the reporter moiety is an analogue of α-tocopherol with a similar chemical reactivity towards peroxyl radicals; the BODIPY flourophore absorbs and emits in the visible region of the spectrum. In addition to **B-TOH**,a control receptor-reporter probe **PM-BHB** was also prepared and investigated. Also, the product **PM-OH** was also retained and investigated.

The photophysical properties of the probes, including absorption and emission spectra, quantum yields, and fluorescence lifetimes of the probes were studied. **PM-BHB** and **PM-OH** have quantum yields similar to that of the parent BODIPY flourophore, however, **B-TOH** has a significantly diminished quantum yield in all solvents studied. In addition, **B-TOH** has a shorter fluorescence lifetime than the control fluorophores, indicating a quenching of the reporter flourophore by the receptor moiety. The quenching rate constant of the BODIPY reporter moiety by the Trolox receptor moiety was determined to be 2.6×10^9 M^{-1} s^{-1} by a Stern-Volmer experiment. A larger quantum yield (and subsequent longer fluorescence lifetime) for **B-TOH** is observed when embedded in DMPC lipid vesicles suspended in phosphate buffer when compared to **B-TOH** in homogeneous solution.

The photophysical properties of **B-TOH** can be attributed to a photoinduced electron transfer (PET) mechanism resulting in the observed intramolecular quenching. Indeed, the intramolecular PET process was shown to be thermodynamically feasible via electrochemical experiments. The increase in the quantum yield of **B-TOH** upon incorporation into lipid vesicles is due to a partial deactivation of said PET mechanism, resulting in the smaller emission growth of **B-TOH** observed in lipid vesicles.

HPLC product studies in homogeneous solution were employed to conclude that the behaviour of **B-TOH** is due to oxidation of the phenol, resulting in an oxidized **B-TOH** product and not via the dissociation of the Trolox quencher from the BODIPY reporter moiety. This oxidized product is shown via fluorescence HPLC analysis to have a significantly higher quantum yield than **B-TOH** as it no longer undergoes intramolecular quenching. Oxidation of **B-TOH** most likely involves the conversion of the phenol of Trolox being converted to a ketone, which has been shown to occur for α-tocopherol in homogeneous solution.

As this probe was designed to be useful in studies involving lipid membranes, it is desirable to have a more remarkable increase in emission of the probe while incorporated into lipid membranes. According to the results presented in the current thesis, this could be achieved via a strengthening of the PET process, which may be accomplished by a shorter distance between the receptor and reporter moieties. It is known that the para- oxygen in the Trolox receptor moiety is needed to stabilize the phenoxy radical; additionally, the six-membered ring ensures the right orientation of the nonbonding orbitals in oxygen.[31] Any shortening of the distance will potentially have, as a secondary affect, a change in the antioxidant activity. An alternative is to work with a BODIPY dye that undergoes reduction more readily, thus ensuring the reaction is endergonic.

Additional future work will include incorporation of B-TOH in whole cells and/or intact mitochondria. Proper characterization in this setting will allow for the use of **B-TOH** in fluorescence microscopy and flow cytometry applications of **B-TOH** in cellular oxidative studies.

Finally, modification of **B-TOH** to aid in its localization should be targeted. For instance, attaching a hydrophobic chain to the BODIPY reporter moiety would allow better hydrophobicity leading to a better partitioning into lipid membranes.

4. EXPERIMENTAL SECTION

4.1 Materials

8-Acetoxymethyl-2,6-diethyl -1,3,5,7-tetramethyl pyrromethene fluoroborate (PM605) was purchased from Exciton, Inc (Dayton, OH). (±) 6-Hydroxy-2,5,7,8-tetramethylchromane-2-carboxylic acid (Trolox®) and Dicumyl peroxide were purchased from Acros Organics (Morris Plains, NJ). 2,2′-Azobis-(2-methylpropionamidine) dihydrochloride (ABAP), N-(3-dimethylaminopropyl)-N'-ethylcarbodiimide (EDC) and Dimethylamino pyridine (DMAP) were purchased from Sigma-Aldrich (Oakville, Ontario, Canada). Dimiristoyl-phosphatidyl-choline was obtained from Avanti Polar Lipids, (Alabaster, Al). 2,2′-Azobis(2-methylpropionitrile) (AIBN) was supplied by Eastman Chemicals. THF was distilled over Na/benzophenone, DCM was distilled over CaH_2. All other solvents were HPLC grade, OmniSolv® brand, from EMD Chemicals (Gibbstown, NJ). They were used without further purification unless otherwise specified in the text. Water was purified by a Millipore MilliQ system.

4.2 Synthesis of Fluorescent Probes

4.2.1 Synthesis of 8-Hydroxymethyl-2,6-diethyl -1,3,5,7-tetramethyl pyrromethene fluoroborate (PMOH or 3)

To an air equilibrated solution of PM605 (50 mg, 0.13 mmol, 1 equiv.) in 110 mL of 1:1 (v:v) distilled deionized H_2O/THF was added LiOH (112 mg, 2.68 mmol, 20.2 equiv.) under stirring. The solution was stirred at room temperature in the dark for 2.5 hours. The reaction was quenched with 10.0 mL of saturated aqueous solution of NH_4Cl. The resulting mixture was extracted with CH_2Cl_2 (100 mL x 3) and dried with anhydrous $MgSO_4$. It was then gravity filtrated and concentrated under reduced

pressure to give a desired alcohol as a pink solid (the yield of the crude mixture is 98%). The compound was used in the next step without further purification. ^{1}H-NMR and ^{13}C spectra are consistent with those previously reported.[93]

4.2.2 Synthesis of 8-((±) 6-Hydroxy-2,5,7,8-tetramethylchromane-2-carbonyloxy)methyl-2,6-diethyl -1,3,5,7-tetramethyl pyrromethene fluoroborate (B-TOH or 1)

To 5 mL of anhydrous CH_2Cl_2 under Argon atmosphere and constant stirring were added PMOH (50.3 mg, 0.15 mmol, 1 equiv.), Trolox® (47.6 mg, 0.19 mmol, 1.25 equiv), EDC (66.0 mg, 0.34 mmol, 2.29 equiv) and DMAP (20.0 mg, 0.16 mmol, 1.09 equiv.). The resulting solution was refluxed under Argon in the dark for 3.5 hours. The reaction mixture was then cooled to room temperature and quenched with 10 mL of saturated aqueous solution of NH_4Cl. The phases were separated and the aqueous phase was extracted with CH_2Cl_2 (10 mL x 3). The combined organic fractions were dried with anhydrous $MgSO_4$, followed by concentration under reduced pressure. The ^{1}H-NMR of the crude reaction mixture reveals *ca.* 50% conversion to the product. Purification by flash chromatography on silica gel was performed as follows: The dispersion of the crude product in hexanes was prepared and loaded on the column. It was first flushed with hexanes and then eluted with a 1/1 CH_2Cl_2/hexanes mixture followed by 3/1 CH_2Cl_2/hexanes to afford a coupling product as a dark purple solid in 37% yield. ^{1}H-NMR (300 MHz, CDCl$_3$) δ ppm 5.31 (d, J_{AB}= 12.0 Hz, 1H), 5.18 (d, J_{BA}= 12.3 Hz, 1H), 4.29 (s, 1H), 2.58-2.34 [m, 13 H, including (2,51 (s, 6H), 2.37 (q, J = 7.5 Hz, 4H))], 1.90-2.10 (m, 16H), 1.65 (s, 3H), 1.04 (t, J = 7.5 Hz, 6H). ^{13}C (75 MHz, CDCl$_3$) δ ppm 174.0, 155.0, 145.9, 145.6, 136.7(x 2), 133.6(x 2), 132.3(x 2), 131.2(x 2), 123.2, 121.8, 119.0, 117.0, 98.4, 58.6, 31.2, 26.0(x 2), 21.4, 17.5(x 2), 15.1(x 2), 13.0, 12.6(x 2), 12.5, 12.1, 11.5. HRMS (ESI) calculated for

$C_{32}H_{41}BF_2N_2O_4$ 566.3127, found 566.3238. IR (neat) v cm^{-1} 3516(sharp, m), 2963 (m), 2930(m), 2876(m), 1737(m), 1557(s), 979(s), 739(m). Absorption λ_{max} = 551 nm in toluene; Emission λ_{max} = 562 nm in toluene.

4.2.3 Synthesis of 3,5-Di-turt-butyl-4-hydroxybenzyloxymethyl-2,6-diethyl - 1,3,5,7-tetramethyl pyrromethene fluoroborate (PM-BHB or 2)

To 5 mL of anhydrous CH_2Cl_2 under Argon atmosphere and constant stirring were added PMOH (15.5 mg, 0.0464 mmol, 1 equiv.), 3,5-Di-turt-butyl-4-hydroxybenzoic acid (11.6 mg, 0.0463 mmol, 1 equiv), EDC (8.9 mg, 0.046 mmol, 1 equiv) and DMAP (5.1 mg, 0.042 mmol, 0.9 equiv.). The resulting solution was refluxed under Argon in the dark for 1 hour. The reaction mixture was then cooled to room temperature and quenched with 10 mL of saturated aqueous solution of NH_4Cl. The phases were separated and the aqueous phase was extracted with CH_2Cl_2 (10 mL x 3). The combined organic fractions were dried with anhydrous $MgSO_4$, followed by concentration under reduced pressure. Purification by flash chromatography on silica gel was performed as follows: The dispersion of the crude product in hexanes was prepared and loaded on the column. It was first flushed with hexanes and then eluted with a 1/1 CH_2Cl_2/hexanes mixture, dried under vacuum, redissolved in $CH_3CH_2OCOCH_3$ (ethyl acetate) and washed 10 times with 10% K_2CO_3 (aq) to afford a coupling product as a dark purple solid in 45% yield. ^{1}H-NMR (400 MHz, CDCl$_3$) δ ppm 8.05 (s, 4H), 5.79 (s, 1H), 5.55 (s, 2H), 2.54 (s, 6H), 2.41 (q, J = 7.6 Hz, 4H), 2.33 (s, 6H), 1.50 (s, 18H), 1.35 (s, 18H), 1.06 (t, J = 7.6 Hz, 6H). ^{13}C (75 MHz, CDCl$_3$) δ ppm 166.9, 158.8, 154.9, 137.0, 136.2, 133.7, 132.8, 132.4, 127.5, 120.3, 58.8, 34.7, 30.5, 17.5, 15.1, 13.1, 13.0. HRMS (ESI) calculated for $C_{33}H_{45}BF_2N_2O_3$ 566.3491, found 566.3604. IR (neat) v cm^{-1} 3586(m), 2963(m), 2934(m), 2876(m), 1713(m), 1556(s), 979(s). Absorption λ_{max} = 549 nm in toluene; Emission λ_{max} = 556 nm in toluene.

4.3 Photophysical Properties of Fluorescent Probes

Absorption spectra were recorded using a Cary 300Bio (Varian) UV-Vis spectrophotometer. Fluorescence spectra were recorded using a Fluoromax-2® fluorometer (Horiba Jobin Yvon). For all absorption and emission experiments the solutions were placed in a 1cm x 1cm quartz cuvette purchased from Luzchem Research, Inc (Morin Heights, Quebec, Canada).

Quantum yields were determined by optically matching the absorbance of the molecule in question with the absorbance of a PM605 in ethanol standard (Φ_{FL} = 0.74) at a particular wavelength. Absorbances were less than 0.1 at the excitation wavelength to avoid self absorption. Next, the solutions were excited at the optically matched wavelength and the complete emission spectra were recorded. The fluorescence quantum yield of the molecule in question was determined via Equation 4-1

$$\Phi_{FL} = \frac{0.74I}{I_{PM605}}$$
(4-1)

where Φ_{FL} is the fluorescence quantum yield of the molecule of interest, 0.74 is the fluorescent quantum yield of the PM605 standard in ethanol, I is the integrated emission (where the abscissa axis is in units of energy, not wavelength) of the molecule of interest excited at the optically matched wavelength, and $I_{BODIPY605}$ is the integrated emission of BODIPY 605 (on an energy scale, not of wavelength) excited at the optically matched wavelength.

The fluorescence lifetime measurements were carried out using the third harmonic (355 nm) pulse from a Continuum PY-61 Nd:YAG laser (35 ps ≤ 4 mJ per pulse) as the excitation source. A Hamamatsu C4334 streak camera was used for time resolved fluorescence detection and data acquisition.[94] The instrument response function is *ca.* 80 ps.

4.4 Electrochemistry of PM605

Voltammetric experiments were conducted with a computer controlled BASi EC Epsilon potentiostat with a BASi C3 cell stand. The working electrode was a 2 mm Pt electrode with a Pt wire auxiliary electrode and a 0.01 M Ag/AgNO3 solution reference electrode. A 0.1 M solution of tetrabutylammonium hexafluorophosphate in dry acetonitrile was used as the electrolyte solvent, in to which the species of interest were dissolved for analysis. The solution was purged with argon with simultaneous stirring and left under a blanket of argon. All values are reported versus ferrocene, with the oxidation of ferrocene explicitly measured and corrected to zero for each experiment.

4.5 Behaviour of Fluorescent Probes under Oxidative Stress

4.5.1 Steady State Studies Monitoring Fluorescence

Stead state fluorescence spectroscopy was carried out using a Fluoromax-2® fluorometer (Horiba Jobin Yvon). For all absorption and emission steady state experiments the solutions were placed in a 1cm x 1cm quartz cuvette purchased from Luzchem Research, Inc (Morin Heights, Quebec, Canada). Absorption spectra were recorded using a Cary 300Bio (Varian) UV-Vis spectrophotometer.

Probe concentrations were determined by measuring the absorption at λ_{max} 551 nm and using a molar absorption coefficient of 70,000 $M^{-1}cm^{-1}$, an average of the reported molar absorption coefficient for PM605 in various solvents.[93]

Probe solutions with a concentration of 3.1 μM in organic solvents and a concentration of 0.54 μM in DMPC 100 nm diameter lipid vesicle suspensions (where [DMPC] = 11 mM, [vesicles] = 110 nM) were

incubated at the desired temperatures in the fluorimeter or the spectrometer cell holders. Fluorescence emission/absorbance values were recorded at the spectra maxima every 5 seconds. The temperature was maintained by circulating a liquid mixture pumped through the cell holder from an external circulating temperature bath. The experiment started following the injection of a small volume of concentrated AIBN (for organic solution) or ABAP (for lipid vesicle suspension) solution into the preconditioned probe solution, to yield a final AIBN concentration of 0.8 mM or a final ABAP concentration of 1.0 mM. The decomposition of azo initiators is thoroughly discussed above (see section 2.3.1 and Scheme 2-3).

4.5.2 Preparation of Lipid Vesicle Suspensions Containing Embedded Probes

Small unilamellar liposomes of pure dimyristoylphosphatidylcholine (DMPC from Avanti Polar Lipids) were prepared by the extrusion method.[95] Aqueous solutions of 20 mM lipids were prepared as follows. DMPC powder of the appropriate weight was dissolved in chloroform. For samples containing probes, aliquots of probe solutions in chloroform of known concentration were added for a final probe/DMPC mole ratio of 1/20000. The solvent was evaporated to dryness by rotating the vial to form a thin layer of probe/lipid on the vial wall to ensure immediate incorporation of the probes into the vesicles (except in the case of the binding constant determination, where a small volume of concentrated probe in methanol was injected into preformed vesicles). Films were further dried under vacuum for at least 1 hour to remove excess solvent. Lipid films were then rehydrated to a final concentration of 11 mM lipids with 150 mM NaCl phosphate buffer pH 7.2 and left to equilibriate for 30 minuntes. The resulting multilamellar lipid vesicle suspensions were

extruded 9 times through a polycarbonate membrane filter (100 nm pore diameter, Whatman, USA) using an extruder device (Avanti Polar Lipids).

4.5.3 HPLC Product Studies of B-TOH in Homogeneous Solution Studies

HPLC product studies were done on an Agilent 1100 Series analytical HPLC using a reverse phase Zorbax SB C8 column (4.6x250 mm from Agilent). UV detection was accomplished with an Agilent 1100 Series DAD unit, and fluorescence detection was accomplished with an Agilent 1100 Series FLD unit. The solvent (100% acetonitrile) eluted at a rate of 0.25 mL/min. Following the extended incubation of acetonitrile solutions containing B-TOH and AIBN under air at 70 °C, they were injected and analyzed via HPLC following extended incubation periods (0, 0.5, 1 and 3 minutes). Acetonitrile solutions of 8-Hydroxymethyl-2,6-diethyl -1,3,5,7-tetramethyl pyrromethene fluoroborate (PMOH) and PM605 were eluted under identical conditions.

HPLC product studies were also done on a WATERS analytical HPLC using a reverse phase Zorbax SB C18 column (4.6x250 mm from Agilent). UV-visible detection was accomplished with a WATERS PDA 996 unit, and mass detection was accomplished with a WATERS TMD unit. The solvent (100% acetonitrile) eluted at a rate of 0.25 mL/min. Acetonitrile solutions containing B-TOH and AIBN were injected and analyzed via HPLC following extended incubation periods under air at 70 °C. Acetonitrile solutions of PMOH and PM605 were eluted under identical conditions.

APPENDIX

A.1 Characterization Data for B-TOH or 1
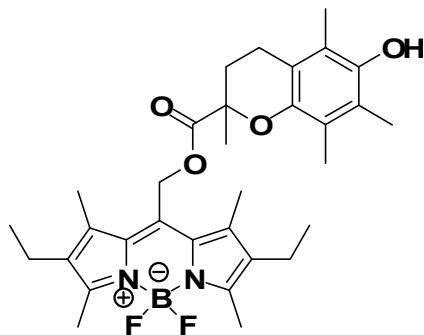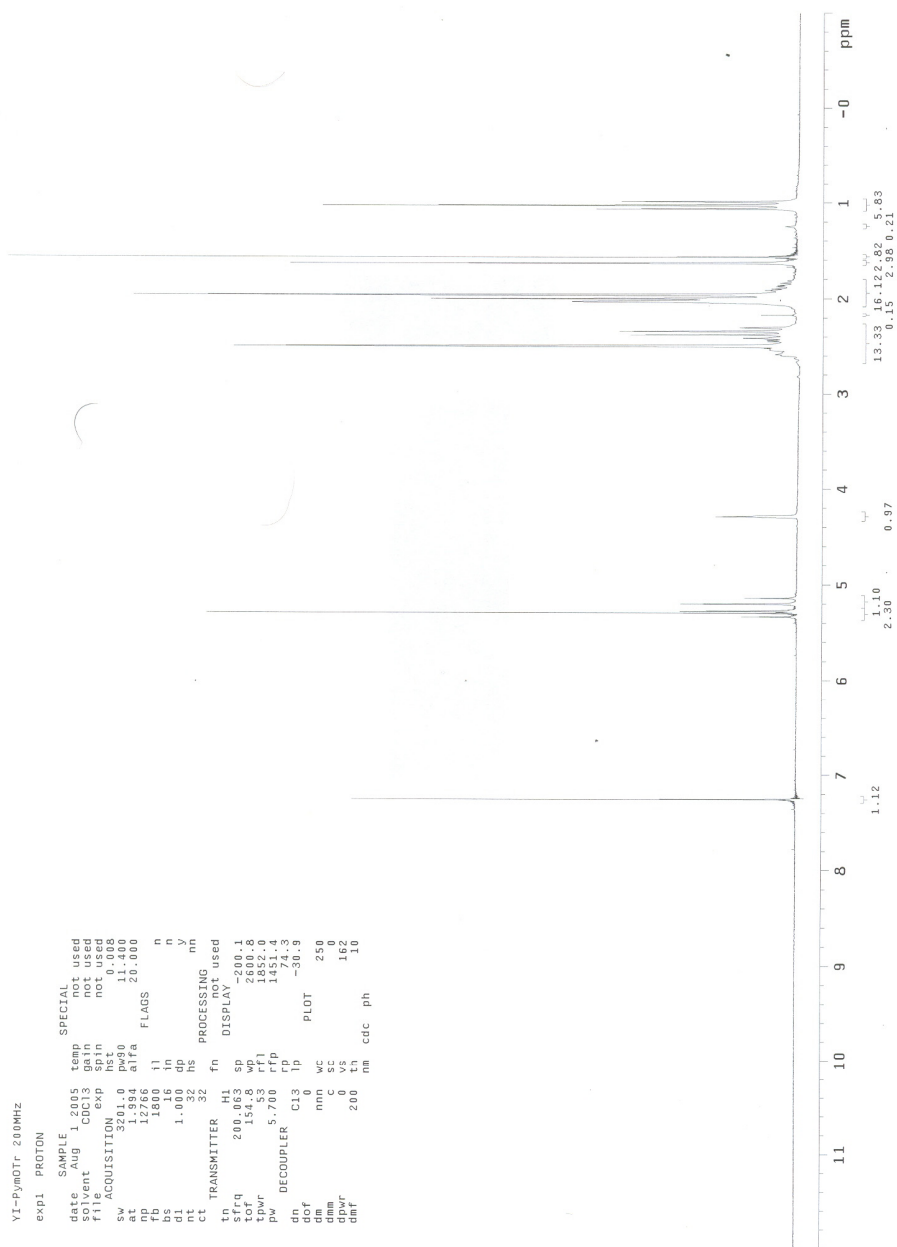
Figure A-1. 200 MHz ^{1}H-NMR spectrum of **B-TOH** or **1** in CHCl$_3$.

YI-PymOTr 13C Spectrum

expl CARBON

SAMPLE   SPECIAL
date   Aug 1 2005   temp   not used
solvent   CDCl3   gain   not used
file   exp   spin   not used
ACQUISITION   nst   0.008
sw   18867.9   pw90   13.800
at   1.815   alfa   20.000
np   68492
fb   64   FLAGS
bs   10400   il   n
d1   3.000   in   y
nt   7788   dp   y
ct   7788   hs   nn

TRANSMITTER   C13   PROCESSING
tn   C13   lb   1.00
sfrq   75.458   fn   not used
tof   742.2   DISPLAY
tpwr   57   sp   -0.1
pw   6.900   wp   15089.7
                     rfl   6967.6
DECOUPLER   H1   rfp   5833.4
dn   0   rp   -157.2
dof   lp   -174.0
dm   yyy
dmm   35   PLOT
dpwr   35   wc   250
dmf   7700   sc   0
                     vs   600
                     th   7
                     nm no ph

Figure A-2. 75 MHz ^{13}C-NMR spectrum of **B-TOH** or **1** in CHCl$_3$.

90

Figure A-3. HRMS (ESI) spectrum of **B-TOH** or **1**.
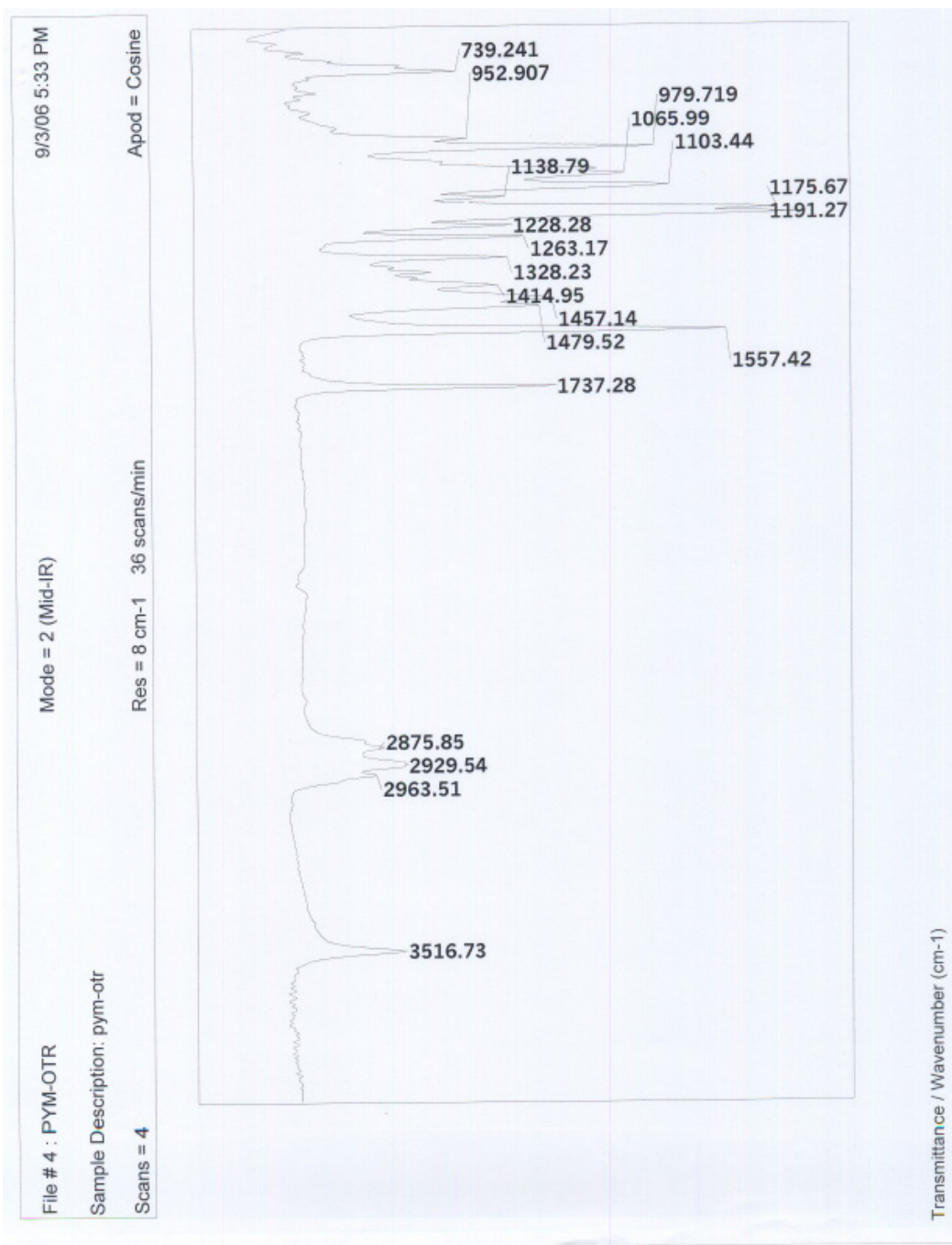
Figure A-4. IR spectrum of **B-TOH** or **1**.

A.2 Characterization Data for PM-BHB or 2
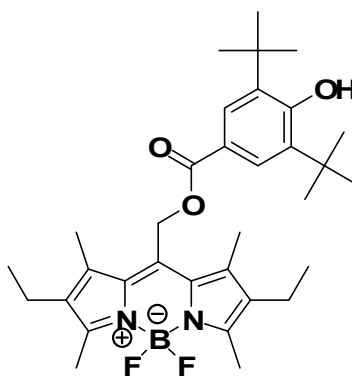
Figure A-5. 400 MHz ^{1}H-NMR spectrum of **PM-BHB** or **2** in CHCl$_3$.

yE-1AA5 Pure PyMDPh

exp1 CARBON

SAMPLE
date   Jul 21 2005
solvent   CDCl3
file   exp

ACQUISITION
sw
at
np
fb
bs
dl
ct

TRANSMITTER C13
tn
sfrq   75.458
tof   742.2
tpwr
pw   6.900

DECOUPLER H1

SPECIAL
temp   not used
gain   not used
spin   not used

FLAGS

PROCESSING

DISPLAY

PLOT

INDEX	FREQUENCY	PPM	HEIGHT
1	12535.776	166.942	8.1
2	11984.839	158.845	8.6
3	11607.433	154.843	6.4
4	10338.593	137.826	6.8
5	10275.253	136.186	18.2
6	10086.387	133.683	6.5
7	10018.441	132.782	4.8
8	9986.196	132.355	6.0
9	9621.706	127.524	26.8
10	9073.245	120.255	9.3
11	5864.020	77.731	158.4
12	5840.400	77.514	6.2
13	5833.150	77.311	162.0
14	5801.193	76.888	160.8
15	4435.079	58.782	9.0
16	2620.119	34.727	27.7
17	2315.514	30.683	3.5
18	2301.695	30.586	84.3
19	2270.025	30.085	6.1
20	1323.965	17.548	15.7
21	1141.721	15.132	19.2
22	988.555	13.102	8.4
23	981.645	13.011	20.1

Figure A-6. 75 MHz ^{13}C-NMR spectrum of **PM-BHB** or **2** in CHCl$_3$.

Figure A-7. HRMS (ESI) spectrum of **PM-BHB** or **2**.

Figure A-8. IR spectrum of **PM-BHB** or **2**.

A.3 Copy of Oleynik, P.; Ishihara, Y.; Cosa, G. J. Am. Chem. Soc.; 2007, 129, 1842 -1843

Design and Synthesis of a BODIPY-α-Tocopherol Adduct for Use as an Off/On Fluorescent Antioxidant Indicator

Paul Oleynik, Yoshihiro Ishihara, and Gonzalo Cosa*

Department of Chemistry, McGill University, 801 Sherbrooke Street West, Montreal, QC, H3A 2K6 Canada

Received September 20, 2006; E-mail: gonzalo.cosa@mcgill.ca

Free radical chain autoxidation of polyunsaturated fatty acyl residues disrupts lipid membrane structure and generates a variety of secondary cytotoxic products which altogether account for various pathological effects such as initiation and development of atherosclerosis,[1,2] neurodegenerative diseases,[3] and cell apoptosis.[4]

The most active lipid antioxidant present in mammalian tissues is α-tocopherol (α-TOH, Scheme 1).[5] The α-TOH consists of a chromanol head, which is located at the water lipid interface, and a long saturated phytyl chain tail, which is buried within the hydrocarbon chains in the lipid bilayers.[5,6] The lipid antioxidant activity of α-TOH arises from its preferential localization within the lipid, its inherently high chemical reactivity toward radicals, and the stability of the phenoxyl radical intermediate (α-TO•) generated.[6,7] In solution, α-TOH traps two chain propagating peroxyl radicals (LOO•), thus effectively terminating two free radical chain autoxidations.[1,6−8] A first peroxyl radical is scavenged, yielding a hydroperoxide and α-TO•; the latter reacts with a second peroxyl radical to give various chromanones such as 8a-(alkyl-dioxy)tocopherone (α-TO(OOL), Scheme 1).[9] An induction period is observed in lipid oxidation studies in the presence of α-TOH, the end of which signals the consumption of α-TOH and the onset of the lipid chain autoxidation.[8,10,11]

Lipid peroxidation studies both in solution and within live cell membranes would dramatically benefit from using a real time off/on fluorescent indicator of the antioxidant status, that is, a probe capable of reporting via emission enhancement the depletion of α-TOH and the onset of the lipid chain autoxidation. Such a probe would allow a noninvasive spatial and temporal monitoring of the system oxidative state. We report herein the synthesis and spectroscopic properties of (to our knowledge) the first off/on hydrophobic fluorescent antioxidant indicator.

Our strategy involves preparing a two segment receptor−reporter type[12] free radical scavenger-fluorophore that fulfills the following solubility, reactivity, and spectroscopic requirements: (i) The antioxidant indicator partitions in hydrophobic media; (ii) the radical scavenging reactivity of the receptor segment compares to that of α-TOH; (iii) the reporter segment absorbs and emits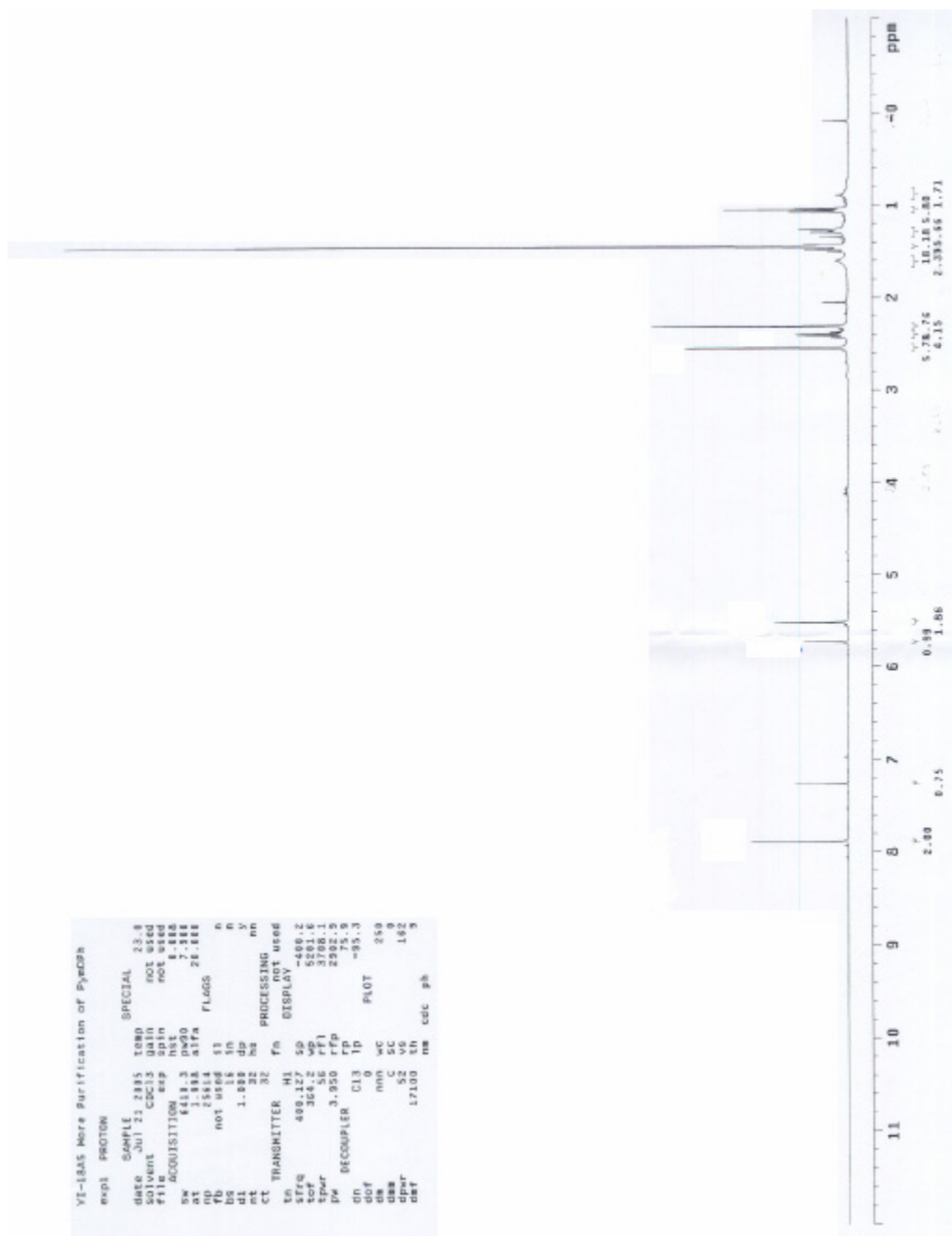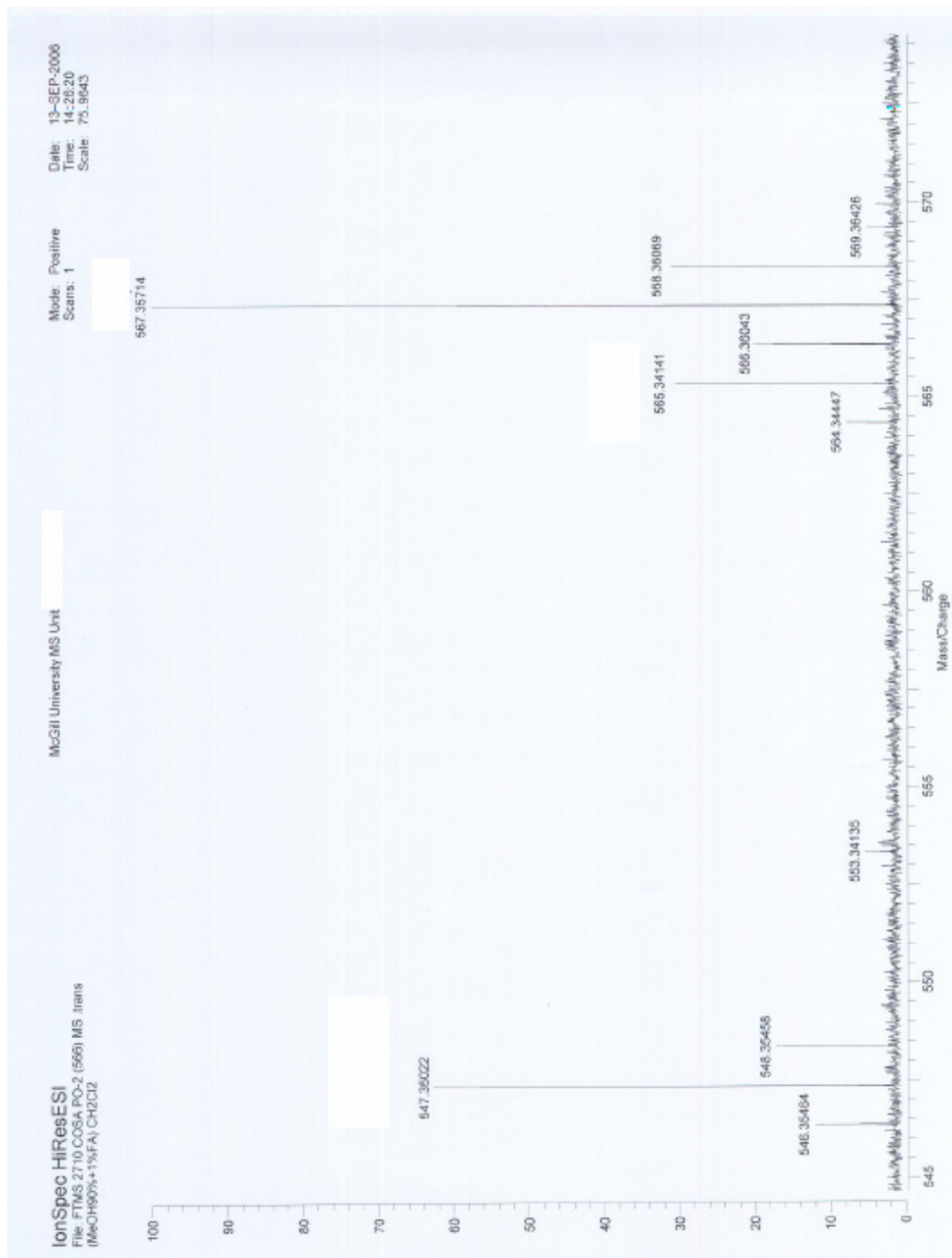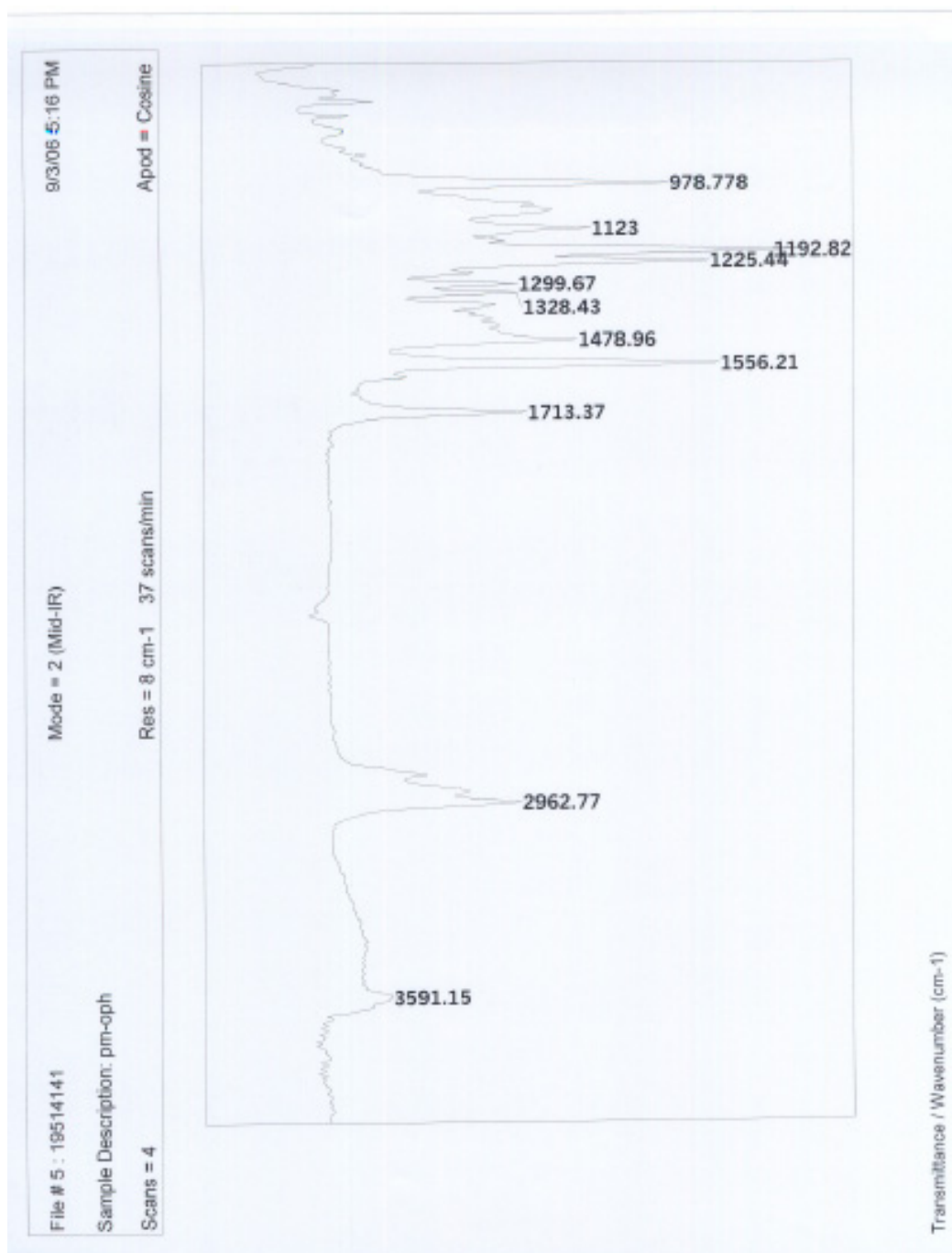 in the visible region of the spectrum; and (iv) the reporter segment undergoes an emission enhancement upon radicals being scavenged by the receptor segment. In order to preserve the free radical scavenging reactivity characteristic of α-TOH, we chose commercially available Trolox,[6,7] a chromanol-based derivative, for the receptor segment. In order to maintain the solubility within hydrophobic media, we coupled to Trolox a dipyrrometheneboron difluoride (BODIPY) fluorescent probe which is known to be retained in phospholipid bilayers.[13] BODIPY dyes fulfill the reporter segment photophysical requirements: they have narrow absorption and emission bands in the visible region of the spectrum, high absorption coefficient and fluorescence quantum yields, and remarkable photostability.

The coupling of the two segments to obtain the fluorescent antioxidant indicator B-TOH was done as shown in Scheme 2.

Scheme 1. Peroxyl Radical Scavenging by α-TOH and α-TO• (refs 7 and 9)
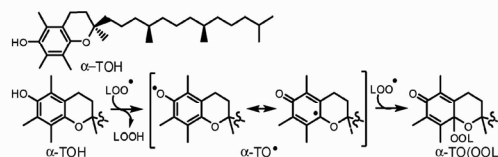
Scheme 2. Synthesis of B-TOH
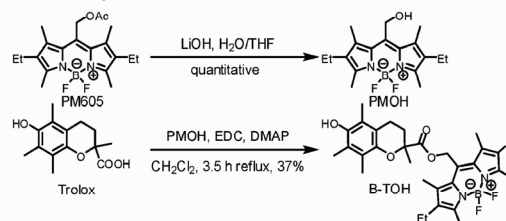
We first studied the spectroscopic properties of B-TOH. There are no significant changes in the absorption and emission spectra of B-TOH compared to those of its precursors PM605 and PMOH (see Scheme 2 for abbreviations). The emission quantum yield of B-TOH is, however, 30-, 15-, and 10-fold smaller than that of PM605 in hexanes (Figure 1), acetonitrile, and toluene, respectively. This dramatic decrease in emission quantum yield arises from an intramolecular emission quenching which we speculate is due to photoinduced electron transfer (PET) from the chromanol moiety to the BODIPY excited singlet state. Consistent with the intramolecular quenching observed, free Trolox efficiently quenches the emission of PMOH in solution. From the ratio of PMOH emission recorded without (I^0) and with (I) increasing Trolox concentration versus [Trolox], we obtain a Stern−Volmer quenching constant K_{SV} of 19.3 M^{-1} in acetonitrile. Given the PMOH fluorescence decay lifetime, $\tau^0 = 7.42$ ns, in acetonitrile and the K_{SV} value (where $K_{SV} = k_q\tau^0$), upon applying eq 1, we calculate a bimolecular quenching constant k_q of 2.6×10^9 M^{-1} s^{-1}.

$$\frac{I^0}{I} = 1 + k_q\tau^0[\text{Trolox}] \qquad (1)$$

We then investigated the emissive properties of B-TOH in the presence of alkoxyl and peroxyl radicals generated at a constant rate either upon 350 nm photolysis of dicumyl peroxide in hexanes under argon or upon thermolysis of 2,2′-azobis(2-methylpropionitrile) (AIBN) in toluene under air, respectively. A ca. 10-fold increase in the emission of 6 μM B-TOH in 0.1 M dicumyl peroxide solutions is observed following irradiation at 350 nm for a 30 s period (Figure 1). No changes are observed in a nonirradiated control sample. A ca. 9-fold increase in the emission is observed upon incubation of 0.8 mM AIBN and 3.1 μM B-TOH in toluene under air at 37, 65, or 75 °C. Control experiments at 75 °C in the

Figure 1. (A) Emission of optically matched hexane solutions of PM605 and B-TOH. (B) Fluorescence enhancement (0−30 s) and decrease (30−120 s) upon 350 nm irradiation of 6 μM B-TOH and 0.1 M dicumyl peroxide hexanes solution under Ar.

Figure 2. Emission intensity time profiles for B-TOH solutions incubated at 75, 37, and 0 °C with AIBN and at 75 °C without AIBN. Also shown are the B-TOH absorption time profile at 65 °C with AIBN and the emission intensity time profile f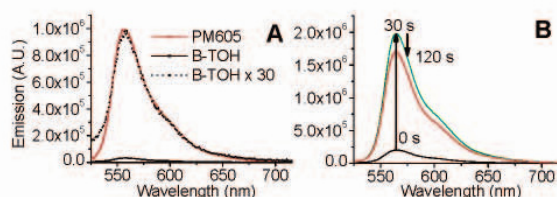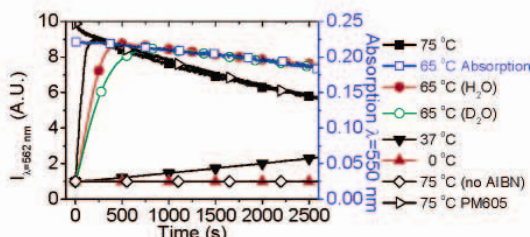or PM605 at 75 °C with AIBN. Two runs at 65 °C illustrate the KIE; in these runs, B-TOH toluene solutions were stirred (1 h) in the presence of either 1% v/v D_2O or 1% v/v H_2O. The phases were then separated, and the AIBN was dissolved in the organic phase incubated at 65 °C. Runs were done with 3.1 μM dye and 0.8 mM AIBN in toluene under air. Data points were taken every 5 s.

absence of AIBN reveal no changes in either absorption or emission over time (Figure 2). The rate of emission enhancement increases with increasing temperature, which is consistent with a larger generation rate of peroxyl radicals (Figure 2 and Supporting Information). No emission enhancement is observed upon incubation at 0 °C, a temperature at which the peroxyl radical generation rate from a 0.8 mM AIBN solution is negligible. A ca. 2-fold kinetic isotope effect (KIE) is observed in the rate of emission enhancement (Figure 2 and Supporting Information), which is consistent with a rate-limiting step involving H-atom abstraction from the chromanol head (first step, Scheme 1).[10] The KIE value measured compares to the 4-fold KIE previously reported for α-TOH in styrene at 30 °C.[10] We further observe no changes in the emission and absorption spectrum or absorption intensity in the visible region during the emission enhancement period; that is, there are no changes to the chromophore chemical structure in this period.

We conclude that the intramolecular emission quenching is deactivated, and the emission is restored upon radicals being scavenged by the receptor segment in B-TOH. Two mechanisms could account for the deactivation of the intramolecular quenching. The first one involves a radical-mediated dissociation of PMOH from B-TOH, effectively separating fluorophore from quencher.[14] An alternative explanation is that radical-mediated oxidation of the chromanol head to various chromanones (which may in turn hydrolyze to quinones)[9] increases the receptor segment redox potential, therefore deactivating the PET quenching mechanism.[12] Under experimental conditions similar to those used in our studies, α-TOH scavenges two peroxyl radicals to yield tocopherones.[9] Tocopherones are also formed in the reaction of α-TOH with alkoxyl radicals.[9] Our HPLC results obtained with UV−vis absorption, emission, and mass spectrometry detectors results support the formation of chromanones upon reaction of B-TOH with peroxyl radicals.

Prolonged exposure to peroxyl and alkoxyl radicals leads to a slow decrease in emission (and parallel decrease in absorption) intensity with time (Figure 2). The intensity decrease is consistent with the onset of radical-mediated BODIPY degradation.[11]

As the antioxidant segment in B-TOH is being consumed, the emission increases, and when the antioxidant is depleted (highest emission point), the BODIPY degradation induction period is over and degradation proceeds at the same rate as that in the absence of antioxidant (compare B-TOH and PM605 emission time profiles at 75 °C in Figure 2).[11] The antioxidant depletion and the onset of radical-mediated oxidation can thus be monitored following emission enhancement over time. Applying the induction period method[10,15] using the highest emission time point, we have calculated the generation rate of peroxyl radicals to be *ca.* 3 × 10^{-8} s^{-1} for 0.8 mM AIBN at 75 °C, which is in close agreement with the expected value (Supporting Information).

Preliminary results reveal a 4-fold increase in emission upon incubating B-TOH intercalated within the lipid bilayer of 100 nm dimyristoyl phosphatidylcholine vesicles in phosphate buffer solution in the presence of water-soluble 2,2′-azobis(2-methylpropion-amidine)dihydrochloride.

In conclusion, we report a novel hydrophobic fluorescent antioxidant indicator with optimum off/on ratio properties. Antioxidant depletion and the onset of radical-mediated oxidation can be monitored following emission enhancement over time.

Supporting Information Available: Emission growth rate analysis, HPLC chromatograms, and synthesis of B-TOH. This material is available free of charge via the Internet at http://pubs.acs.org.

References

(1) Bowry, V. W.; Ingold, K. U. *Acc. Chem. Res.* **1999**, *32*, 27−34.
(2) Steinberg, D. *Lancet* **1995**, *346*, 36−38.
(3) (a) Barnham, K. J.; Masters, C. L.; Bush, A. I. *Nat. Rev. Drug Discovery* **2004**, *3*, 205−214. (b) Montine, T. J.; Neely, M. D.; Quinn, J. F.; Beal, M. F.; Markesbery, W. R.; Roberts, L. J.; Morrow, J. D. *Free Radical Biol. Med.* **2002**, *33*, 620−626.
(4) Kagan, V. E.; Fabisiak, J. P.; Shvedova, A. A.; Tyurina, Y. Y.; Tyurin, V. A.; Schor, N. F.; Kawai, K. *FEBS Lett.* **2000**, *477*, 1−7.
(5) Burton, G. W.; Doba, T.; Gabe, E.; Hughes, L.; Lee, F. L.; Prasad, L.; Ingold, K. U. *J. Am. Chem. Soc.* **1985**, *107*, 7053−7065.
(6) Niki, E.; Noguchi, N. *Acc. Chem. Res.* **2004**, *37*, 45−51.
(7) Burton, G. W.; Ingold, K. U. *Acc. Chem. Res.* **1986**, *19*, 194−201.
(8) Barclay, L. R. C. *Can. J. Chem.* **1993**, *71*, 1−16.
(9) (a) Liebler, D. C.; Baker, P. F.; Kaysen, K. L. *J. Am. Chem. Soc.* **1990**, *112*, 6995−7000. (b) Liebler, D. C.; Burr, J. A.; Matsumoto, S.; Matsuo, M. *Chem. Res. Toxicol.* **1993**, *6*, 351−355.
(10) Burton, G. W.; Ingold, K. U. *J. Am. Chem. Soc.* **1981**, *103*, 6472−6477.
(11) (a) Yoshida, Y.; Shimakawa, S.; Itoh, N.; Niki, E. *Free Radical Res.* **2003**, *37*, 861−872. (b) Naguib, Y. M. A. *Anal. Biochem.* **1998**, *265*, 290−298.
(12) (a) de Silva, A. P.; Gunaratne, H. Q. N.; Gunnlaugsson, T.; Huxley, A. J. M.; McCoy, C. P.; Rademacher, J. T.; Rice, T. E. *Chem. Rev.* **1997**, *97*, 1515−1566. (b) Ueno, T.; Urano, Y.; Kojima, H.; Nagano, T. *J. Am. Chem. Soc.* **2006**, *128*, 10640−10641. (c) Ueno, T.; Urano, Y.; Setsukinai, K.; Takakusa, H.; Kojima, H.; Kikuchi, K.; Ohkubo, K.; Fukuzumi, S.; Nagano, T. *J. Am. Chem. Soc.* **2004**, *126*, 14079−14085. (d) Gabe, Y.; Urano, Y.; Kikuchi, K.; Kojima, H.; Nagano, T. *J. Am. Chem. Soc.* **2004**, *126*, 3357−3367.
(13) Johnson, I. D.; Kang, H. C.; Haugland, R. P. *Anal. Biochem.* **1991**, *198*, 228−237.
(14) Heyne, B.; Maurel, V.; Scaiano, J. C. *Org. Biomol. Chem.* **2006**, *4*, 802−807.
(15) Boozer, C. E.; Hammond, G. S.; Hamilton, C. E.; Sen, J. N. *J. Am. Chem. Soc.* **1955**, *77*, 3233−3237.

JA066789G

Design and synthesis of a BODIPY®-α-tocopherol adduct for use as an off-on fluorescent antioxidant indicator

Paul Oleynik, Yoshihiro Ishihara and Gonzalo Cosa*
Department of Chemistry, McGill University, 801 Sherbrooke St. West, Montreal, QC, H3A 2K6, Canada

*To whom correspondence should be addressed:
Phone: 1 (514) 398-6932   **Fax:** 1 (514) 398-3797   **Email:** gonzalo.cosa@mcgill.ca

This section includes:
- Materials.
- Methods.
  - Steady state experiments.
  - Analysis of emission growth rate.
  - HPLC Chromatograms.
  - UV irradiation conditions.
  - Fluorescence lifetime experiment.
- Synthesis of PMOH and B-TOH and characterization of B-TOH.
- B-TOH ^{1}H-NMR spectrum.
- B-TOH ^{13}C spectrum.

Materials. 8-Acetoxymethyl-2,6-diethyl -1,3,5,7-tetramethyl pyrromethene fluoroborate (PM605) was purchased from Exciton, Inc (Dayton, OH). (±) 6-Hydroxy-2,5,7,8-tetramethylchromane-2-carboxylic acid (Trolox®) and Dicumyl peroxide were purchased from Acros Organics (Morris Plains, NJ). 2,2´-Azobis-(2-methylpropionamidine) dihydrochloride, N-(3-dimethylaminopropyl)-N'-ethylcarbodiimide (EDC) and Dimethylamino pyridine (DMAP) were purchased from Sigma-Aldrich (Oakville, Ontario, Canada). Dimyristoyl-phosphatidyl-choline was obtained from Avanti Polar Lipids, (Alabaster, Al). 2,2´-Azobis-(2-methylpropionitrile) (AIBN) was supplied by Eastman Chemicals. THF was distilled over Na/benzophenone, DCM was distilled over CaH$_2$. All other solvents were HPLC grade, OmniSolv® brand, from EMD Chemicals (Gibbstown, NJ). They were used without further purification unless otherwise specified in the text. Water was purified by a Millipore MilliQ system.

Methods. Steady state fluorescence spectroscopy was carried out using a Fluoromax-2® fluorometer (Horiba Jobin Yvon). Absorption spectra were recorded using a Cary 300Bio (Varian) UV-Vis spectrophotometer. For all steady state absorption and emission experiments the solutions were placed in a 1cm x 1cm quartz cuvette purchased from Luzchem Research, Inc (Morin Heights, Quebec, Canada).

B-TOH concentrations were determined by measuring the absorption at λ_{max} 550 nm and using a molar absorption coefficient of 70,000 $M^{-1}cm^{-1}$, an average of the reported molar absorption coefficient for PM605 in various solvents.[1]

Solutions of B-TOH in organic solvents were incubated at the desired temperatures in the fluorimeter or the spectrometer cell holders. The temperature was maintained by circulating a liquid mixture pumped through the cell holder from an external circulating temperature bath. The experiment started following the injection of a small volume of AIBN solution into the preconditioned B-TOH solution, to yield a final AIBN concentration of 0.8 mM.

It is well established that AIBN decomposes thermally to yield two carbon centered radicals which in solutions under air trap molecular oxygen to yield two peroxyl radicals (see Scheme S1).[2,3] The peroxyl radicals in our experiments were generated at a constant rate via thermolysis of 0.8 mM AIBN in toluene under air (AIBN thermolysis half-life times are 8.5×10^3s, 32×10^3s, 2.1×10^6s and 1.8×10^9s at 75 °C, 65 °C, 37 °C, and 0 °C, respectively. The data was calculated from the preexponential value (2.89×10^{15} s^{-1}) and the activation energy value (130.23 kJ/mol) for the unimolecular thermolysis of AIBN, reported by Akzo Chemie).
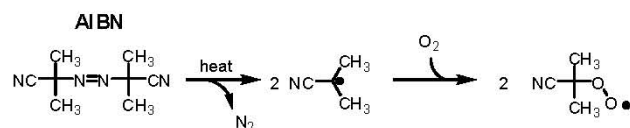
Scheme S1: Thermolysis of AIBN in the presence of Oxygen.

An induction period in the radical-mediated BODIPY® degradation is observed on the absorption curves (see for example the B-TOH absorption time profile at 65 °C with AIBN in Figure 2). The induction period coincides with the emission enhancement period shown in Figure 2. We have calculated the rate of generation of peroxyl radicals R_g by using the inhibitor method[2-4] following the antioxidant consumption directly via emission enhancement rather than doing HPLC product studies. Briefly, in this method a phenolic antioxidant capable of scavenging two peroxyl radicals, such as α-TOH or B-TOH (whereupon we assume B-TOH has similar radical scavenging activity as Trolox® and α-TOH), is added to a solution in a known concentration *[B-TOH]*. The time required to deplete the antioxidant via reaction with peroxyl radicals, *i.e.*, the inhibition or induction period τ, is then determined. Given that 50% of peroxyl radicals are scavenged by B-TOH and the other 50% are scavenged by B-TO•, the generation rate of peroxyl radicals R_g and the consumption rate of antioxidant will be equal.[4] Using Equation S1 the rate of generation of peroxyl radicals can then be directly determined.

Equation S1:
$$R_g = \frac{2[B\text{-}TOH]}{\tau}$$

We have used the fluorescence enhancement period, which reaches a maximum upon antioxidant depletion, to calculate R_g at 75 °C, 65 °C and 37 °C both for B-TOH and B-TOD (see Figure S1 and Table S1 below).

The rate of generation of peroxyl radicals can be further estimated from the known AIBN thermolysis rate constant (also known as initiation rate constant k_i,) the AIBN concentration *[AIBN]* and the efficiency of escape of the geminate radical pair e by applying Equation S2.[4] We have used a value of 0.64 for e (measured at 30 °C[3]), and have calculated k_i from the preexponential value and activation energy for the thermolysis of AIBN reported by Akzo Chemie (vide supra).

Equation S2:
$$R_g = 2e[AIBN]k_i$$

The values calculated according to Equation S2 and using the parameters reported by Akzo Chemie, are consistent with those calculated via Equation S1 and using the experimentally measured fluorescence enhancement period.

We have also determined the initial rates of fluorescence enhancement at each temperature (see Table S1). With these values we have calculated the KIE to be *ca.* 2.
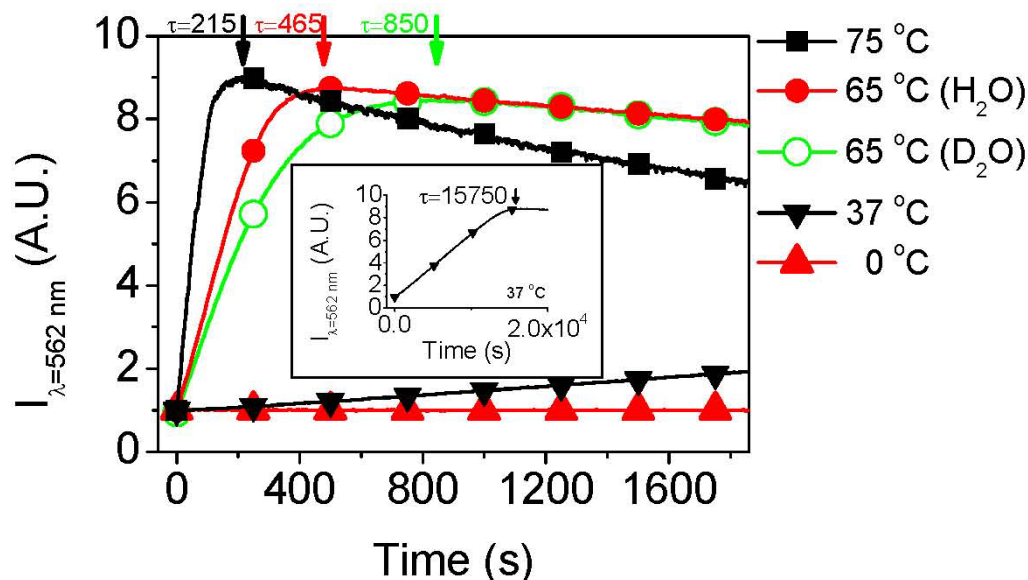
Figure S1: Emission intensity time profiles for B-TOH solutions incubated at 75 °C, 37 °C and 0 °C with AIBN. Also shown are two runs at 65 °C to illustrate the KIE. In these runs B-TOH toluene solutions were stirred (1 h) in the presence of either 1%V/V D_2O or 1%V/V H_2O. The phases were then separated and the AIBN was dissolved in the organic phase incubated at 65 °C. All runs were done in 3.1 μM dye and 0.8 mM AIBN in toluene under air. Excitation was performed at 516 to 518 nm, and emission was recorded at 562 nm. Datapoints were taken every 5 seconds. Inset: full range of the emission intensity time profile measured at 37 °C.

Table S1: Kinetic parameters determined from the fluorescence time trajectories.

Sample	τ highest emission time point	R_g (s^{-1}) Determined via Equation S1	R_g (s^{-1}) Determined via Equation S2	Initial rates of emission enhancement (s^{-1})
75 °C, B-TOH	21×10^1 s	2.9×10^{-8}	8.4×10^{-8}	8.22×10^{-2}
65 °C, B-TOH	46×10^1 s	1.3×10^{-8}	2.2×10^{-8}	2.70×10^{-2}
65 °C, B-TOD	85×10^1 s	7.3×10^{-9}	N.A.	2.09×10^{-2}
37 °C, B-TOH	15.7×10^3 s	3.9×10^{-10}	3.4×10^{-10}	5.04×10^{-4}
0 °C, B-TOH	N.A.	N.A.	3.7×10^{-13}	0

HPLC RESULTS:

HPLC product studies were done on two different instruments provided with UV absorption and emission detectors and a Zorbax SB C8 column, and with UV-visible absorption and MS detectors and a Zorbax SB C18 column, respectively. Absorption chromatograms obtained following incubation of B-TOH with AIBN under air in acetonitrile bared a high resemblance to each other. In both cases the retention time of B-TOH was larger than that of the dominant oxidized B-TOH product observed. The oxidized B-TOH in turn had larger retention times than PMOH in both columns. PM605 appeared at retention times different to those of PMOH, B-TOH and oxidized B-TOH. The UV absorption vs. fluorescence analysis and UV-visible absorption vs. MS analysis are described below. Two proposed mechanisms could account for the deactivation of the intramolecular quenching in B-TOH leading to its marked fluorescence enhancement following reaction with peroxyl radicals. Our MS, UV-visible and fluorescence HPLC results support the formation of chromanones upon reaction of the receptor segment in B-TOH with peroxyl radicals.

1) FLUORESCENCE AND UV ABSORPTION HPLC STUDIES: HPLC product studies were done on an Agilent 1100 Series analytical HPLC using a reverse phase Zorbax SB C8 column (4.6x250 mm from Agilent). UV detection was accomplished with an Agilent 1100 Series DAD unit, and fluorescence detection was accomplished with an Agilent 1100 Series FLD unit. The solvent (100% acetonitrile) eluted at a rate of 0.25 mL/min. Acetonitrile solutions containing B-TOH and AIBN were injected and analyzed via HPLC following extended incubation periods (0, 0.5, 1 and 3 minutes) under air at 70 $^{\circ}$C. Acetonitrile solutions of 8-Hydroxymethyl-2,6-diethyl -1,3,5,7-tetramethyl pyrromethene fluoroborate (PMOH) and PM605 were eluted under identical conditions. Retention times were obtained for pure B-TOH (12.9 minutes), PMOH (11.5 minutes), PM605 (13.3 minutes), and the product formed upon radicals scavenging by the receptor segment in B-TOH (12.4 minutes) (Figure S2, red and blue traces for emission and absorbance, respectively).

Following incubation of 0.180 mM B-TOH with 22 mM AIBN at 70 $^{\circ}$C under air, a decrease in the B-TOH absorption peak and the appearance of a newly formed product whose retention time is different to that of B-TOH, PMOH and PM605, is readily observed (Figure S2). Prolongued incubation (3 minutes) leads to a substantial, *ca.* 50%, consumption of B-TOH, the dominant formation of the species with retention time of 12.42 minutes, as well as the appearance (minor peak) of a new species with a retention time of 11.9 minutes (see Figure S2 bottom right). We can not exclude that the retention time 11.9 min. species is a secondary product arising from subsequent reaction of oxidized B-TOH with free radicals. The following analysis focuses on the dominant product whose retention time is 12.4 min. on a Zorbax SB C8 column (and 16.8 minutes on a Zorbax SB C18 column, see below).

Changes in the corresponding emission chromatograms are more evident than in the absorption chromatograms. The formation of a new emissive species whose chromatogram emission peak is as intense as that of B-TOH is observed after 0.5 minutes incubation, whereas the absorption of the new species is undetectable in the absorption chromatogram (less than 5% of B-TOH absorption). Following 1 minute incubation, the newly formed species absorption peak is *ca.* 10 fold less intense than that of B-TOH, yet its emission is 2 fold larger (Figure S2 bottom row, left). Considering that the absorption extinction coefficients for B-TOH and its oxidized product reveal no significant differences at 228 nm, the wavelength at which the absorption chromatogram was acquired (see Figures S3, S4 and discussion below), the previous

HPLC studies are consistent with the formation of a highly emissive species (10 to 20 fold more emissive than B-TOH) following B-TOH radical-mediated oxidation.
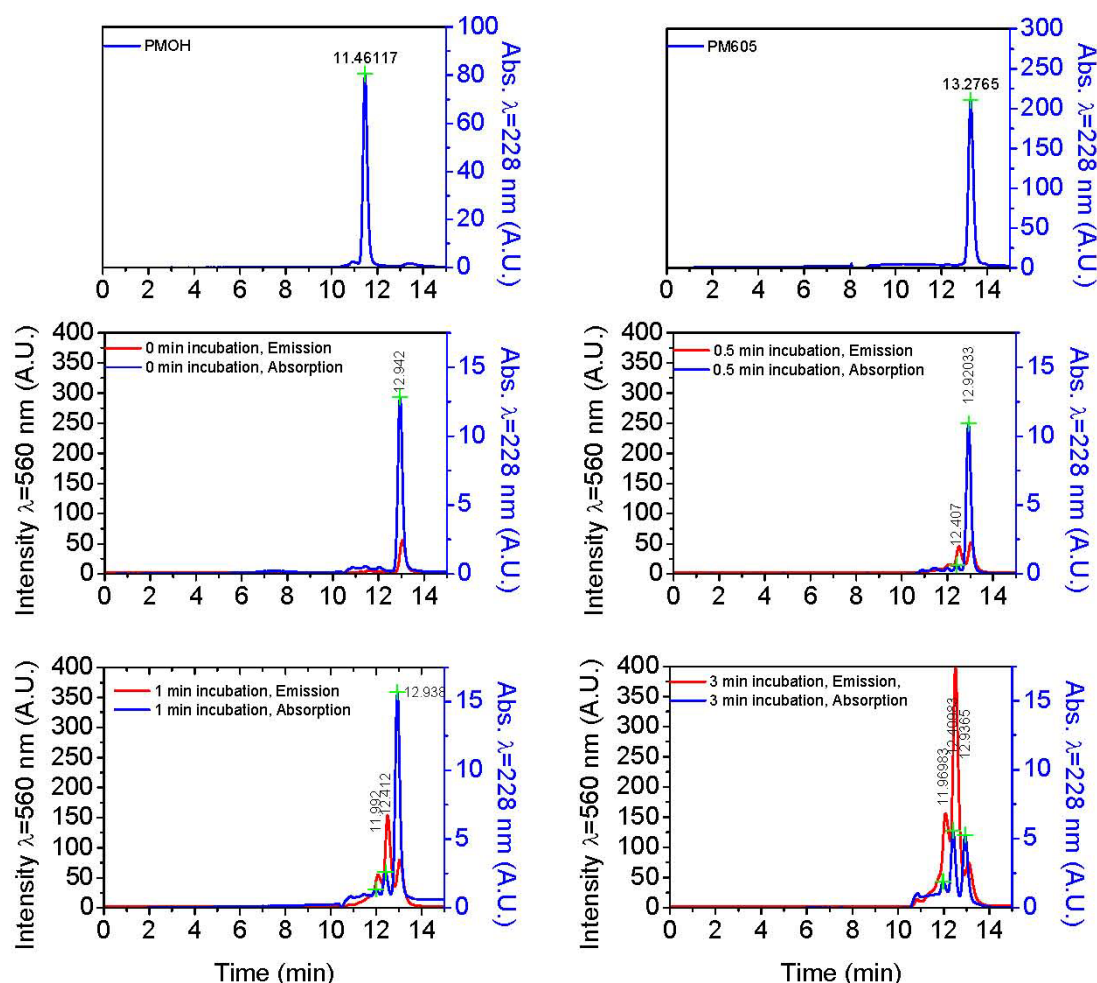
Figure S2: Top row: absorption chromatograms of: Left: PMOH; Right: PM605. Middle and bottom rows: absorption (blue trace) and fluorescence (red trace) chromatograms of: a 0.180 mM B-TOH sample following incubation at 70 °C with AIBN 22 mM in air equilibrated acetonitrile: middle row, left: 0 minute incubation period, middle row, right: 0.5 minute incubation period; bottom row, left: 1 minute incubation period and bottom row, right: 3 minutes incubation period. All chromatograms were recorded following the absorption over time at 228 nm, and the emission over time at 560 nm upon excitation at 550 nm.

2) MS AND UV-VISIBLE ABSORPTION HPLC STUDIES: HPLC product studies were also done on a WATERS analytical HPLC using a reverse phase Zorbax SB C18 column (4.6x250 mm from Agilent). UV-visible detection was accomplished with a WATERS PDA 996 unit, and mass detection was accomplished with a WATERS TMD unit. The solvent (100% acetonitrile) eluted at a rate of 0.25 mL/min. Acetonitrile solutions containing B-TOH and AIBN were injected and analyzed via HPLC following extended incubation periods under air at 70 °C. Acetonitrile solutions of PMOH and PM605 were eluted under identical conditions. Retention times were obtained for pure B-TOH (17.6 minutes), PMOH (13.5 minutes), PM605

(14.6 minutes), and the product formed upon radicals scavenging by the receptor segment in B-TOH (16.8 minutes) (Figure S3).
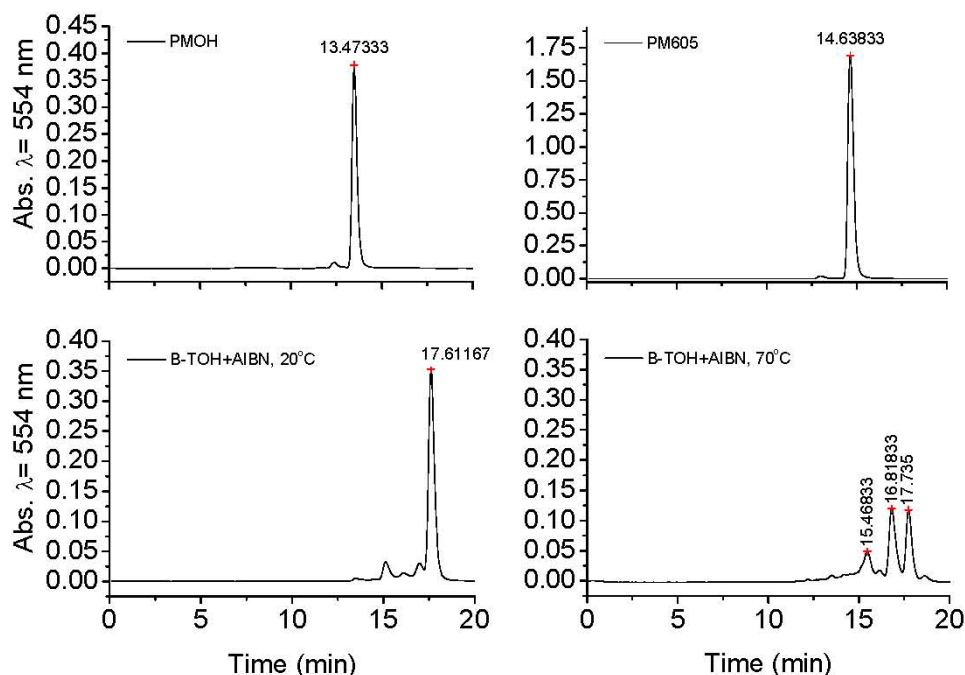
Figure S3: Absorption chromatograms of: Top row, left: PMOH; top row, right: PM605; bottom row, left: a 0.430mM B-TOH sample with AIBN 11 mM kept at room temperature; bottom row, right: a 0.430mM B-TOH sample following 30 minutes incubation at 70 °C with AIBN 11 mM in air equilibrated acetonitrile. All chromatograms were recorded following the absorption over time at 554 nm.

Following incubation of 0.430 mM B-TOH with 11 mM AIBN at 70 °C under air, a decrease in the B-TOH absorption peak and the appearance of a newly formed product with a retention time different to that of B-TOH, PMOH and PM605, is readily observed (Figure S3). The chromatogram has a significant resemblance to that obtained following 3 minute incubation of 0.180 mM B-TOH with 22 mM AIBN at 70 °C under air (shown in Figure S2 bottom right,).

The absorption spectrum of the newly formed species matches that of B-TOH in all the visible range. Differences however appear at wavelengths below 325 nm (Figure S4). An analysis of the absorption spectra of Trolox®, PMOH, B-TOH, and oxidized B-TOH product reveals that the B-TOH absorption band centered at 297 nm and the shoulder at 225 nm (which can be assigned to absorptions from the chromanol chromophore in B-TOH) disappear following reaction of B-TOH with peroxyl radicals. In addition, the molar absorption coefficient of oxidized B-TOH reveals a 2 fold increase at 240 nm in comparison to that of B-TOH or PMOH.

The disappearance of the B-TOH absorption band at ca. 297 nm (corresponding to the 292 nm band in Trolox®), and the 2 fold enhancement of the molar absorption coefficient at 240 nm (from 15,000 to 30,000 $M^{-1}cm^{-1}$) in going from B-TOH to oxidized B-TOH, are consistent with oxidation of the chromanol to chromanone/s. An analysis based on Woodward's rules for enones indicate that the formed tocopherone/s should have an intense ($\varepsilon \sim 1 \times 10^4$ $M^{-1}cm^{-1}$)

absorption in the 240 nm to 250 nm region, a value similar to the observed molar absorption coefficient enhancement at 240 nm, upon oxidation of B-TOH by peroxyl radicals.

Figure S4: Molar absorption coefficients for Trolox[®], PMOH, PM605, B-TOH and oxidized B-TOH. In all cases but Trolox[®], the absorption spectra were extracted at the indicated retention times from the HPLC 3D data (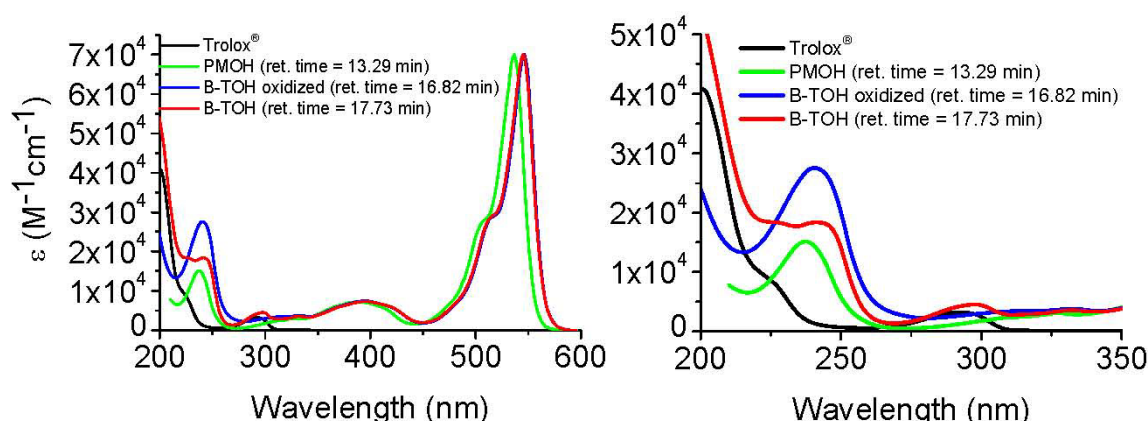absorbance *vs.* time *vs.* wavelength) and further analyzed with Origin software. Spectra were normalized to the λ_{max} absorption coefficient value of 70,000 $M^{-1}cm^{-1}$, an average of the reported absorption coefficient for PM605 in various solvents.[1] Trolox[®] absorption coefficient was obtained from a Beer-Lambert analysis. Note the absorption peaks of Trolox[®] at 292 nm and the shoulder at ca. 225 nm.

The newly formed species has a molecular weight equal to or larger than that of B-TOH. This is revealed by the presence of a fragment with m/z= 565, i.e. one unit less than the molecular ion peak of B-TOH, at the elution time corresponding to the major product obtained following B-TOH oxidation (Figure S5). A comparison of the mass spectra for B-TOH and oxidized B-TOH, extracted from the HPLC 3D data (intensity *vs.* time *vs.* m/z) reveal the presence of ion fragments whose m/z value is one unit higher for B-TOH than for oxidized B-TOH. Thus we find peaks at m/z 566 (B-TOH molecular ion peak), 546 (loss of HF) and 318 for B-TOH and m/z 565, 345 and 317 for oxidized B-TOH. These results support the hypothesis that the oxidation product results from the addition of a reactive species to B-TOH (which would lead to a m/z=565 fragment upon ionization), rather than the fragmentation of B-TOH (which would give rise to a molecular ion peak with m/z $\ll$ 566). Arguably, the oxidation product arises from the addition of a peroxyl radical to the chromanyl radical in B-TOH to yield tocopherones. The full characterization of oxidized B-TOH is however beyond the scope of this work.

Two proposed mechanisms could account for the deactivation of the intramolecular quenching in B-TOH leading to its marked fluorescence enhancement following reaction with peroxyl radicals. Our MS, UV-visible and fluorescence HPLC results rule out the radical-mediated dissociation of PMOH from B-TOH, and support the formation of chromanones upon reaction of the receptor segment in B-TOH with peroxyl radicals.
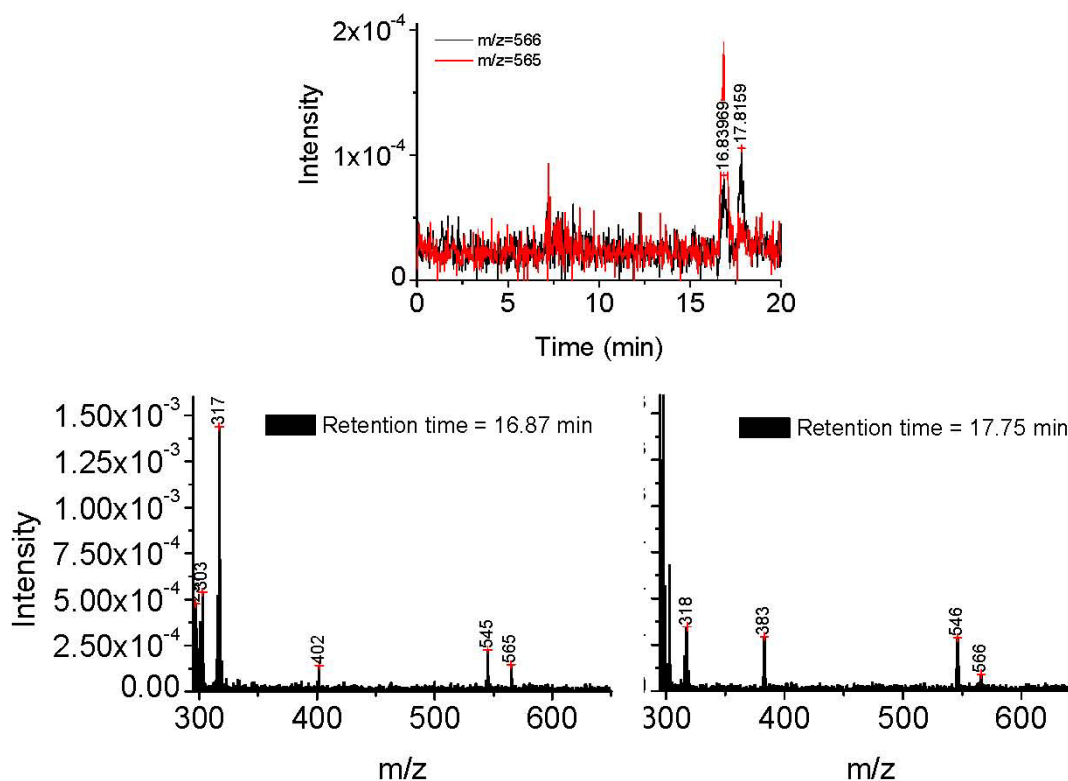
Figure S5: Top: HPLC m/z chromatograms of a 0.430mM B-TOH sample following 30 minutes incubation at 70 °C with AIBN 11 mM in air equilibrated acetonitrile. Red trace: m/z=565. Black trace: m/z=566. Also shown at the bottom are the mass spectra corresponding to: Left) oxidized B-TOH, retention time 16.87 m. Right) B-TOH, retention time 17.75 m.

The alkoxyl radicals were generated at a constant rate upon 350 nm photolysis of 0.1 M dicumyl peroxide solution in hexanes under Argon (Scheme S2). Samples containing cumiloxyl peroxide and the respective controls were irradiated in a Luzchem LZC4 photoreactor (Luzchem Research, Inc) conditioned with filtered mercury lamps with an output wavelength centered at 350 nm (model LZC UVA). Only two lamps, each located on opposite sides of the photoreactor, were simultaneously used. Following extended irradiation periods the emission were monitored in the fluorometer.
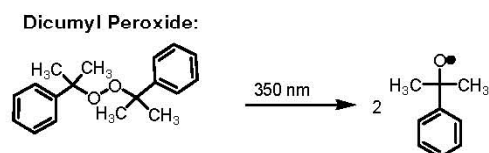
Scheme S2: Photolysis of dicumyl peroxide.

The fluorescence lifetime measurement of PM605 was carried out using the third harmonic (355 nm) pulse from a Continuum PY-61 Nd:YAG laser (35 ps ≤ 4 mJ per pulse) as

the excitation source. A Hamamatsu C4334 streak camera was used for time resolved fluorescence detection and data acquisition.[6] The instrument response function is ca. 80 ps.

Synthesis. **8-Hydroxymethyl-2,6-diethyl -1,3,5,7-tetramethyl pyrromethene fluoroborate (PMOH):**[1,7] To an air equilibrated solution of PM605 (50 mg, 0.13 mmol, 1 equiv.) in 110 mL of 1:1 (v:v) distilled deionized H_2O/ THF was added LiOH (112 mg, 2.68 mmol, 20.2 equiv.) under stirring. The solution was stirred at room temperature in the dark for 2.5 hours. The reaction was quenched with 10.0 mL of saturated aqueous solution of NH_4Cl. The resulting mixture was extracted with CH_2Cl_2 (100 mL x 3) and dried with anhydrous $MgSO_4$. It was then gravity filtrated and concentrated under reduced pressure to give a desired alcohol as a pink solid (the yield of the crude mixture is 98%). The compound was used in the next step without further purification. ^{1}H-NMR and ^{13}C spectra are consistent with those previously reported.[1]

8-((±) 6-Hydroxy-2,5,7,8-tetramethylchromane-2-carbonyloxy)methyl-2,6-diethyl - 1,3,5,7-tetramethyl pyrromethene fluoroborate (B-TOH): To 5 mL of anhydrous CH_2Cl_2 under Argon atmosphere and constant stirring were added PMOH (50.3 mg, 0.15 mmol, 1 equiv.), Trolox® (47.6 mg, 0.19 mmol, 1.25 equiv), EDC (66.0 mg, 0.34 mmol, 2.29 equiv) and DMAP (20.0 mg, 0.16 mmol, 1.09 equiv.). The resulting solution was refluxed under Argon in the dark for 3.5 hours. The reaction mixture was then cooled to room temperature and quenched with 10 mL of saturated aqueous solution of NH_4Cl. The phases were separated and the aqueous phase was extracted with CH_2Cl_2 (10 mL x 3). The combined organic fractions were dried with anhydrous $MgSO_4$, followed by concentration under reduced pressure. The ^{1}H-NMR of the crude reaction mixture reveals *ca.* 50% conversion to the product. Purification by flash chromatography on silica gel was performed as follows: The dispersion of the crude product in hexanes was prepared and loaded on the column. It was first flushed with hexanes and then eluted with a 1/1 CH_2Cl_2/hexanes mixture followed by 3/1 CH_2Cl_2/hexanes to afford a coupling product as a dark purple solid in 37% yield. ^{1}H-NMR (300 MHz, $CDCl_3$) δ ppm 5.31 (d, J_{AB} = 12.0 Hz, 1H), 5.18 (d, J_{BA} = 12.3 Hz, 1H), 4.29 (s, 1H), 2.58-2.34 [m, 13 H, including (2,51 (s, 6H), 2.37 (q, J = 7.5 Hz, 4H))], 1.90-2.10 (m, 16H), 1.65 (s, 3H), 1.04 (t, J = 7.5 Hz, 6H). [13]C (75 MHz, $CDCl_3$) δ ppm 174.0, 155.0, 145.9, 145.6, 136.7(x 2), 133.6(x 2), 132.3(x 2), 131.2(x 2), 123.2, 121.8, 119.0, 117.0, 98.4, 58.6, 31.2, 26.0(x 2), 21.4, 17.5(x 2), 15.1(x 2), 13.0, 12.6(x 2), 12.5, 12.1, 11.5. HRMS (ESI) calculated for $C_{32}H_{41}BF_2N_2O_4$ 566.3127, found 566.3238. IR (neat) ν cm^{-1} 3516(sharp, m), 2963 (m), 2930(m), 2876(m), 1737(m), 1557(s), 979(s), 739(m). Absorption λ_{max} = 551 nm in toluene; Emission λ_{max} = 562 nm in toluene.

References.
1.   Amat-Guerri, F.; Liras, M.; Carrascoso, M. L.; Sastre, R., *Photochem. Photobiol.* **2003,** 77, 577-584.
2.   (a) Boozer, C. E.; Hammond, G. S.; Hamilton, C. E.; Sen, J. N., *J. Am. Chem. Soc.* **1955,** 77, 3233-3237. (b) Niki, E.; Saito, T.; Kawakami, A.; Kamiya, Y., *J. Biol. Chem.* **1984,** 259, 4177-4182.
3.   Burton, G. W.; Ingold, K. U., *J. Am. Chem. Soc.* **1981,** 103, 6472-6477.
4.   Bedard, L.; Young, M. J.; Hall, D.; Paul, T.; Ingold, K. U., *J. Am. Chem. Soc.* **2001,** 123, 12439-12448.
5.   Heyne, B.; Maurel, V.; Scaiano, J. C., *Org. Biomol. Chem.* **2006,** 4, 802-807.
6.   Mohtat, N.; Cozens, F. L.; Scaiano, J. C., *J. Phys. Chem.: B* **1998,** 102, 7557-7562.
7.   Amat-Guerri, F.; Delgado, F., J., Personal Communication.

YI-PymOTr 200MHz

exp1 PROTON

SAMPLE
date   Aug 1 2005
solvent   CDCl3
file   exp

ACQUISITION
sw   3201.0
at   1.994
np   12766
fb   1800
bs   16
d1   1.000
nt   32
ct   32

TRANSMITTER   H1
tn
sfrq   200.063
tof   154.8
tpwr   53
pw   5.700

DECOUPLER   C13
dn
dof   0
dm   nnn
dmm   c
dpwr   0
dmf   200

SPECIAL
temp   not used
gain   not used
spin   not used
hst   0.008
pw90   11.400
alfa   20.000

FLAGS
il   n
in   n
dp   y
hs   nn

PROCESSING
fn   not used

DISPLAY
sp   -200.1
wp   2600.8
rfl   1852.0
rfp   1451.4
rp   74.3
lp   -30.9

PLOT
wc   250
sc   0
vs   162
th   10
nm   cdc   ph

13.33 16.1 22.82   5.83
0.15   2.98 0.2

0.97

1.10
2.30

1.12

ppm   0   1   2   3   4   5   6   7   8   9   10   11

S10

YI-PynOTf 13C Spectrum

expl CARBON

SAMPLE   SPECIAL
date   Aug 1 2005   temp   not used
solvent   CDCl3   gain   not used
file   exp   spin   not used
                      hst   0.008
ACQUISITION   pw90   13.800
sw   18867.9   alfa   20.000
at   1.815
np   68492   FLAGS
fb   19400   il   n
bs   64   in   n
d1   3.000   dp   y
nt   7788   hs   nn
ct   7788
                      PROCESSING   1.00
TRANSMITTER   C13   lb   not used
tn   75.458   fn
sfrq   742.2   DISPLAY
tof   57   sp   -0.1
tpwr   6.900   wp   15089.7
pw   rfl   6967.6
                      rfp   5833.4
DECOUPLER   H1   rp   -157.2
dn   0   lp   -174.0
dof   yyy
dm   35   PLOT
dmm   7700   wc   250
dpwr   sc   0
dmf   vs   600
                      th   7
                      nm no ph

ppm
180 160 140 120 100 80 60 40 20

S11

REFERENCES

(1)   Falkowski, P. G.; Katz, M. E.; Knoll, A. H.; Quigg, A.; Raven, J. A.; Schofield, O.; Taylor, F. J. *Science* **2004**, *305*, 354-60.

(2)   Kasting, J. F.; Siefert, J. L. *Science* **2002**, *296*, 1066-8.

(3)   Nisbet, E. G.; Sleep, N. H. *Nature* **2001**, *409*, 1083-91.

(4)   Lesser, M. P. *Annu Rev Physiol* **2006**, *68*, 253-78.

(5)   Gerschman, R.; Gilbert, D. L.; Nye, S. W.; Dwyer, P.; Fenn, W. O. *Science* **1954**, *119*, 623-6.

(6)   Gerschman, R.; Gilbert, D. L.; Nye, S. W.; Fenn, W. O. *Proc Soc Exp Biol Med* **1954**, *86*, 27-9.

(7)   Gerschman, R.; Nye, S. W.; Gilbert, D. L.; Dwyer, P.; Fenn, W. O. *Proc Soc Exp Biol Med* **1954**, *85*, 75-7.

(8)   Keele, B. B., Jr.; McCord, J. M.; Fridovich, I. *J Biol Chem* **1970**, *245*, 6176-81.

(9)   Keele, B. B., Jr.; McCord, J. M.; Fridovich, I. *J Biol Chem* **1971**, *246*, 2875-80.

(10)   McCord, J. M.; Fridovich, I. *J Biol Chem* **1969**, *244*, 6049-55.

(11)   McCord, J. M.; Keele, B. B., Jr.; Fridovich, I. *Proc Natl Acad Sci U S A* **1971**, *68*, 1024-7.

(12)   Carlioz, A.; Touati, D. *Embo J* **1986**, *5*, 623-30.

(13)   Cadenas, E. *Annu Rev Biochem* **1989**, *58*, 79-110.

(14)   Imlay, J. A. *Annu Rev Microbiol* **2003**, *57*, 395-418.

(15)   Halliwell, B. *Nutr Rev* **1997**, *55*, S44-9; discussion S49-52.

(16)   Stief, T. W. *Med Hypotheses* **2003**, *60*, 567-72.

(17)   Albers, A. E.; Okreglak, V. S.; Chang, C. J. *J. Am. Chem. Soc.* **2006**, *128*, 9640-9641.

(18)   Apel, K.; Hirt, H. *Annu Rev Plant Biol* **2004**, *55*, 373-99.

(19)   Chen, S. X.; Schopfer, P. *Eur J Biochem* **1999**, *260*, 726-35.

(20)   Ashok, B. T.; Ali, R. *Exp Gerontol* **1999**, *34*, 293-303.

(21) Lee, J.; Koo, N.; Min, D. B. *Comprehensive Reviews in Food Science and Food Safety* **2003**, *3*, 21-33.

(22) Thomas, M. J. *Crit Rev Food Sci Nutr* **1995**, *35*, 21-39.

(23) Wickens, A. P. *Respir Physiol* **2001**, *128*, 379-91.

(24) Spiteller, G. *Exp Gerontol* **2001**, *36*, 1425-57.

(25) Cohen, J. H.; Kristal, A. R.; Stanford, J. L. *J Natl Cancer Inst* **2000**, *92*, 61-8.

(26) Niki, E. *Free Radic Res* **2000**, *33*, 693-704.

(27) Criegee, R.; Pilz, H.; Flygare, H. *Ber.* **1939**, *72*, 1799-1804.

(28) Farmer, E. H.; Koch, H. P.; Sutton, D. A. *J. Chem. Soc.* **1943**, 541-547.

(29) Burton, G. W.; Doba, T.; Gabe, E.; Hughes, L.; Lee, F. L.; Prasad, L.; Ingold, K. U. *J. Am. Chem. Soc.* **1985**, *107*, 7053-7065.

(30) Burton, G. W.; Ingold, K. U. *J. Am. Chem. Soc.* **1981**, *103*, 6472-6477.

(31) Burton, G. W.; Ingold, K. U. *Acc. Chem. Res.* **1986**, *19*, 194-201.

(32) Ingold, K. U. *Chem. Rev.* **1961**, *61*, 563-589.

(33) Ingold, K. U. *Acc. Chem. Res.* **1969**, *2*, 1-9.

(34) Ingold, K. U. *Spec. Publ.-Chem.Soc.* **1971**, *24*, 285-293.

(35) Porter, N. A.; Weber, B. A.; Weenen, H.; Khan, J. A. *J. Am. Chem. Soc.* **1980**, *102*, 5597-5601.

(36) Barclay, L. R. C. *Can. J. Chem.* **1993**, *71*, 1-16.

(37) Niki, E.; Noguchi, N. *Acc Chem Res* **2004**, *37*, 45-51.

(38) Girotti, A. W. *J Lipid Res* **1998**, *39*, 1529-42.

(39) Maillard, B.; Ingold, K. U.; Scaiano, J. C. *J. Am. Chem. Soc.* **1983**, *105*, 5095-5099.

(40) Bowry, V. W.; Ingold, K. U. *Acc. Chem. Res.* **1999**, *32*, 27-34.

(41) Burton, G. W.; Ingold, K. U. *Accounts of Chemical Research* **1986**, *19*, 194-201.

(42)   Bowry, V. W.; Ingold, K. U. *Accounts of Chemical Research* **1999**, *32*, 27-34.

(43)   Barclay, L. R. C. *Canadian Journal of Chemistry* **1993**, *71*, 1-16.

(44)   Niki, E.; Noguchi, N. *Accounts of Chemical Research* **2004**, *37*, 45-51.

(45)   Liebler, D. C.; Baker, P. F.; Kaysen, K. L. *Journal of the American Chemical Society* **1990**, *112*, 6995-7000.

(46)   Liebler, D. C.; Burr, J. A.; Matsumoto, S.; Matsuo, M. *Chemical Research in Toxicology* **1993**, *6*, 351-355.

(47)   Burton, G. W.; Ingold, K. U. *Journal of the American Chemical Society* **1981**, *103*, 6472-6477.

(48)   Yoshida, Y.; Shimakawa, S.; Itoh, N.; Niki, E. *Free Radical Research* **2003**, *37*, 861-872.

(49)   Naguib, Y. M. A. *Analytical Biochemistry* **1998**, *265*, 290-298.

(50)   Boozer, C. E.; Hammond, G. S.; Hamilton, C. E.; Sen, J. N. *J. Am. Chem. Soc.* **1955**, *77*, 3233-3237.

(51)   Soh, N. *Anal. Bioanal. Chem.* **2006**, *386*, 532-543.

(52)   Lakowicz, J., R *Principles of Fluorescence Spectroscopy, Third Edition*; 3 ed.; Springer: New York, 2006.

(53)   Jablonski, A. *Z. Phys.* **1935**, *94*, 38-46.

(54)   Goodwin, P. M.; Ambrose, W. P.; Keller, R. A. *Acc. Chem. Res.* **1996**, *29*, 607-613.

(55)   Lewis, A.; Lieberman, K. *Anal. Chem.* **1991**, *63*, 625-632.

(56)   Moerner, W. E. *Acc. Chem. Res.* **1996**, *29*, 563-571.

(57)   Orrit, M.; Bernard, J. *Phys Rev Lett* **1990**, *65*, 2716-2719.

(58)   Yeung, E. S. *Acc. Chem. Res.* **1994**, *27*, 409-414.

(59)   Grynkiewicz, G.; Poenie, M.; Tsien, R. Y. *J Biol Chem* **1985**, *260*, 3440-50.

(60)   Minta, A.; Kao, J. P.; Tsien, R. Y. *J Biol Chem* **1989**, *264*, 8171-8.

(61)   Tsien, R.; Pozzan, T. *Methods Enzymol* **1989**, *172*, 230-62.

(62)   Tsien, R. Y. *Biochemistry* **1980**, *19*, 2396-404.

(63)   Haugland, R. P. *Handbook of fluorescent probes and research chemicals*; 9th ed.; Molecular Probes Inc.: Eugene, OR, 1996.

(64)   de Silva, A. P.; Gunaratne, H. Q. N.; Gunnlaugsson, T.; Huxley, A. J. M.; McCoy, C. P.; Rademacher, J. T.; Rice, T. E. *Chem. Rev.* **1997**, *97*, 1515-1566.

(65)   Gershkovich, A. A.; Kholodovych, V. V. *J Biochem Biophys Methods* **1996**, *33*, 135-62.

(66)   Wang, Q.; Scheigetz, J.; Gilbert, M.; Snider, J.; Ramachandran, C. *Biochim Biophys Acta* **1999**, *1431*, 14-23.

(67)   Zhou, M.; Upson, R. H.; Diwu, Z.; Haugland, R. P. *J Biochem Biophys Methods* **1996**, *33*, 197-205.

(68)   Fischer, R. T.; Cowlen, M. S.; Dempsey, M. E.; Schroeder, F. *Biochemistry* **1985**, *24*, 3322-31.

(69)   Hale, J. E.; Schroeder, F. *Eur J Biochem* **1982**, *122*, 649-61.

(70)   Schroeder, F.; Barenholz, Y.; Gratton, E.; Thompson, T. E. *Biochemistry* **1987**, *26*, 2441-8.

(71)   LeBel, C. P.; Ischiropoulos, H.; Bondy, S. C. *Chem. Res. Toxicol.* **1992**, *5*, 227-231.

(72)   Naguib, Y. M. *Anal Biochem* **1998**, *265*, 290-8.

(73)   Packer, L. *Methods Enzymol.* **1994**, *233*.

(74)   Gabe, Y.; Urano, Y.; Kikuchi, K.; Kojima, H.; Nagano, T. *J. Am. Chem. Soc.* **2004**, *126*, 3357-3367.

(75)   Ueno, T.; Urano, Y.; Kojima, H.; Nagano, T. *J. Am. Chem. Soc.* **2006**, *128*, 10640-10641.

(76)   Ueno, T.; Urano, Y.; Setsukinai, K.; Takakusa, H.; Kojima, H.; Kikuchi, K.; Ohkubo, K.; Fukuzumi, S.; Nagano, T. *J. Am. Chem. Soc.* **2004**, *126*, 14079-14085.

(77)   Johnson, I. D.; Kang, H. C.; Haugland, R. P. *Anal Biochem* **1991**, *198*, 228-37.

(78) Joseph H. Boyer, A. M. H. G. S. M.-L. S. K. T. T. G. P. *Heteroatom Chemistry* **1993**, *4*, 39-49.

(79) Brigati, G.; Lucarini, M.; Mugnaini, V.; Pedulli, G. F. *J Org Chem* **2002**, *67*, 4828-32.

(80) Lucarini, M.; Pedulli, G. F.; Cipollone, M. *J. Org. Chem.* **1994**, *59*, 5063-5070.

(81) Oleynik, P.; Ishihara, Y.; Cosa, G. *J. Am. Chem. Soc.* **2007**, *129*, 1842-1843.

(82) Amat-Guerri, F.; Liras, M.; Carrascoso, M. L.; Sastre, R. *Photochem Photobiol* **2003**, *77*, 577-84.

(83) Kondo, A.; Iwatsuki, S. *J. Org. Chem.* **1982**, *47*, 1965-1968.

(84) Arbeloa, T. L.; Arbeloa, F. L.; Arbeloa, I. L.; Garcia-Moreno, I.; Costela, A.; Sastre, R.; Amat-Guerre, F. *Chemical Physics Letters* **1999**, *299*, 315-321.

(85) Rehm, D.; Weller, A. *Isr. J. Chem* **1970**, *8*, 259.

(86) Williams, L. L.; Webster, R. D. *J. Am. Chem. Soc.* **2004**, *126*, 12441-12450.

(87) Chemicals, A. N.; Akzo Nobel Chemicals: Chicago, 2006; Vol. 2007.

(88) Bedard, L.; Young, M. J.; Hall, D.; Paul, T.; Ingold, K. U. *J. Am. Chem. Soc.* **2001**, *123*, 12439-12448.

(89) Liebler, D. C.; Baker, P. F.; Kaysen, K. L. *J. Am. Chem. Soc.* **1990**, *112*, 6995-7000.

(90) Liebler, D. C.; Burr, J. A.; Matsumoto, S.; Matsuo, M. *Chem Res Toxicol* **1993**, *6*, 351-5.

(91) Liao, K.; Yin, M. *J Agric Food Chem* **2000**, *48*, 2266-70.

(92) Brault, D.; Vever-Bizet, C.; Le Doan, T. *Biochim Biophys Acta* **1986**, *857*, 238-50.

(93) Amat-Guerri, F.; Liras, M.; Carrascoso, M. L.; Sastre, R. *Photochemistry and Photobiology* **2003**, *77*, 577-584.

(94) Mohtat, N.; Cozens, F. L.; Scaiano, J. C. *J. Phys. Chem.: B* **1998**, *102*, 7557-7562.

(95) Hope, M. J.; Bally, M. B.; Web, G.; Cullis, P. R. *Biochem. Biophys. Acta* **1985**, *858*, 161-168.